UNIVERSITY OF SOUTHAMPTON

FACULTY OF MEDICINE, HEALTH AND LIFE SCIENCES

School of Medicine

The role of the MAP Kinase Signal Integrating Kinases in the proliferation and survival of cancer cells

by

Matthew James Wheater

Thesis for degree of Doctor of Philosophy

May 2011

UNIVERSITY OF SOUTHAMPTON

ABSTRACT

FACULTY OF MEDICINE, HEALTH AND LIFE SCIENCES

School of Medicine

Doctor of Philosophy

The role of the MAP Kinase Signal Integrating Kinases in the proliferation and survival of cancer cells

By Matthew James Wheater

Eukaryotic initiation factor 4E (eIF4E) is an oncogene over-expressed in a variety of cancers. It is responsible for regulation of synthesis of proteins involved in progression to the malignant phenotype, including cyclin D1, Mcl-1 and VEGF. The oncogenic activity of eIF4E has been shown to be dependent on phosphorylation at serine 209 by the mitogen-activating protein kinase signal integrating kinases (MNKs).

This work investigates the role of the MNK proteins in the proliferation and survival of breast and kidney cancer cells. Inhibition of the MNKs with a chemical kinase inhibitor resulted in inhibition of proliferation through cell cycle arrest, with no induction of apoptosis. This is consistent with a reduction in cyclin D1 protein. Combination of mTOR inhibition and inhibition of the MNK proteins in kidney cancer cells resulted in an additive but not synergistic effect on inhibition of proliferation. siRNA knockdown of the MNKs resulted in a reduction in eIF4E phosphorylation but did not inhibit proliferation or induce cell cycle arrest in a renal cancer cell line. The generation of an eIF4E mutant with phospho-mimetic activity induced partial insensitivity to the MNK kinase inhibitor suggesting some specificity of activity of this agent through the MNK proteins.

Inhibition of the MNKs resulted in a reduction in cyclin D1 mRNA with no reduction in transcription. An accumulation of cyclin D1 RNA was seen in the nuclear compartment following treatment with MNK inhibitor suggesting inhibition of nuclear export of cyclin D1 RNA and subsequent degradation. Gene expression array analysis revealed regulation of genes with key functions in cellular metabolism.

The MNK kinases are thus worthy of further investigation as a therapeutic target in breast and renal cancer. More potent and specific inhibitors of the MNK kinases than CGP57380 are required for this to be clinically relevant.

List of Contents

List of Figures

List of tables

DECLARATION OF AUTHORSHIP

I, Matthew James Wheater, declare that this thesis entitled 'The role of the MAP Kinase Signal Integrating Kinases in the proliferation and survival of cancer cells' and the work presented in the thesis are both my own, and have been generated by me as a result of my own original research. I confirm that:

- this work was done wholly or mainly while in candidature for a research degree at this University;
- where any part of this thesis has previously been submitted for a degree or any other qualification at this University or any other institution, this has been clearly stated;
- where I have consulted the published work of others, this is always clearly attributed;
- where I have quoted from the work of others, the source is always given. With the exception of such quotations, this thesis is entirely my own work;
- I have acknowledged all main sources of help;
- where the thesis is based on work done by myself jointly with others, I have made clear exactly what was done by others and what I have contributed myself;
- parts of this work have been published as: Wheater M, Johnson PW, Blaydes JP; The role of MNK proteins and eIF4E phosphorylation in breast cancer cell proliferation and survival. *Cancer Biol Ther*. 2010; 10 (7) 728-735

Signed:.....

Date:.....

ACKNOWLEDGEMENTS

I would like to thank and acknowledge the support of Dr Jeremy Blaydes and Professor Peter Johnson who acted as supervisors for the work presented in this thesis.

I would like to acknowledge Mr Matthew Darley, Dr Anna Philips and Dr Charles Birts in Dr Blaydes laboratory for instruction on the laboratory techniques that I have used in this work. I would like to thank Professor Chris Proud for advice and discussion, particularly regarding 4-thiouracil labeling of RNA.

I acknowledge Graham Broadley and Alison Donlevy who worked as students under my supervision and contributed to figures as indicated in this work.

I would like to thank my family for their encouragement and support in allowing me the time to complete this thesis.

Finally I am grateful to Cancer Research UK who funded my position as a Clinical Research Fellow which allowed me to undertake this work.

List of Abbreviations

4E-BP	4E-binding protein
4E-SE	4E-sensitivity element
4TU	4-thiouracil
ADP	adenosine di-phosphate
ANOVA	analysis of variance
AOI	area of interest
ARE	AU rich element
ARE	antioxidant response elements
ATP	adenosine tri-phosphate
CaMK	calcium/calmodulin regulated kinases
CAPP	ceramide-acivated protein phosphatases
CDK	cyclin dependent kinase
CK1	casein kinase 1
CML	chronic myeloid leukaemia
CSD	cystein rich domain
DAG	diacylglycerol
DAPI	4',6-diamidino-2-phenylindole
DAVID	database for annotation, visualisation and integrated discovery
DKO	double knockout
DMEM	Dulbecco's modified Eagle's medium
DMF	dimethylformamide
DMSO	dimethyl sulfoxide
DTT	Dithiothreitol
EASE	expression analysis systematic explorer
EDTA	Ethylenediaminetetraacetic acid
EGFR	epidermal growth factor receptor
eIF4E	eukaryotic initiation factor 4E
EMEM	Eagle's minimal essential medium
ER	oestrogen receptor
ERK	extracellular signal-regulated kinase
EYFP	enhanced yellow fluorescent protein
FGF2	fibroblast growth factor 2

FITC	Fluorescein isothiocyanate
GAP	GTPase activating protein
Grb2	growth factor receptor bound protein 2
HDAC	histone deacetylase
HGF/SF	hepatocte growth factor / scatter factor
HIF	hypoxia inducible factor
hnRNP A1	heterogenous nuclear ribonuclear protein A1
HRP	horseradish peroxidase
HRPC	hereditary papillary renal cancer carcinoma
IDC	invasive ductal carcinoma
IHC	immunohistochemistry
ILC	invasive lobular carcinoma
IP3	inositol 1,4,5-triphosphate
JNK	c-Jun n terminal kinase
KSR	kinase suppressor of ras
M^7GTP	7-methyl guanosine triphosphate
MAP3K	MAPKK kinase
MAPK	mitogen activated protein kinase
MAPKAPK	MAPK activated protein kinase
MAPKK	MAPK kinase
Mcl-1	myeloid cell leukaemia sequence 1 protein
MKK1	MAPK kinase 1
MNK	Mitogen activated protein kinase signal integrating kinase
mTORC1	mammalian target of rapamycin complex 1
NES	nuclear export sequence
MTS	3-(4,5-dimethylthiazol-2-yl)-5-(3-carboxymethoxyphenyl)-2-(-4-sulfophenyl)-2H-tetrazolium inner salt
NF-κB	nuclear factor- κB
NLS	nuclear localisation sequence
ODD	oxygen degradation domain
p90RSK	p90 ribosomal S6 kinase
PABP	poly-A binding protein
PAGE	poly-acrylamide gel electrophoresis
PBS	phosphate buffered saline

PCR	polymerase chain reaction
PDGF	platelet derived growth factor
PDK1	3-phosphoinositide dependent kinase
PI3K	phosphoinositide 3 kinase
PIP2	phophotidylinositol-4,5-bisphosphate
PIP3	phosphotidylinositol-3,4,5–triphosphate
PML	promyelocytic leukaemia protein
PR	progesterone receptor
PTEN	phosphatase and tensin homolog
PTK	protein tyrosine kinase
Rb	retinoblastoma protein
RBD	ras binding domain
RGC	receptor guanylate cyclase
RTK	receptor tyrosine kinase
SDS	sodium dodecyl sulphate
SH2	src-homology 2
SH3	src-homology 3
siRNA	small interfering RNA
snRNA	small nuclear RNA
snRNP	small nuclear ribonuclear protein
SOS	son of sevenless
TBS	tris buffered saline
TG	tris-glycine
TGF	transforming growth factor
TSC	tuberous sclerosis complex
UTR	untranslated region
VEGF	vascular endothelial growth factor
VHL	von Hippel-Lindau

1. Introduction

An increasing understanding of the molecular characteristics underlying the development of cancer has led to a revolution in the development of cancer therapeutics, with many agents now in use designed to inhibit known signaling pathways critical to cancer cell proliferation and survival. Although these agents have improved the outlook for many with cancer, in the face of advanced disease, cure remains elusive for the majority. There is thus an imperative to investigate novel pathways involved in the development and maintenance of the malignant phenotype, and strategies for their inhibition.

Many intracellular signaling events are controlled by post-translational modification of proteins including phosphorylation; indeed many of the cellular functions which become dysregulated as the hallmarks of cancer[1] are controlled by protein kinase signaling cascades. As such interest has developed in the understanding of protein kinases, and synthesis of specific inhibitors which are now starting to see widespread use in the clinical treatment of cancer.

1.1. Eukaryotic Initiation Factor 4E (eIF4E)

eIF4E is a translation factor involved in the preferential translation of a variety of proteins including many which regulate cell growth, proliferation and invasion. These include the cell cycle regulatory protein cyclin D1[2], the transcription factor c-Myc and growth factors such as vascular endothelial growth factor (VEGF) and fibroblast growth factor 2 (FGF2)[3]. eIF4E has dual functions, regulating translation through mRNA cap binding, and through control of mRNA nuclear export.

eIF4E regulation of translation via mRNA cap binding

Regulation of cap dependent translation is achieved through binding of eIF4E to the 7-methyl guanosine tri-phosphate (GTP) cap structure present at the 5' end of all mRNA molecules. Following binding of eIF4E to the cap structure a scaffold protein eIF4G is recruited, leading to the further recruitment of eIF4A, a RNA helicase, to form the eIF4F complex. Poly-A binding protein (PABP) binds eIF4G to the poly-adenylated tail at the 3' end of the mRNA creating a loop structure. Subsequent binding of the 40S ribosome subunit and methionyl tRNA leads to

translation initiation on reaching the AUG initiation codon in the open reading frame (Fig 1:1). eIF4E is the rate limiting component of the eIF4F complex and thus translation is sensitive to the presence of increasing availability of eIF4E.
A subset of mRNA molecules include a long and complex 5' untranslated region (UTR) rich in cytosine and guanine, with features such as repeat stem loop structures. These mRNA molecules often code for proteins implicated in malignant transformation such as c-myc and VEGF as described above. Those mRNA molecules with a complex 5' UTR are particularly sensitive to the presence of the helicase eIF4A for efficient translation. Most mRNAs have short 5' UTRs and are efficiently translated at low levels of eIF4F, however in response to growth signaling, increasing amounts of eIF4E are available for formation of the eIF4F complex. This then allows increased translation of those mRNAs with complex 5'UTRs.

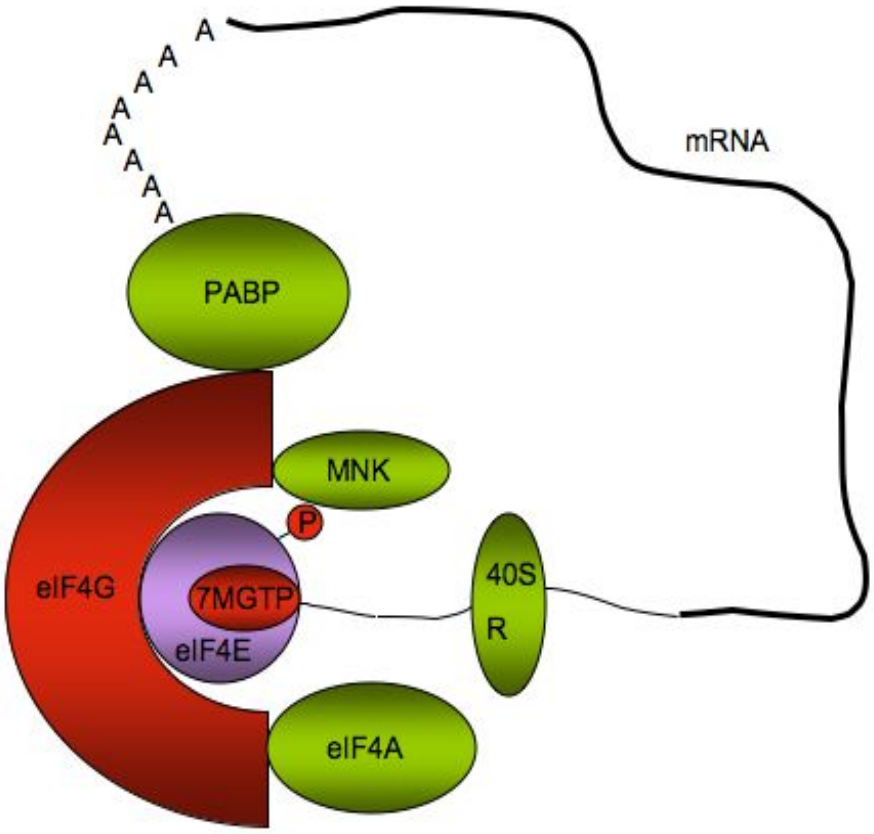

Figure 1:1 Structure of the eIF4F complex

AAAAAAA…. Poly A tail; PABP Poly A Binding Protein; eIF4G eukaryotic initiation factor 4G; eIF4E eukaryotic initiation factor 4E; MNK mitogen activating protein kinase signal integrating kinase; M^7GTP 7 methyl guanine triphosphate cap; eIF4A eukaryotic initiation factor 4A; 40SR 40S ribosomal subunit

eIF4E is essential for cell survival, with knockdown producing cell death in HeLa cells[3], and lethality in yeast[4]. Overexpression however causes deregulated cell growth and malignant transformation[3,5]; indeed patients with node positive breast cancer and high levels of eIF4E expression have a significant increase in relative risk for cancer recurrence[6]. Increased expression has also been identified as an adverse prognostic factor in head and neck cancer[7], and lung cancer[8,9] and with progression from adenoma to carcinoma in colorectal cancer[9]. Regulation of eIF4E is thus critical both to normal development and avoidance of a malignant phenotype.

The activity of the eIF4F complex is regulated by competitive binding of eIF4E to 4E binding proteins (4E-BPs) at the same binding site as eIF4G. Sequential phosphorylation of 4E-BP reduces its affinity for eIF4E allowing formation of the eIF4F complex. 4E-BP phosphorylation is under the control of the mammalian target of rapamycin complex 1 (mTORC1) and thus through the phosphoinositide 3-kinase (PI3 kinase)/AKT pathway, such that a variety of mitogenic and growth stimulatory factors, signalling through receptor tyrosine kinases, cause up-regulation of protein translation via eIF4E[10] .

Further input to the eIF4E translation initiation factor is through phosphorylation by the mitogen activated protein kinase (MAPK) signal-integrating kinases (MNKs). The MNKs themselves undergo activating phosphorylation through both extracellular signal-regulated kinase (ERK) and p38 MAP-kinase, and are therefore downstream of the MAP-kinase pathway (Fig 1:2).

eIF4E regulation of RNA nuclear export

Additional control of gene expression at the post-transcriptional level can be achieved via the control of mRNA export, with enhanced nuclear export of mRNA messages facilitating increased ribosomal recruitment and hence enhanced translation. The majority of large mRNA molecules are transported through nuclear pore complexes following completion of splicing via the binding of an exporter complex, consisting of a heterodimer of Tap (NXF1) and NXT[11]. An alternative export pathway, CRM1, predominantly regulates export of ribosomal RNA and small nuclear RNA (snRNA) prior to cytoplasmic incorporation into small nuclear ribonuclear proteins (snRNPs)

The role of eIF4E in promoting nuclear export of mRNA appears related to its phosphorylation at serine 209 by MNKs, with phosphorylation promoting nuclear export and contributing to the transforming ability of eIF4E[12].

In cytoplasmic fractions of whole cell lysates eIF4E is able to bind all mRNA molecules due to the presence of a 5' m^7GTP cap on the mRNA molecule as described above. It appears however that eIF4E binding in nuclear fractions is restricted to a subset of mRNA molecules with specific characteristics.

Experiments using eIF4E mutants deficient in particular functions have shown that binding to the mRNA cap is essential, however a mutant inactive in translation, and unable to bind the eIF4G scaffold, remains able to promote nuclear export. Using reporter constructs of the cyclin D1 3'UTR, a 100-nt region has been identified which is essential for nuclear export and is conserved between species. This 4E sensitivity element (4E-SE) appears to be the defining characteristic of mRNA molecules for which eIF4E regulates nuclear export[13], and is an example of the way in which coordinated regulation of expression of functionally related genes can occur at a post-transcriptional level. Such elements in the 5' or 3'UTR of mRNA molecules have been termed untranslated sequence elements for regulation, or USER codes[14].

The mechanism underlying nuclear export of mRNA as regulated by eIF4E appears specific, and independent of bulk mRNA transport via NXF1 (Tap). siRNA knockdown of NXF1 failed to affect the nuclear export of 4E-SE containing reporter constructs, however leptomycin B caused nuclear accumulation, suggesting CRM1 to be the nuclear export mechanism through which eIF4E mediated mRNA export occurs[14].

Whereas cytoplasmic regulation of eIF4E is predominantly through binding to 4E-BPs, in the nucleus the export function of eIF4E is controlled through binding of the RING domain of promyelocytic leukaemia protein (PML)[15]. A large portion of cellular eIF4E is located in the nucleus where it is associated with nuclear bodies. Whereas over-expression of eIF4E induces increased nuclear export of cyclin D1, over-expression of PML causes a reduction in cyclin D1 mRNA in the cytoplasmic compartment, suggesting a negative regulatory role of PML in eIF4E induced nuclear export. In addition PML can be detected by pull down of eIF4E by immunoprecipitation, suggesting a direct interaction between these two proteins[16].

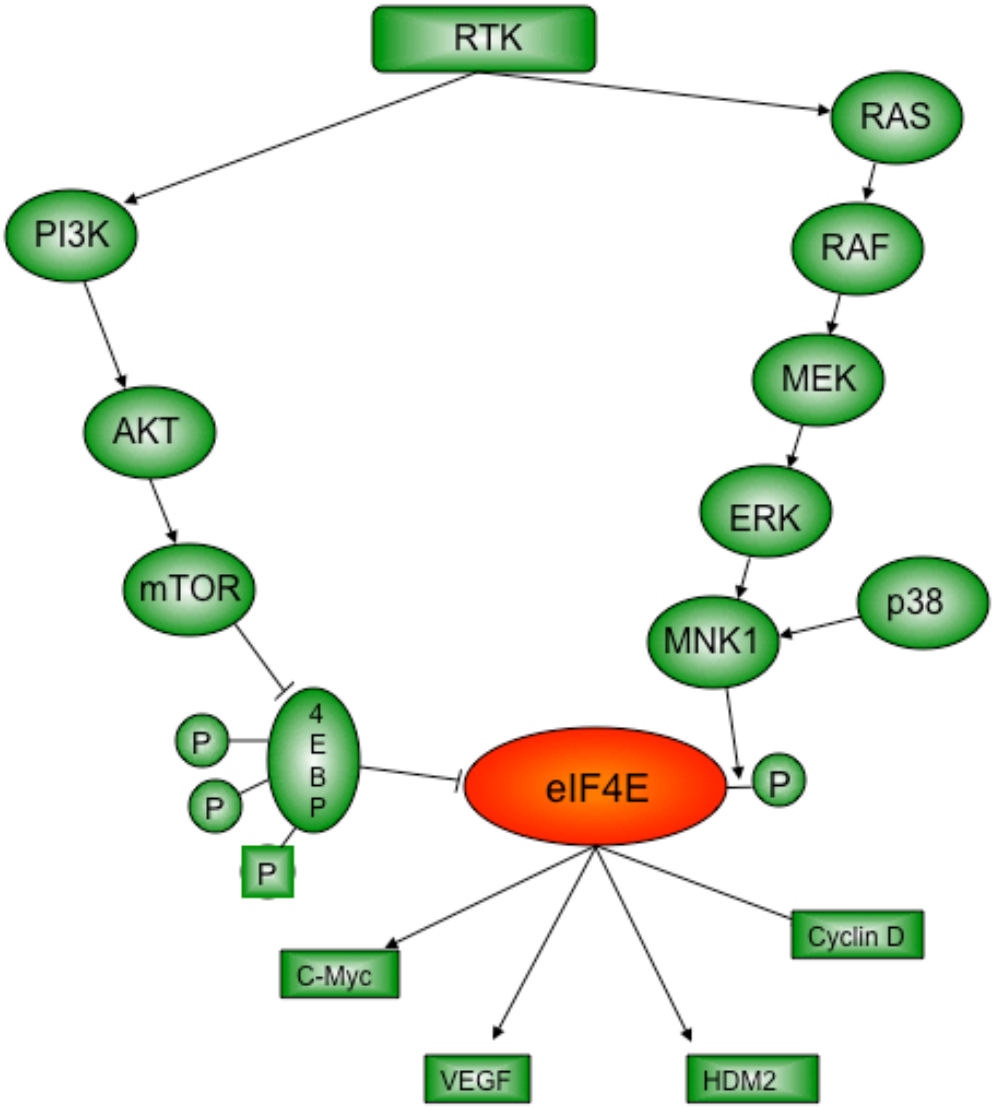

Figure 1:2 eIF4E is regulated by the PI3K and MAPK pathways
Activation of receptor tyrosine kinases (RTK) through ligand binding leads to sequential activation of members of the PI3K/AKT/mTOR, or MAPK (RAS/RAF/MEK/ERK) pathways. Activation of mTOR leads to phosphorylation of 4E binding proteins (4EBP) and their dissociation from eIF4E allowing recruitment to the eIF4F complex. Activation of MNK1 via MAPK signaling leads to phosphorylation of eIF4E with a subsequent reduction in cap binding affinity and promotion of mRNA nuclear export.

eIF4E as a therapeutic target

eIF4E has become a therapeutic target via its regulation by 4E-BP. mTOR inhibitors are now used in the clinic both as anti-neoplastic and immunosuppressant drugs. Both temsirolimus[17], and everolimus[18], analogues of the naturally occurring mTOR inhibitor rapamycin, have shown activity in advanced renal cancer and are licensed for use in the first and second line respectively. Alternative therapeutic strategies are being investigated with the clinical development of anti-sense technology targeted at eIF4E[19].

Pre-clinical work has shown that inhibition of eIF4E with rapamycin can cause a paradoxical rise in eIF4E phosphorylation in a PI3K dependent fashion[20]. The implication of this finding remains at present uncertain, but could represent a mechanism of resistance to mTOR inhibition in cancer therapy, however the further study of pathways controlling the activity of eIF4E is clearly warranted.

1.2. Signalling pathways regulating eIF4E

Growth and mitogenic signals, following transduction by transmembrane receptors, are relayed to their cytoplasmic and nuclear targets by a complex set of intracellular signaling molecules. Two molecular pathways define much of this signaling, namely the PI3K/mTOR and MAPK pathways. eIF4E is regulated by input from both the PI3K and MAPK signaling cascades, and is therefore potentially a critical node in the regulation of signalling inputs under many different conditions.

PI3K/mTOR

The best defined regulatory interaction of eIF4E is through the PI3K/mTOR pathway, via 4E-BP1. In its unphosphorylated form, 4E-BP1 binds eIF4E, preventing its interaction with the eIF4G scaffold protein and therefore preventing assembly of the eIF4F complex[21]. The phosphorylation of 4E-BP1 is regulated by mTOR, in complex with raptor as mTORC1. 4E-BP1 undergoes four sequential phosphorylation events leading to its dissociation from eIF4E and up-regulation of translation of target mRNAs[22].

mTOR exists as two complexes in mammals, mTORC1 in complex with raptor and mLST8, and mTORC2 together with rictor and mLST8[23]. The function of mTORC1 is the best defined and accounts for most of the knowledge of mTOR function. mTORC1 is able to integrate a variety of extracellular and intracellular signals including growth factors[24], amino acids[25], insulin[24] and intracellular energy supply in the form of ATP/ADP ratios[26].

mTORC1 is directly activated by Rheb via binding to its catalytic domain. Rheb is a GTPase and only activates mTORC1 in the presence of GTP, having an inhibitory effect in its absence[27]. Rheb is inactivated by tuberous sclerosis complex 2 (TSC2), a GTPase activating protein (GAP) which forms a complex with TSC1, by converting Rheb from its GTP to its GDP bound form[28]. TSC2 is itself inactivated by signalling from AKT, which phosphorylates TSC2, inhibiting its GAP activity[29]. TSC also has inhibitory input from ERK, which inhibits the association of TSC1 and TSC2 in response to signaling from the MAPK pathway, ultimately resulting in activation of mTOR[30].

AKT is recruited to the cell membrane by phosphotidylinositol-3,4,5–triphosphate (PIP3), and activated by phosphorylation at two sites[31]. 3-phosphoinositide dependent kinase (PDK1), itself recruited and bound by PIP3, phosphorylates AKT at Thr 308 on the activation-loop[32]. A second phosphorylation event at Ser 473 occurs via mTORC2[33].

Activation of cell surface receptor tyrosine kinases results in a conformational change through which tyrosine residues are phosphorylated, leading to the binding of PI3K via SH2 domains. PI3K consists of two subunits, p85, a regulatory unit, and p110 which has a catalytic function, phosphorylating phophotidylinositol-4,5-bisphosphate (PIP2) to form PIP3. PI3K can also be directly activated by Ras, a further interaction between the MAPK and mTOR pathways[34]. The action of PI3K in phosphorylating PIP2 is antagonised by the tumour suppressor phosphatase and tensin homolog (PTEN)[35]. This phosphatase inhibits signalling through the PI3K/mTOR axis, and is mutated either in the germ line, or as a somatic mutation in a wide variety of cancers[36].

Once activated mTORC1 up-regulates both eIF4E (via inhibitory phosphorylation of 4EBP), and activates S6K. This results in both up-regulation of ribosomal synthesis, but also in an inhibitory negative feedback loop to PI3K (fig 1:3).

PIP2 is involved in an additional intracellular signalling pathway, which can also be activated by receptor tyrosine kinases, as well as antigen receptors on the surface of cells of the immune system and phorbol esters. PIP2 can be converted, not only to PIP3 by PI3K, but also to inositol 1,4,5-triphosphate (IP3) and diacylglycerol (DAG), by phospholipase C. IP3 binds receptors on the endoplasmic reticulum resulting in release of calcium, and the propagation of a signalling cascade through calcium flux. DAG however is an activator both of protein kinase C and of Ras GTPase. Activation of protein kinase C plays a critical role in control of immune function, in part through activation of NF-κB as well as through the interplay between the MAPK signalling cascade and the calmodulin, calcineurin pathway (reviewed in [37]).

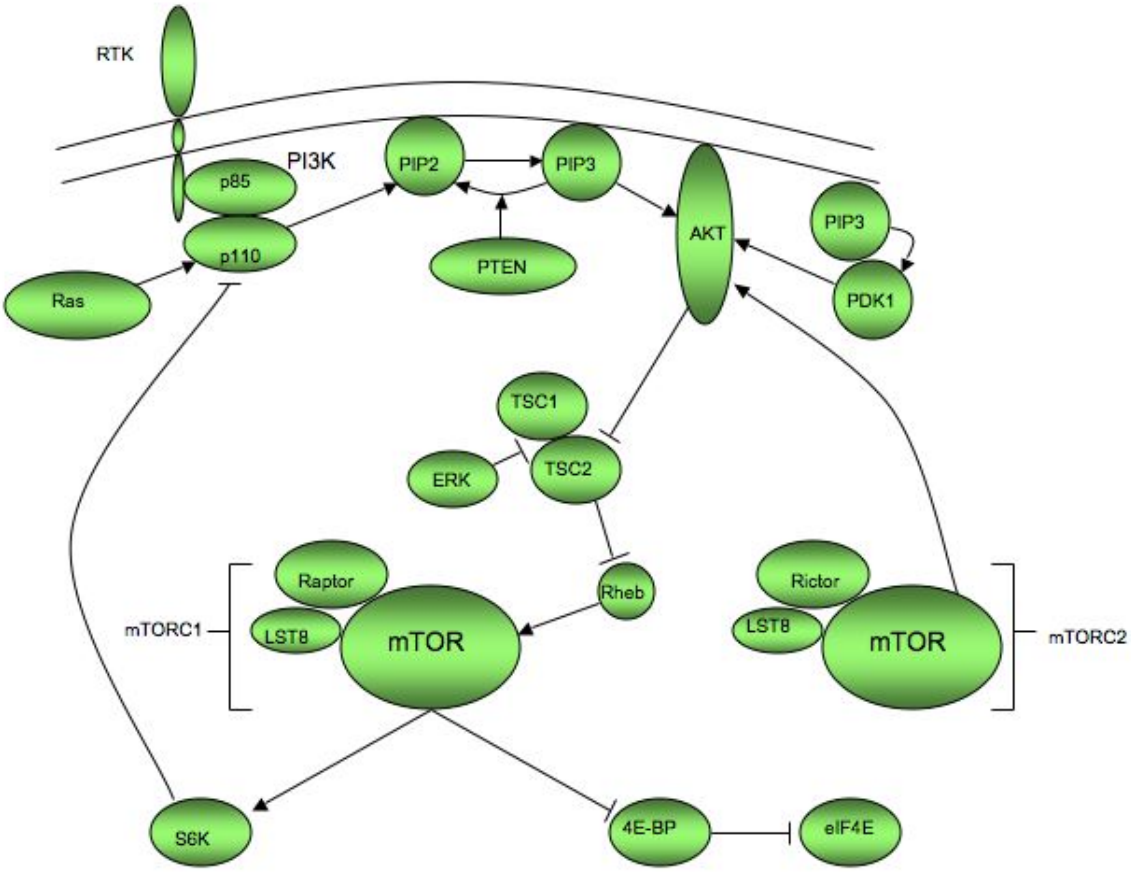

Figure 1:3 PI3K/AKT signaling activates eIF4E via mTOR
Activation of receptor tyrosine kinases via ligand binding leads to recruitment of the p85 and p110 subunits of phosphatidylinositol 3-kinase (PI3K) and subsequent phosphorylation of phosphatidylinositol (3,4)-bisphosphate (PIP2) to phosphatidylinositol (3,4,5)-triphosphate (PIP3), a reaction antagonised by phosphatase and tensin homolog (PTEN). PIP3 recruits AKT to the inner cell membrane where it is phosphorylated and activated by 3-phosphoinositide dependent kinase (PDK1). Activated AKT phosphorylates tuberous sclerosis complex 2 (TSC2) preventing its inhibitory activity on Rheb, which also results from ERK activation preventing the binding of TSC2 and tuberous sclerosis complex 1. Rheb therefore remains in its activated form and activates mammalian target of rapamycin (mTOR) as mTOR complex 1 (mTORC1) bound to Raptor and mammalian LST8. This in turn results in phosphorylation of 4E-binding proteins (4E-BPs) preventing their association with eIF4E allowing recruitment to the eIF4F complex. mTOR additionally phosphorylates and activates ribosomal S6 kinase, which has a negative regulatory effect on PI3K. mTOR exists in a second complex (mTORC2) which has activity in promoting signaling through the PI3K/AKT pathway through activation of AKT.

MAPK Signalling

The MAPK signalling cascade is a complex system of sequential kinases that can be divided into three major cascades, with four main levels of signaling. The three major cascades include the ERK MAPK pathway which is involved in transduction of proliferative signaling, with activating mutations in several of its constituent kinases implicated in carcinogenesis[38,39]. p38 and c-Jun N-terminal kinase (JNK) MAPK pathways are involved in stress response, with ERK and p38 shown to have activity in regulating eIF4E[40].

Each of these signalling pathways has analogous levels of signaling, terminating in the MAPK molecules ERK, JNK and p38. These MAPK molecules are themselves activated by phosphorylation by a MAPK kinase (MAPKK). Moving up the chain of signaling molecules are also found MAPKK kinases (MAP3K) (fig 1:4).

The best described of the MAPK pathways is the ERK pathway. Phosphorylation of receptor tyrosine kinases results in the activation of membrane bound RAS GTPase, through recruitment of adaptor proteins. Growth factor receptor-bound protein 2 (Grb2) is an adaptor protein, bound to Son of Sevenless (SOS) by a Src homology 3 (SH3) domain. Once the Grb2/SOS complex is bound to the activated receptor tyrosine kinase, SOS acts as a guanine exchange factor to Ras, switching it to its active GTP bound form[41]. Three Ras genes exist in humans; *K-Ras*, *H-Ras*, and *N-Ras*, giving rise to four proteins; K-RAS4A, K-RAS4B, H-RAS and N-RAS. These are ubiquitously expressed with tissue specific variations in ratios of particular proteins[42].

Activated Ras binds Raf-1, a serine/threonine kinase via two binding sites on Raf-1, a cystein rich domain (CSD), and Ras binding domain (RBD). Raf-1 undergoes a conformational change during this binding process, leading to activation of its kinase function, and phosphorylation of MAPK/ERK kinase (MEK)[43]. MEK, a family of dual specific tyrosine/threonine kinases in turn phosphorylate ERK1 and ERK2 on both tyrosine and threonine residues[44]. Co-ordination of this sequence of phosphorylation events is facilitated by the translocation of kinase suppressor of ras (KSR), a scaffold protein which binds Raf-1, MEK and ERK, to the plasma membrane[45]. ERK 1 and 2 target a variety of effector molecules including protein kinases (MAPK activated protein kinases (MAPKAPK) I (p90RSK) and II)[46], and transcription factors such as the Ets family including Elk-1[47].

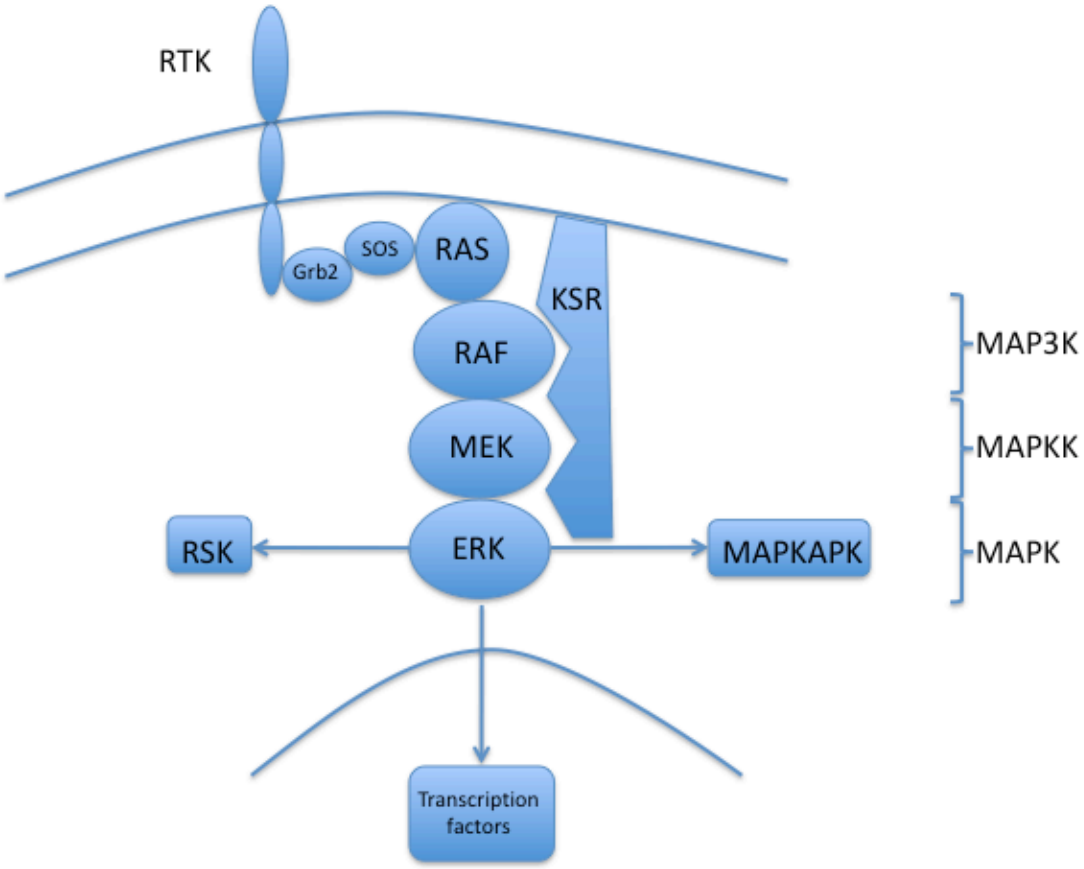

Figure 1:4 Signalling through the ERK MAPK pathway
Activation of receptor tyrosine kinases (RTK) through ligand binding results in the recruitment of adaptor proteins Growth Factor Receptor-bound Protein 2 (Grb2) and Son of Sevenless (SOS). As a result Ras becomes activated leading to sequential phosphorylation of Raf (Mitogen Activating Protein Kinase Kinase Kinase (MAP3K)), Map/Erk Kinase (MEK) (Mitogen Activating Protein Kinase Kinase (MAPKK)) and Extracellular Regulated Signalling Kinase (ERK) (Mitogen Activating Protein Kinase (MAPK)). These phosphorylation events are facilitated by binding to the scaffold protein Kinase Suppressor of Ras (KSR). Activation of ERK leads to phosphorylation of Ribosomal S6 Kinase (RSK), Map Kinase Activating Protein Kinases (MAPKAPK) and activation of transcription factors within the nucleus.

1.3. Mitogen activated protein kinase (MAPK) signal-integrating Kinases

Mitogen activated protein kinase (MAPK) signal-integrating Kinases (MNKs) 1 and 2 are two protein kinases that phosphorylate eukaryotic initiation factor 4E (eIF4E) at serine 209. Murine Mnks 1 and 2, and human MNK1, were identified in 1997 as downstream targets of both the extracellular signal-regulated kinases (ERK) and p38 MAPK pathways, responsible for phosphorylation of eIF4E in response to extracellular mitogens or stress[40,48]. Subsequently the human *MNK2* gene was identified in 2000[49]. Since then, despite extensive work on their role in both normal and deregulated cell function, uncertainty persists as to their function.

The MNK proteins have similarity with other protein kinase targets of MAP kinases, the ribosomal S-6 kinase (RSK) proteins. They contain a C terminal ERK interacting domain, a T loop, which contains MAPK phosphorylation sites, and a catalytic domain, however unlike the RSKs they lack a second N terminal kinase domain[40]. Two splice variants of both the *MNK* genes exist in humans; *MNK1a* and *MNK1b*[49,50]. Both MNK1b and MNK2b are truncated proteins, lacking the C terminal MAPK binding domain, however they retain their ability to phosphorylate eIF4E in vitro (fig 1:5).

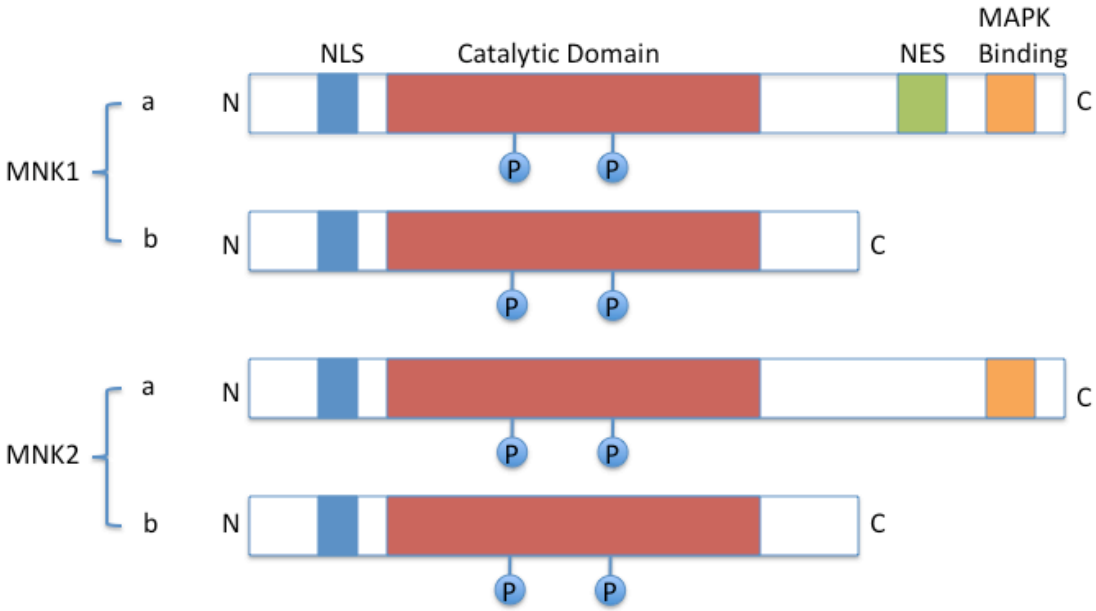

Figure 1:5 Domain structure of the MNK proteins
MNK1 and MNK2 a isoforms consist of a nuclear localization sequence (NLS) at the N termini and a catalytic domain with two phosphorylation sites. MNK1a has a nuclear export sequence (NES) towards the C terminus and both MNK1a and MNK2a have MAPK binding sites at the C terminus. The b isoforms of both proteins have a truncated C terminus lacking the MAPK binding and NES motifs.

There are differences in the binding affinity of MNK1 and MNK2 for MAP kinases. MNK1 is phosphorylated by both ERK and p38 MAPK but not Jun N-terminal kinases (JNKs). MNK2 is phosphorylated by ERK alone, suggesting a differential effect in the signaling pathways able to activate the MNKs[40]. The regulation and activity of the two proteins also differ, related to multiple factors including their catalytic domains, and C termini[51]. MNK1 has a low baseline level of activity that is readily inducible by activation of the MAPK pathway, and inhibited by blocking signalling through either the ERK or p38 MAPK pathways. MNK2 however has much greater basal activity, with little effect from either the induction of, or blockade of ERK signaling[52].

Three phosphorylation sites have been identified in MNK1 and MNK2[52,53]. Two of these, Thr 197 and Thr 202 are within the T-loop, the third, Thr 332, is close to the C terminus. All are within consensus MAPK phosphorylation sites. Alanine substitutions at Thr 197 and Thr 202 have shown these sites to be essential for activation, and kinase activity. Alanine substitution at Thr 332 in MNK1 surprisingly showed enhanced activation of MNK1, however the same substitution in MNK2 inhibited kinase function. It may therefore be this site that is responsible for the high basal activity of MNK2.

Both MNK1 and MNK2 contain an eIF4G binding domain in the N terminus which overlaps with a polybasic nuclear localisation sequence[53,54]. Mutation of this sequence, preventing MNK1 from binding eIF4G inhibits the ability of MNK1 to phosphorylate eIF4E. In addition MNK1 must be phosphorylated through MAPK signalling for eIF4G binding to occur[55]. Thus both eIF4E and activated MNKs bind to eIF4G as part of the eIF4F complex before eIF4E can be phosphorylated at serine 209[56].

The cellular distribution of the full length and truncated MNK proteins is variable, as a consequence of the combination of effects of the nuclear localisation and nuclear export motifs (fig 1:5). Both MNK1a and MNK2a are cytoplasmic in distribution. In MNK1a this is due to the nuclear export sequence at the C terminus which facilitates exportin 1 (CRM1) mediated nuclear export. The N terminal domain binds importin α, and when nuclear export is blocked with leptomycin B, MNK1a localises to the nucleus, suggesting that it is able to shuttle from the nucleus to the cytoplasm[57]. In the case of MNK2a a key amino acid in the nuclear export domain

is substituted, suggesting that nuclear localisation should predominate. It has been shown however that the C terminal of MNK2a is able to interfere with access to the N terminal basic region, reducing access to the nuclear localisation domain, hence its cytoplasmic localisation[57]. Both MNK1b and MNK2b lack the C terminal NES seen in the full length transcripts and as such predominantly localise to the nucleus[50].

The impact of eIF4E phosphorylation on mRNA binding and translation remains controversial. Early in vitro assays investigating the phosphorylated form of eIF4E suggested enhanced binding affinity for the mRNA m7GTP cap structure. This was initially thought to account for increased protein synthesis and cellular growth in the context of phosphorylated eIF4E[58]. More recently however data has suggested that phosphorylation may in fact reduce mRNA binding affinity, but that this may allow progression of the eIF4F complex beyond the mRNA cap structure, still allowing increased protein synthesis[59]. Contrary to this model, a bicistronic reporter assay, allowing assessment of both cap-dependent and cap-independent translation in response to eIF4E phosphorylation has suggested a negative regulatory role of eIF4E phosphorylation on both global and cap-dependent translation[60]. Further work on recovery from cellular stress has shown induction of 4E-BP and eIF4E phosphorylation, but that inhibition of the MNKs and subsequent reduction in eIF4E phosphorylation does not affect either formation of the eIF4F complex, or initiation of translation[61].

Phosphorylated eIF4E plays an additional role in the control of mRNA export from the nucleus to cytoplasm. This was first defined with respect to cyclin D1 where enhanced eIF4E expression led to an increase in cytoplasmic cyclin D1 mRNA, but not total cyclin D1 mRNA levels[2]. More recently it has been shown that eIF4E phosphorylation is required for this function, with introduction of a phospho-resistant form of eIF4E (ST209/210AA) rendering cells resistant both to increases in cyclin D1 export and to transformation to the malignant phenotype[12]. The transport function of phosphorylated eIF4E is important in the regulation of other proteins, including MDM2, where inhibition of eIF4E phosphorylation has also shown a reduction in nuclear export of mRNA[62].

Data on the role of MNK1 driven phosphorylation of eIF4E in normal growth and development is conflicting. By generating a serine 251 to alanine mutation in eIF4E in Drosophila (the equivalent position to serine 209 in mammalian eIF4E), eIF4E

was rendered resistant to phosphorylation as demonstrated by the uptake of radiolabelled phosphate. Flies containing the mutant eIF4E allele were rendered smaller, and developed more slowly than unmutated controls[63]. This is contrary to a mouse model in which the MNK proteins were found not to be essential for normal growth or development. Both *Mnk1* and *Mnk2* single knockout, as well as double knockout mice have been developed, none of which show any phenotypic abnormality. Embryonic fibroblasts derived from these mice have confirmed that Mnk1 is responsible for inducible eIF4E phosphorylation, whereas Mnk2 is responsible for constitutive eIF4E phosphorylation, however in the complete absence of eIF4E phosphorylation, fibroblasts develop normally[64]. A role for the Mnk proteins in induction of apoptosis has also been identified in fibroblasts derived from *Mnk1* and *Mnk2* double knockout mice. These fibroblasts had increasing sensitivity to apoptosis on serum withdrawal compared to wild-type cells, an effect which was replicated with an inhibitor of the MNK proteins applied to wild-type cells[65].

Although eIF4E is the best described target of the MNKs, the MNK proteins have kinase activity towards additional proteins in addition to eIF4E. Sprouty2 is an antagonist of several receptor tyrosine kinases including fibroblast growth factor receptor and vascular endothelial growth factor receptor, and is involved in the negative feedback of RTK signaling. Phosphorylation of Sprouty2 at serines 112 and 121 mediated by MNK1 result in its stabilisation and thus enhanced activity[66]. Cytosolic phospholipase A_2, which regulates eicosanoid synthesis from phospholipids during inflammatory responses, is activated both by increasing intracellular calcium, but also by phosphorylation at serine 727 by MNK1. This mode of activation has been implicated in thrombin stimulation of platelets[67]. The heterogenous nuclear ribonuclear protein A1 (hnRNP A1) is one of three hnRNPs known to be targets of the MNKs, the others being hnRNP A0 and JKT BP. hnRNP binds the AU rich element (ARE) in the 3'UTR of TNFα mRNA, promoting mRNA stability, and thus the MNK proteins have been implicated in the control of TNFα biosynthesis[68], and are therefore implicated in the regulation of inflammatory processes.

The MNK proteins have shown importance in tumour development in a mouse

lymphoma model. Here, introduction of either wild type eIF4E or a phosphomimetic in which serine 209 was mutated to a positively charged aspartic acid (S209D), caused an increase in tumour formation. This effect was negated with the use of the phospho-resistant form in which serine 209 was mutated to alanine (S209A)[69]. This model also identified Mcl-1 as a target for regulation by eIF4E phosphorylation.

A second lymphoma model driven by PTEN knockout has confirmed the importance of the MNKs in tumourigenesis. In this model, conditional knockout of PTEN in T cells leads to the development of lymphoma by approximately 10 weeks, with significant levels of eIF4E phosphorylation found in thymic tumours from these mice. When MNK 1 and 2 double knockout (MNK-DKO) mice were crossed with PTEN null mice to generate mice deficient both in MNK 1 and 2, and PTEN, tumours formed with increased latency, and at smaller size, with no measureable eIF4E phosphorylation in tumours derived from these mice[70].

Equally the significance of phosopho-resistant eIF4E in impairing carcinogenesis has been confirmed in a second study using a pre-clinical prostate cancer model. Here knock-in mice expressing eIF4E S209A were crossed with a conditional knockdown of PTEN in prostate epithelium. The PTEN deficient mice with wild-type eIF4E developed prostate cancers by 5 to 8 months of age, however in mice crossed with eIF4E S209A knock-in, no invasive tumours were found, and pre-invasive prostatic intraepithelial neoplasia was of a lower grade. Of note high levels of eIF4E phosphorylation were seen in the eIF4E wild-type tumours, with no phosphorylation seen in those from eIF4E S209A knock-in mice[71].

Not only has eIF4E been implicated in carcinogenesis; by correlation of expression with outcome in clinical cases, phosphorylated eIF4E is also associated with clinical cancer progression. In a series of 300 patients with non-small cell lung cancer, high levels of eIF4E phosphorylation in the primary tumour was associated with shorter survival[72]. Similarly in prostate cancer higher levels of phosphorylated eIF4E are associated both with increased pathological grading as defined by the Gleason score, and progression from normal prostate tissue, through prostatic intraepithelial neoplasia to invasive malignancy[71].

The inhibition of eIF4E phosphorylation as a potential therapeutic target has been investigated in cell line models. Lung cancer cell lines[20] and a HER2 over-expressing breast cancer line[73] have shown sensitivity to inhibition of proliferation

by inhibition of the MNK proteins. Prostate cancer cell lines with wild type PTEN have also shown sensitivity to inhibition of MNKs with growth inhibition and accumulation of cells in G1 on cell cycle analysis[74]. In addition inhibition of MNKs with CGP57380 in a murine primary CNS lymphoma xenograft model showed a significant reduction in tumour size compared with vehicle control treated animals[75].

The effective regulation of cell signaling pathways not only involves phosphorylation events, but also in order to prevent continuous signaling following activation of a particular pathway, de-phosphorylation must occur. It is thus a balance between phosphorylation by kinases, and de-phosphorylation by phosphatases which regulates any particular signal. The phosphatase responsible for the de-phosphoryaltion of both eIF4E and MNK1 itself has recently been identified as phosphatase PP2A[76]. PP2A is the phosphatase involved in the majority of serine-threonine de-phosphorylation in eukaryotic cells and thus regulates multiple pathways. Rather than being a single molecule it is a trimeric complex consisting of a scaffold and catalytic complex together with a third (B) subunit which provides specificity for localisation of the target and specificity of the substrate[77]. Through a combination of different members of the scaffold, catalytic and B subunits over 75 different holo-enzymes can be formed leading to involvement in a diverse range of cellular functions[78].

PP2A is regulated on a variety of different levels. PP2A can itself be phosphorylated on tyrosine 307, part of the catalytic subunit, by several kinases including the epidermal growth factor receptor, an event which leads to inactivation of phosphatase activity[79]. PP2A can however act as an autophosphatase, and reactivate itself following de-activating phosphorylation. In addition phosphorylation of the B subunit can modify the target specificity of PP2A, providing another layer of regulation[80].

PP2A can undergo additional post-translational modification by methylation of the carboxy group at leucine 309, within the same motif as tysrosine 307 within the C-terminal of the catalytic motif[81]. The role of carboxy methylation appears to be related to the binding of the catalytic subunit for particular B subunits, hence changing the specificity of phosphatase activity[82].

Second messengers, such as the lipid second messenger ceramide have a role in

regulation of PP2A. Ceramide may be formed by the hydrolysis of sphingomyelin in response to stress signaling, for example through tumour necrosis factor α. This subsequently activates ceramide-activated protein phosphatases (CAPPs), which include PP2A, and can result in activation of a variety of signaling molecules, for example protein kinase Cα and c-Jun[83]. Additionally c-Jun may be regulated by the interaction of one of two inhibitors of PP2A, I_1^{PP2A} and I_2^{PP2A}, which increases c-Jun concentration and DNA binding through inhibition of phosphorylation at serine 63[84].

Thus MNK activity is highly regulated in a complex fashion, both through activation via MAPK signaling and phosphorylation, but also through de-phosphorylation both of MNK itself and of its target, eIF4E, by PP2A.

1.4. Regulated Targets of eIF4E phosphorylation

Cyclin D1

Cyclin D1 is a critical regulator of the cell cycle, where it translates mitogenic stimuli into progression through the cell cycle from G1[85]. Upregulation of cyclin D1 through chromosomal translocation and gene amplification has been implicated in several cancers including breast[86] and oesophageal cancer[87] and mantle cell lymphoma[88].

Cyclin D1 is the binding partner of the two cyclin dependent kinases CDK4 and CDK6. Following binding to cyclin D1, CDK4 leads to phosphorylation of retinoblastoma protein (Rb), releasing E2F transcription factors, which up-regulate many genes involved in DNA synthesis and cell cycle progression, including cyclins and cyclin dependent kinases involved in subsequent stages of the cell cycle. The cyclin D/CDK4-6 complex also binds the cell cycle inhibitors p27 and p21, titrating them away from cyclin E/CDK2, facilitating complete phosphorylation of Rb and further progression through the cell cycle (fig 1:6)[89]. Cyclin D1 has additional cell cycle independent functions including regulation of transcription factors with regulatory activity towards both the oestrogen[90] and androgen receptors[91] independent of binding to CDK4.

A variety of approaches have been taken to investigate inhibition of cyclin D1 as an anti-cancer therapy. In pre-clinical models the histone deacetylase inhibitor trichostatin A causes reduced proliferation and cell cycle arrest as a consequence

of cyclin D1 inhibition through regulation of NF-κB[92]. Inhibition of cyclin D1 through enhanced degradation has shown cell cycle arrest in breast and colon cancer cell lines[93]. In the clinical setting, inhibitors of the kinase activity of the cyclin D1/CKD 4 complex have been developed. The cyclin dependent kinase inhibitor flavopiridol is being investigated in a variety of clinical settings and has shown both single agent and combination activity in leukaemia[94]. In most cases it is the cell cycle regulatory function of cyclin D1 that has been investigated with respect to overexpression in cancer, however in a study of breast cancer tissue samples a gene expression profile independent of E2F activity, and consistent with inhibition of the transcription factor C/EBPβ, was seen[95] suggesting the importance of both cell cycle regulatory and transcription control for cyclin D1 in cancer.

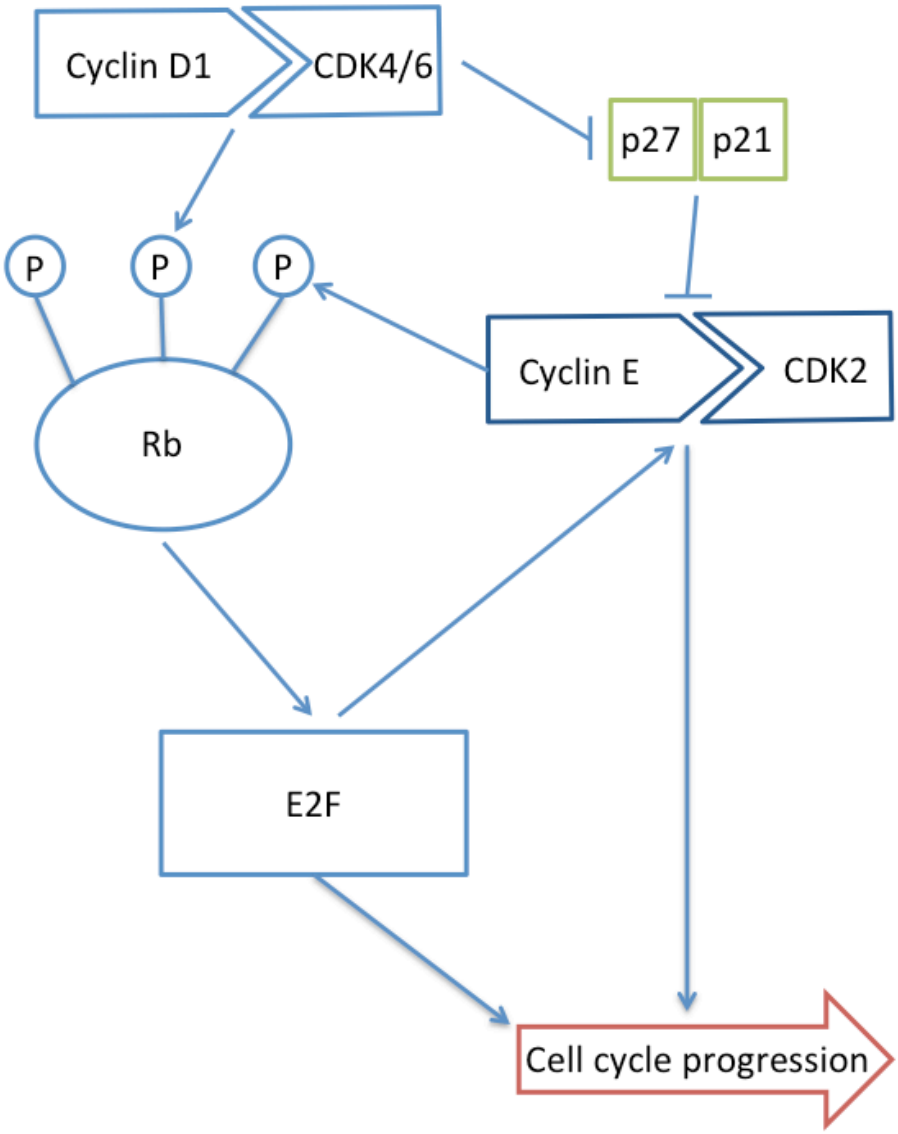

Figure 1:6 Cell cycle control. The role of cyclin D1
Cyclin D1 binds cyclin dependent kinases (CDK) 4 and 6 and phosphorylates retinoblastoma protein (Rb). Phosphorylated Rb releases E2F transcription factors which activate transcription of Cyclin E, as well as other genes involved in cell cycle progression. Cyclin D1/CDK 4/6 bind and inhibit the inhibitors of cyclin E/CDK 2, p27 and p21, resulting in enhanced phosphorylation of Rb.

1.5. Post translational modification of proteins

Although the 20 amino acids that make up proteins provide an almost limitless variety of structure and function, following translation of the genetic code to formation of a protein, additional modifications may be made, further influencing the way in which a given protein may function. Perhaps the most common of these is phosphorylation; the addition of a phosphate group, usually to a tyrosine, serine or threonine amino acid, catalysed by a protein kinase. This addition is frequently involved in the activation or deactivation of enzymatic function and is described in detail below.

Other modifications include the addition of polypeptides to larger proteins targeting them for degradation, such as ubiquitination leading to protein degradation via the proteosome. The addition of other small ubiquitin-like peptides which bind proteins but cause changes in function other than degradation have also been described. One example of this is the small ubiquitin-related modifier proteins (SUMO) of which eIF4E is a known target[96].

Modification of histone proteins by either methylation or acetylation is a mechanism by which post-translational modification of a protein is able to influence transcription. Histone proteins provide the structure for chromatin by acting as a structural support around which the DNA molecule is packaged. Post translational modification of histone proteins results in changes in the conformation of chromatin and as such promoter regions of genes become more or less accessible to transcription factors, either up or down-regulating gene expression. This has been exploited clinically with the use of histone deacetylase (HDAC) inhibitors, which are able to induce cell cycle arrest and apoptosis in cancer cell models. For example the HDAC inhibitor vorinostat has shown clinical activity in the treatment of advanced cutaneous T cell lymphoma[97].

Prenylation involves the addition of a hydrophobic prenyl moiety to the C terminal cystein of a protein and affects its location via either interaction with cell lipid membranes, or protein-protein interactions. A notable example is Ras, part of the MAPK and AKT signalling pathways, which must be membrane bound for oncogenic activity. Ras undergoes prenylation by an enzyme farnesyl-transferase for which inhibitors have been generated, and are currently in clinical testing[98].

Over the last 10 years, small cell permeable molecules that are able to selectively target protein kinases have moved from laboratory tools, to having routine use in clinical practice.

There are over 500 protein kinases in the human proteome[99]. Many of these are membrane bound receptor tyrosine kinases, however others are soluble proteins which form signalling intermediates in the transduction of extracellular signals to a wide range of intracellular changes. All kinases belong to a superfamily of proteins with a common kinase catalytic domain. Within this domain have been described 12 smaller subdomains which contain sequences of conserved amino-acids and are likely representative of the common function of these enzymes. The kinases have been further classified according to common structural and functional features. An initial classification by Hanks et al according to amino acid sequence homology established four groups of proteins which were named AGC (after constituent families protein kinase A, G and C), CaMK (calcium/calmodulin regulated kinases), CMGC (containing cyclin-dependent kinases, MAP kinases, glycogen synthase 3, and casein kinases) and PTK ('conventional' protein-tyrosine kinases)[100]. This classification was updated in 2003 following an extensive search of the human genome for sequences with homology to the eukaryotic protein kinase domain. Four additional groups were added to give a total of ten. These were as follows: Tyrosine kinases, Tyrosine kinase-like, AGC, CAMK, CK1 (casein kinase 1), CMGC, STE (MAP kinase cascade kinases, homologs of yeast Ste kinases), RGC (receptor guanylate cyclase) and Atypical[99].

Protein kinases catalyse the addition of a phosphate group to other proteins within the cell through the hydrolysis of adenosine triphosphate (ATP) to adenosine diphosphate, and the addition of a phosphate group at the hydroxyl moiety of tyrosine, serine and threonine amino acids. There are two broad groups based on the amino acid residue targeted for phosphorylation, with the majority of kinases either targeting tyrosine, or serine/threonine, and a minority able to target all three residues. This post-translational modification of the target gives rise to changes in activity, most commonly as a result of conformational change, and may result in enzymatic activation of the target[53], inhibition of the target[101], changes in distribution[102], or destruction of the target molecule through targeting for degradation[103].

The basic structure of protein kinases is conserved such that each has an ATP binding pocket formed by the association of N and C terminal domains. The crystal structure of this catalytic domain was first identified during structural analysis of cyclic adenosine monophosphate-dependent protein kinase[104]. Within this cleft are conserved amino acid sequences for nucleotide binding, protein binding and for the catalytic activity of the kinase[105].

The activity of protein kinases is controlled via conformational change, often brought about by phosphorylation of additional sites within the protein molecule. The activation loop is typically located at the mouth of the catalytic domain, defined as spanning the region between two conserved sequences DFG and APE (using single letter amino acid notation). This loop can inhibit ATP and substrate binding when in its inactive conformation, however phosphorylation of the loop results in either ATP or the peptide substrate gaining access to the catalytic domain, and therefore increased function of the kinase[106].

Activation of protein kinases may involve interaction with other proteins, and as such many kinases contain putative protein-protein interaction domains. Examples of these include the Src homology 2 (SH2)[107] and Src homology 3 (SH3)[108] domains. These represent consensus sequences of amino acids which allow binding to phosphorylated tyrosine residues and proline-rich motifs respectively on interacting proteins which may result in activation or inactivation of the kinase through interaction with the activation loop as described above. Alternatively these sites may represent interactions within the kinase molecule such that the kinase function is altered by conformational changes brought about by association between phosphorylated residues within the molecule and SH2 domains.

Crystal structure of the kinase domains of both MNK1[105] and MNK2[109] have been studied, following expression in E.coli and purification. The kinase fragments were shown to have kinase activity by phosphorylating eIF4E in response to ERK in vitro. The characteristic bilobar kinase structure was identified. The secondary structure of the N-terminal lobe consists of predominantly β strands and is responsible for ATP binding. It contains a Glycine rich loop previously shown to interact with non-transferable phosphates within the ATP nucleotide. The majority of the secondary structure of the C-terminal lobe is α helices. It is here that the peptide substrate binds and the elements required for phosphate transfer are

found. A magnesium binding loop, catalytic loop and activating loop are located in this region.

The activating loop in the MNK proteins is extended by the insertion of additional amino-acids to the two α helices EF and F. This results in a stable inhibitory conformation of the activating loop in the non-phosphorylated state, which crosses the kinase cleft and interacts with the αC helix of the N terminal lobe. Interaction of phenylalanine (Phe) 230 of the activation loop, with Phe 192 of the DFD motif in the magnesium loop results in Phe 192 occupying the ATP-binding pocket and inhibiting ATP binding. Interaction of arginine residues in helix αC and the activation loop stabilise the inhibitory conformation. When activating phosphorylation by ERK or p38 MAPK occurs, the phosphorylated residues in the activation loop engage with the RD pocket, also formed by arginine residues in the αC helix and a further arginine upstream of the catalytic loop. This releases the activating loop from the N terminal lobe, freeing up the ATP binding site, and allowing the substrate to access the catalytic cleft.

1.6. Inhibition of protein kinases with small molecules

The identification of a wide variety of protein kinases as oncogenes, with activating mutations found in many cancers, has led to interest in these as therapeutic targets.

An early example of a naturally occurring kinase inhibitor is staurosporine, a natural product produced by the actinomycete Streptomyces identified during a screen for microbial alkaloids[110]. Molecular characterisation identified staurosporine as an indolocarbazole compound with chemical synthesis achieved in 1996[111]. During further investigation, staurosporine and its derivatives were found to be protein kinase inhibitors, initially as potent inhibitors of protein kinase C[112] and v-src[113] kinase, with anti-tumour properties in animal models[114], and subsequently as non-specific inhibitors of many other kinases[115].

Identification of the crystal structure of staurosporine bound to the kinase domain of protein kinase C showed the tight binding of staurosporine to the adenosine binding pocket, and identified many of the interactions between the inhibitor and the surrounding residues of the kinase[116].

Knowledge of the crystal structure of a variety of protein kinases, in many cases bound to inhibitors has allowed the generation of pharmacophore models in order to rationalise the structure of compounds developed through screening programmes[117]. Several classes of compound with activity as protein kinase inhibitors have thus been identified and modified to induce specificity for particular kinase molecules.

CIBA Geigy developed a kinase inhibitor screening programme, and identified CGP57148, a 2-phenylaminopyrimidine with activity against the Abl protein kinase and platelet-derived growth factor[118]. This compound has growth inhibitory effects on cells containing the BCR-Abl fusion protein characteristic of chromic myeloid leukaemia (CML) [119]. Clinical trials of what by then was known as imatinib showed dramatic effects in CML. By switching off signalling through the fusion protein, responses were seen in 95% of patients treated with imatinib with clearance of the fusion protein by cytogenetic analysis in 74%[120].

One major success of imatinib has been its specificity for a small number of protein kinases, a feature that has been difficult to achieve with other agents. One reason for this is likely to be the binding of imatinib to the inactive form of the kinase. The active, or open form of many kinases results in a similar conformation of the catalytic cleft[121], making the design of molecules to specifically recognise a particular kinase more difficult. When in the inactive form the conformation is much more specific to an individual protein and as such small molecules can be tailored to an individual kinase domain.

A subset of patients has primary resistance to therapy with imatinib, or develops resistance during therapy. It has become apparent that a single amino acid mutation can result in a conformational change, preventing binding of the imatinib molecule to the catalytic cleft, for example by disruption of the inhibitory conformation[122]. As a consequence alternative compounds which bind the active conformation have been developed to target such resistant cases[123].

CGP57380 (4-amino-3-(p-fluorophenylamino)pyrazolo[3,4-d]pyrimidine) was identified in 2001 and described as a specific inhibitor of MNK1[60]. The compound showed inhibition of MNK1 kinase activity with both in vitro kinase assays and cellular kinase activity with an IC_{50} of 2.2 μM and 3 μM respectively. It was found to have no inhibitory activity on other kinases including p38, JNK1, ERK1 and 2,

protein kinase C and Src-like kinases. Additional analysis of the specificity of CGP57380 has shown both MNK1 and MNK2 inhibition with some inhibitory activity towards MKK1, ERK2, RSK1 and p38 MAPKα, but at significantly higher concentrations than those required for inhibition of MNK1/MNK2[68]. Questions have been raised however as to how specific CGP57380 is in a broader kinase screen. When tested against a panel of 80 protein kinases, three other kinases were identified with inhibition at similar concentrations to MNK1, namely MAP Kinase Kinase 1 (MKK1), Casein Kinase 1 (CK1) and Brain selective kinase 2 (BRSK2)[124]. Although some questions remain as to the specificity of CGP57380 as an inhibitor of the MNK proteins, it has been investigated in several models to demonstrate the importance of eIF4E phosphorylation in cancer cell survival. A lung cancer cell line model used CGP57380 at up to 5 μM to demonstrate modest inhibition of cell proliferation, with enhanced effects for the addition of CGP57380 to rapamycin[20]. Similarly a single HER2 overexpressing breast cancer cell line showed growth inhibition in a long-term colony assay in a dose dependent fashion with CGP57380 up to 50 μM[73].

1.7. Cancer models for eIF4E regulation

As HER2 signalling may be mediated via both the mTOR and MAPK signalling pathways then HER2 overexpressing breast cancer cells may be particularly sensitive to inhibition of the MNK proteins.

mTOR inhibition has now become part of routine care for certain patients with advanced renal cancer, however this is not effective for all. The interesting cell line data suggesting an increase in eIF4E phosphorylation in response to inhibition of the MNK proteins[20] may therefore be particularly relevant to this patient cohort.

Breast Cancer

Breast cancer represents a major health problem. As the commonest malignancy in females, and the third most common malignancy overall, more than 40,000 cases are diagnosed annually in the United Kingdom.

Breast cancer has historically been at the forefront of biological research with an advanced understanding of the molecular pathogenesis underlying what is increasingly seen as a heterogeneous disease. The concept of therapy targeted at specific molecular pathways has been, perhaps unknowingly, in existence for over a century, since it was first discovered that performing an oophorectomy in a case

of advanced breast cancer could lead to regression of metastatic disease[125]. Since then it has become apparent that it is in fact a subset of breast cancers over-expressing the oestrogen receptor that respond to oestrogen deprivation, and a variety of therapeutic manoeuvres have been designed to achieve this[126].

The 1980s and 1990s saw the identification of the *ERBB2* oncogene, and its protein product the HER2 cell surface receptor tyrosine kinase[127]. This member of the EGFR family is overexpressed due to gene amplification in around 20% of breast cancers and accounts for a more aggressive pattern of disease with a worse prognosis[128]. The production of a therapeutic monoclonal antibody targeting the external domain of the HER2 receptor (trastuzumab) has significantly changed the outlook for patients with this subtype of breast cancer, however as with other subtypes, in the face of metastatic disease breast cancer remains almost universally fatal[129].

The advent of high throughput gene expression profiling has allowed further work to be carried out in characterising breast cancer and defining prognostic groups by their pattern of gene expression. Profiling of a number of breast cancers has defined signatures for 5 groups of patients, namely normal breast–like, luminal A, luminal B, basal and HER2[130]. These groups differ in both their genetic and molecular signatures. Normal breast-like tumours are characterised on the basis of their similarity to normal breast ductal and adipose tissue. Luminal tumours have expression patterns similar to cells of the breast duct luminal epithelium, and typically have high expression of the oestrogen receptor (*ER*) gene, with a further subclassification into A and B partly reflecting the level of *ER* expression, p53 mutation status and other luminal specific genes. Those classified as basal have similar expression patterns to the basal epithelium with low expression of *ER* and non-amplified *ERBB2*, and HER2 tumours have high levels of *ERBB2* expression, with low levels of *ER*. Subsequent correlation of this genetic data with clinical outcome has revealed distinct patterns of survival dependent on the gene expression grouping[131].

In order to allow clinical application of these subgroups attempts have been made to define these groups on the basis of protein expression, allowing conventional diagnostic immunohistochemical (IHC) tests to be used to classify tumours. In this way luminal cases are typically defined by high levels of ER on IHC with absence of HER2 over-expression. The HER2 group have consistently high levels of HER2

overexpression, low levels of ER and are typically of a high nuclear grade. Basal-like tumours include all tumours of the 'triple negative' class with absent ER and progesterone receptor (PR) staining on IHC and absence of HER2 over-expression. These tumours are almost always of high nuclear grade, and respond poorly to conventional chemotherapy[132].

In summary a great deal of information is available on the influence of a variety of molecular factors on breast cancer outcomes. Cell line models have been integrated into these classification systems such that the influence of specific pathways can be modeled on the clinical spectrum of breast cancers[133].

Renal Cancer

Renal Cancer represents the 8th most common malignancy in the United Kingdom, and with just under 8000 new cases annually it represents 3% of cancer diagnoses.

Currently renal cancers are distinguished by light microscopic appearance with three major subtypes of malignant tumour derived from the tubular epithelium of the proximal convoluted tubule, and a fourth derived from the collecting duct system[134]. The most common subtype representing 75% of cases is conventional or clear cell renal cell carcinoma, so described due to the presence of a majority of cells containing clear cytoplasm. Papillary renal carcinoma represents 10-15% of cases with the majority of cells forming papillary architecture. Chromophobe tumours account of around 5% of cases and consist of cells which have condensed cytoplasm around the nucleus and vary in size. Finally collecting duct carcinomas represent less than 1% of renal cancers. Although these tumours vary in histological appearance they typically consist of cellular channels lined by abnormal epithelium. All of the above tumours may consist of areas of sarcomatoid appearance which is regarded as high grade tumour of the histological subtype of origin, rather than a distinct subtype of its own.

Different genetic abnormalities have been associated with each different histological subtype, and as a greater understanding of the molecular defects underlying these tumours is achieved, so more effective therapies have been developed.

Clear cell renal cell carcinomas are commonly associated with loss of material from chromosome 3p. The von Hippel-Lindau (VHL) tumour suppressor gene was

identified as the germ line mutation in the von Hippel-Lindau cancer syndrome in which patients develop multiple bilateral clear cell renal tumours from a young age, as well as haemangioblastomas and tumours of the central nervous system, adrenals, pancreas and epididymis[135]. The VHL gene is located at chromosome 3p25 with frequent chromosomal loss in sporadic clear cell renal cancer[136] . Mutations in the VHL gene have subsequently been identified in up to 60%[137] of patients with sporadic clear cell kidney cancer, with up to a further 20% showing promoter hypermethylation[138]. The deranged cellular signaling which occurs as a consequence is the target for several new therapies for advanced renal cancer. Under normoxic conditions VHL protein acts as a tumour suppressor by regulating HIFα transcription factors (HIF1α , HIF2α, HIF3α) in response to oxygen availability[139]. HIFα contains an oxygen degradation domain (ODD)[140] where a proline residue can undergo hydroxylation, catalysed by HIF proline hydroxylase[141]. Hydroxylated proline is recognised by a hydroxyproline binding pocket in VHL protein[142] as part of an E3 ubiquitin ligase complex together with Cul2, elongin B, elongin C[143] and Rbx1[144]. Under hypoxic conditions HIFα is no longer proline hydroxylated and therefore does not bind to VHL and accumulates. When VHL is non-functioning or absent, either due to chromosomal loss, mutation, or hypermethylation, HIFα is no longer degraded and accumulates under normoxic conditions. HIFα is then able to bind one of the HIFβ family to form an active transcription factor. This results in up-regulation of genes normally associated with hypoxic stress, including *VEGF,* platelet derived growth factor β (*PDGF-B),* transforming growth factor α (*TGF-*α*),* glucose transporter 1 (*Glut 1*), carbonic anhydrase IX and erythropoietin[145] (fig 1:7).

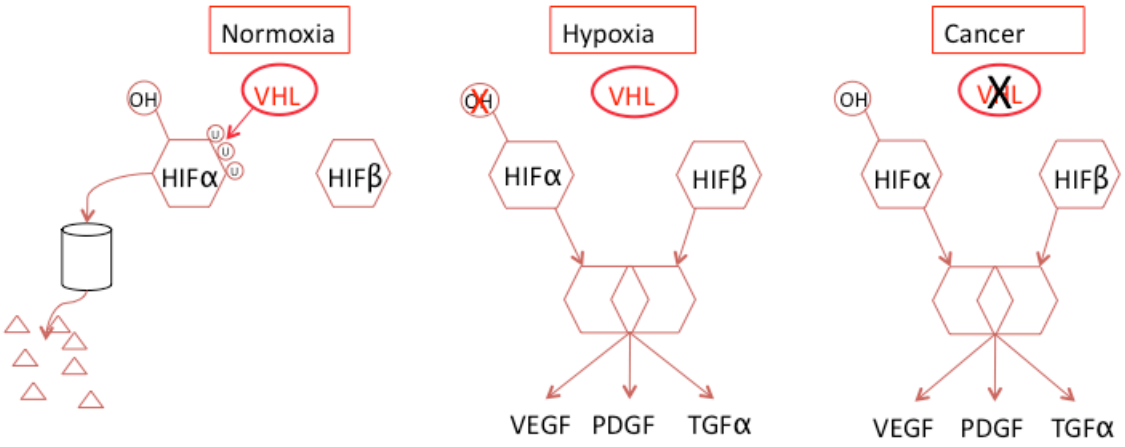

Figure 1:7 HIF regulation by VHL
Under normoxic conditions HIFα is hydroxylated, and thus targeted for ubiquitination by VHL and degraded within the proteosome. Under hypoxic conditions HIFα is no longer hydroxylated and therefore not targeted by VHL. HIFα accumulates and binds HIFβ forming a transcription factor and upregulating target genes including vascular endothelial growth factor, platelet derived growth factor and transforming growth factor alpha. In clear cell renal cancers with VHL inactivation a pseudo-hypoxic phenotype is seen.

Study of a familial syndrome of multiple bilateral papillary renal cancers (hereditary papillary renal cancer carcinoma HRPC) has led to the identification of the MET oncogene as critical to the development of papillary renal cancers. Papillary tumours are characterised in cytogenetic studies by trisomies including chromosome 7. Activating mutations in the MET oncogene on chromosome 7 have been identified both in families with HRPC, and in sporadic cases of multiple papillary renal cancers[146,147]. Although MET mutations have not been identified in all cases studied, the ligand of MET, hepatocyte growth factor/scatter factor (HGF/SF) is also located on chromosome 7, as are several other cytokines known to increase the expression of MET[148]. MET is a receptor tyrosine kinase which undergoes dimerisation and phosphorylation in response to binding of its ligand HGF/SF, and subsequent signaling through the ERK MAPK cascade[149]. This results in an increase in cell motility, invasiveness and proliferation[150].

Early stage kidney cancer confined to a single kidney is conventionally treated by surgical resection, although organ preserving techniques such as partial nephrectomy, or ablative techniques such as cryoablation and radiofrequency ablation, are increasingly used. The outlook for early stage disease following surgical resection is stage dependent. Resected disease can be stratified as to recurrence risk using the Leibovich pathological scoring system[151], which takes into account nuclear grade, degree of histologically defined necrosis, tumour size, and tumour and nodal stage. Using this system patients may be stratified to good prognosis with a 97% 5 year metastasis free survival, compared with a poor risk group with 31.2% 5 year metastasis free survival. For advanced renal cancer, however the outlook is poor. Historically survival has been short with a median survival of 6 months in untreated patients. The only treatment option until recently was immunotherapy with interferon, with or without interleukin 2. Response rates were low with minimal effect on survival[152].

The advent of VEGF targeted therapy has however made a significant difference to the management of advanced renal cancer. The multi-targeted kinase inhibitors sunitinib and sorafanib have both shown significant activity in advanced renal cancer in the first and second line respectively. These agents share target specificity towards VEGF receptors , PDGF receptors, and KIT, with sorafenib additionally targeting Raf and RET kinases. The median survival following

treatment with sunitinib is 26 months[153]. Similar results were seen with the combination of bevacizumab, a VEGF targeted monoclonal antibody, in combination with interferon[154]. The two mTOR inhibitors temsirolimus and everolimus have also shown activity and are now licensed for use in advanced renal cancer. The phase III trial of temsirolimus specifically targeted a poor prognosis group of patients and although it only showed a median survival of 11 months, this was significantly better than 7 months seen in the interferon treated control group[17]. Everolimus is licensed in the second line after failure of tyrosine kinase inhibitor therapy having shown an improvement in progression free survival of an additional 2 months over placebo control. At the time of publication of the trial data in 2009 the median survival for the placebo group was 8.8 months and had not been reached in the everolimus group[18].

2. Aims

Although significant advances in the management of advanced malignancies have been made in recent decades, even in the face of apparent curative surgery patients with early stages of disease may still relapse, and in the setting of advanced disease cures remain elusive for the majority of solid tumours. An imperative therefore exists both for a greater understanding of the biology underlying this disease, and for novel therapeutic options.

The role of the MNK kinases in the transforming ability of cells has become apparent. It is clear that eIF4E is overexpressed in some solid tumours with enhanced expression being associated with inferior prognosis. Increasing data suggest that inhibition of eIF4E phosphorylation may be a valid therapeutic target in certain cancers.

The aims of this project are four fold:

Firstly to establish the effect of inhibition of eIF4E phosphorylation on the proliferation and survival of breast and kidney cancer cell lines. Limited data suggest that inhibition of the MNK proteins inhibits the proliferation of HER2 over-expressing breast cancer cell lines, however this project aims to further investigate this effect in the wider context of the full spectrum of phenotypes of breast cancer. The effects of inhibition of eIF4E phosphorylation have not previously been investigated in renal cancer, however HIF has been established both as significant in the pathogenesis of the majority of clear cell renal cancers and as a target of eIF4E.

Secondly the mechanisms underlying any effect on the proliferation or survival of these cancer cell lines will be investigated. In particular assays to assess the relative contribution of cell cycle control and induction of apoptosis will be performed.

Thirdly the specificity of the chemical inhibitor of the MNK kinases, CGP57380, will be investigated by using alternative strategies to inhibit eIF4E phosphorylation.

Finally the molecular mechanisms underlying the transcriptional and translational regulation of targets of eIF4E will be investigated, both by investigating the effects

on established targets of eIF4E phosphorylation in breast and kidney cancer cell lines, and identifying novel targets.

3. Materials and Methods

3.1. Materials

Solutions and Buffers

Phosphate Buffered Saline (30X) (PBS)	NaCl 600 g
	KCl 15 g
	Na2HPO4 108 g
	KH2PO4 18 g
	Water to 2.5 l
	pH 7.4
Tris Buffered Saline (10X) (TBS)	Tris Base 24.2 g
	NaCl 80 g
	Water to 1 l
	pH 7.6
Urea Lysis Buffer	8 M Urea
	10% Triton X-100
	5 M NaCl
	1 M HEPES pH 7.6
	1 M DTT (in 0.01M NaAc pH 5.2)

Polyacrylamide Gels

Running Gel (12%)	40% Acrylamide-Bis (29:1)	3 ml
	Water	5.35 ml
	1.5 M Tris pH 8.8	2.5 ml
	10% SDS	100 ml
	10% APS	100 ml
	TEMED	5 ml
Stacking Gel	40% Acrylamide-Bis (29:1)	3 ml
	Water	6.35 ml
	1.5 M Tris pH 8.8	2.5 ml
	10% SDS	100 ml
	10% APS	100 ml
	TEMED	10 ml
SDS Sample Loading Buffer (4X)	EDTA 10 mM	
	SDS 4% (w/v)	
	Glycerol 20% (w/v)	
	Tris pH 6.8 20 mM	
	Bromophenol Blue Dye to colour	
	DTT 200 mM	

PAGE Running Buffer (10X stock)	Tris Base	30 g
	Glycine	144 g
	SDS	10 g
	Water	to 1 l
TG Buffer (10X stock)	Tris Base	29 g
	Glycine	145 g
	Water	to 1 l
Propidium Iodide staining solution	PBS	10 ml
	Triton X 100	0.2%
	RNAse A	2 mg
	Propidium Iodide 1mg/ml	20 ml
Annexin V binding buffer (10X)	0.1 M Hepes/NaOH (pH 7.4)	
	1.4 M NaCl	
	25 mM $CaCl_2$	
MPG Buffer	1 M NaCl	
	10 mM EDTA	
	100 mM Tris-Cl pH 7.4	
M^7GTP pulldown extraction buffer	25 mM Tris-Cl pH 7.6	
	50 mM β-glycerophosphate	
	0.2 mM EDTA	
	50 mM KCl	
Immediately before use added	20 X Protease inhibitor mix (Roche)	
	1% Triton X 100	
	0.5 mM $NaVO_3$	
	50 mM NaF	
	100 mM DDT	

Cell Culture

The breast cancer cell lines, MCF7, T47D, ZR75.1, SKBr3, BT474 and MDA-MB-231 were from Dr Blaydes laboratory. Cells were cultured in complete Dulbecco's Modified Eagle Medium (DMEM) consisting of DMEM (Invitrogen) supplemented by Foetal Calf Serum (10% v/v Autogen Bioclear), penicillin G/streptomycin (100 μg/ml), and L-glutamine (2 mM). Cells were maintained in exponential growth at 37° in a CO_2 controlled incubator at 10% (Hera cell, Haraeus).

The renal cancer cell lines, Caki2, 786-O, 769-P, A498 and ACHN were a gift from Dr Sahota. A498 and ACHN cells were cultured in Eagle's minimal essential medium (EMEM, Lonza), 37° 5% CO_2. Caki-2 cells were cultured in McCoy's 5a medium (Lonza), 37° 10% CO_2. 786-O and 769-P cell lines were cultured in RPMI-1640 (Lonza) 37° 5% CO_2. All medium was supplemented with foetal calf serum, penicillin G/streptomycin and L-glutamine as above.

siRNA

The following siRNA oligonucleotides were obtained from Ambion

MNK1 (s16321)

sense	GGAGUAGGGUGUUUCGAGA
antisense	UCUCGAAACACCCUACUCC

MNK1 (s16319)

sense	GCCCUUGACUUCCUGCAUA
antisense	UAUGCAGGAAGUCAAGGGC

MNK2 (s6095)

sense	GCCUUGGACUUUCUGCAU
antisense	UAUGCAGAAAGUCCAAGGC

MNK2 (s6094)

sense	GCAGCGGCAUCAAACUCAA
antisense	UUGAGUUUGAUGCCGCUGC

Antibodies

The following antibodies were used for immunoblotting at dilutions as indicated. Antibodies were diluted as indicated in 3% fat free milk / 0.1% Tween 20 / TBS except for phospho-eIF4E which was diluted in 5% bovine serum albumin (fraction V) / 0.1% Tween 20 / TBS

Target	**Species**	**Manufacturer**	**Catalogue No**	**Concentration**
Primary antibodies				
eIF4E	Rabbit polyclonal	Cell Signalling Technology	9742	1:2000
Phospho eIF4E (serine 209)	Rabbit polyclonal	Cell Signalling Technology	9741	1:400
MNK1	Rabbit polyclonal	Cell Signalling Technology	2196	1:2000
MNK2	Rabbit polyclonal	Santa Cruz Biotechnology	Sc-28781	1:500
Cyclin D1	Mouse monoclonal (Ab-3)	Calbiochem	CC12	1:500
Mcl-1	Rabbit polyclonal	Santa Cruz Biotechnology	SC819	1:500
Actin	Rabbit polyclonal	Sigma	A5060	1:3000
Secondary antibodies (Horse radish peroxidase (HRP) conjugated)				
anti rabbit	Goat	Dako	PO448	1:2000
Anti mouse	Sheep	Amersham Bioscience		1:2000

Table 3:1 Antibodies used for immunoblotting

Taqman Gene Expression Assays

The following Taqman gene expression assays were obtained from Applied Biosystems

Cyclin D1 (CCND1) Hs00277039_m1 NM_053056.2 (FAM)

GAPDH 4326317E NM_002046.3 (VIC)

3.2. Methods

3.2.1. Cell Biology

Cell Treatments

Cells were plated to 60mm dishes at 0.5 X 10^6 cells per dish in 3 ml complete medium. At 24 h the medium was removed and the inhibitor of the MNK proteins, CGP57380 (Tocris bioscience) added at varying concentrations with a final concentration of 0.5% v/v DMSO vehicle, before returning the medium to the cells. At varying time points cells were rinsed once in PBS before being scraped, centrifuged at 1000*g* for 4 minutes at 4° and the pellets snap frozen in liquid nitrogen.

MTS Proliferation Assay

The MTS assay involves the conversion of a soluble tetrazolium compound 3-(4,5-dimethylthiazol-2-yl)-5-(3-carboxymethoxyphenyl)-2-(-4-sulfophenyl)-2H-tetrazolium inner salt (MTS) to a water soluble formazan compound. This results in a colour change, with the Formosan compound absorbing light at 490 nm. This colour change can be used as a surrogate for cellular proliferation. The reaction relies on the reducing capacity of intracellular NADH in metabolically active cells. Cells were plated in triplicate with serial dilutions from 8000 to 500 cells per well in 96 well plates in 120 μl medium. 24 h later 110 μl medium was removed from each well and pooled. CGP57380 (Tocris) was added to give a final concentration of 20 μM and 0.5% v/v DMSO vehicle, and 100 μl was added back to each well. This was repeated on the same plate for CGP57380 concentrations of 10 μM and 5 μM, as well as for 0.5% DMSO control. After 72 h incubation 20 μl MTS reagent (CellTiter 96Aqueous One Solution, Promega) was added to each well and the plates incubated at 37° C for two h. Absorbance at 490 nm was measured on a Varioskan Flash plate reader (Thermo Electron Corporation).

CyQuant Proliferation assay

A second assay of cell proliferation was also used. The CyQuant Direct Cell Proliferation Assay (Invitrogen) uses a fluorescent nuclear stain as a surrogate for

cell number. A second masking dye only permeable to dead cells with compromised cell membrane integrity prevents dead cells from being counted. To assess the ability of this assay to assess cell number, cells were plated at increasing number in triplicate wells of 96 well plates in 100 μl medium. 24 h later cell number was assayed as follows.

The following were combined in a 15 ml tube:

11.7 ml PBS

48 μl CyQuant Direct nucleic acid stain

240 μl CyQuant Direct background suppressor I

100 μl of the above mix was added to each well in the 96 well plate and incubated for 1 h at 37°C for 1h. Fluorescence was then measured on a bottom reading Varioskan Flash plate reader (Thermo Electron Corporation) using an excitation wave length of 480 nm and emission 535nm. Results were plotted as fluorescence intensity against cell number (Fig 2:2).

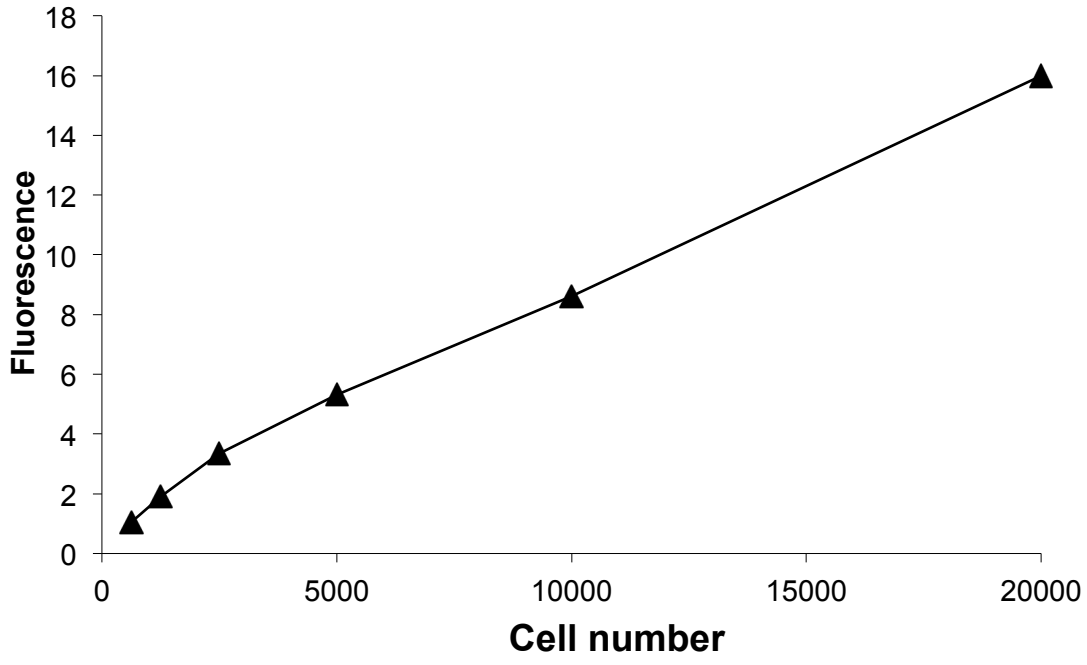

Figure 3:1 Validation of CyQuant proliferation assay
A498 cells were plated at the cell numbers as shown in 100 μl medium in 96 well plates. 24 h later proliferation was assayed using the CyQuant Direct assay. Results represent mean of triplicate wells.

For proliferation experiments 1000 cells per well were plated in 120 μl medium in 96 well plates. 24 h later the medium was removed and CGP57380 added to give a final concentration of 20 μM in 0.5% DMSO. 100 μl was returned to each well. This was repeated for treatments at a final concentration of 10 μM, 5 μM and 0.5% DMSO vehicle control. Cells were incubated at 37° C for 72 h and proliferation assayed as described above.

Live Cell Imaging

Cells were plated in 24 well plates at 4000 cells per well in 1 ml medium. At 24 h the medium was removed and CGP57380 added to give a final concentration of 20 μM in 0.5% DMSO, or 0.5% DMSO alone as a vehicle control. The medium was returned to the cells which were incubated for a further 24 h. Time-lapse photography was used to obtain 20X images at fifteen-minute intervals for a further twenty-four hours using an Olympus IX81 microscope with CO_2 and temperature controlled environmental chamber, controlled by SIS Cell P software. Three fields were imaged for each well at each time point. The images were used to count cell numbers at the beginning and end of the time course. The number of apoptotic and mitotic events at each time point were identified, and the total number over the time course expressed as a fraction of the starting cell number (fig 2:3).

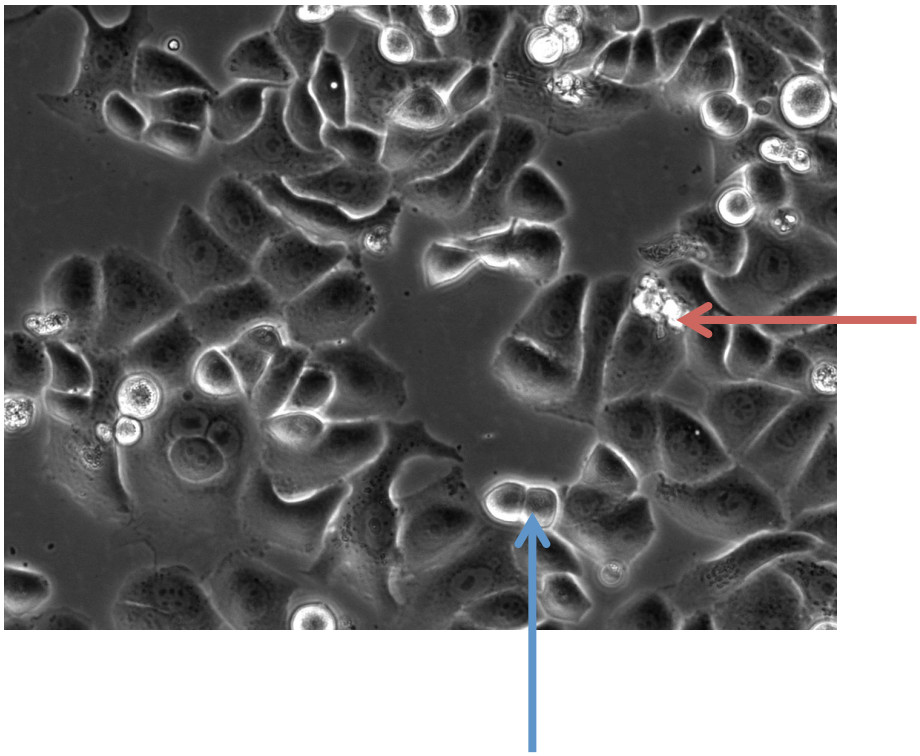

Figure 3:2 Live cell imaging of SKBr3 cells
A photomicrograph at 20 X magnification of SKBr3 cells following treatment with CGP57380 at 20 μM for 24 h and then undergoing time lapse microscopy. Image indicates a cell undergoing mitosis (blue arrow) and apoptosis (red arrow).

Cell Cycle Analysis

Cells were plated in 60mm dishes with 25 x 10^4 cells per dish in 2 ml medium. 24 hours after plating the medium was removed and CGP57380 added to give a final concentration of 20 μM or DMSO vehicle control at 0.5% v/v. The medium was returned and the cells incubated for 72 h. Cells were harvested by trypsinisation with retention of the original medium and washes. Cell suspensions were centrifuged at 1000*g* for 4 min and the supernatant aspirated. The cell pellet was resuspended in 1 ml ice cold PBS and the suspension once again centrifuged at 1000*g* for 4 minutes with no braking. Again the supernatant was aspirated and the cells suspended in 300 μl ice cold PBS. 700 μl ice cold ethanol was then added dropwise while gently vortexing the cell suspension. The cells were fixed for at least 2 h at 4° C. They were then centrifuged at 1000*g* for 4 min, washed once in PBS and then resuspended in propidium iodide staining solution and maintained at room temperature for 30 min. Analysis was performed using a FACScaliber (Becton Dickinson).

siRNA Transfection

Cells were plated to 60mm dishes at 0.5 X 10^6 cells per dish in 2.4 ml complete medium on the day prior to transfection.

The transfection mix was created as follows: siRNA was added to 0.6 ml Optimem serum free medium (Invitrogen) at a volume to give the required final concentration of siRNA in 3 ml medium. 20 μl of Interferin reagent (Polyplus transfection) was added and the sample mixed by vortex. Following ten minutes incubation at room temperature the transfection mix was added dropwise to cells. Fresh medium was applied four hours later.

siRNA Duplex	**Stock concentration**	**Quantity added to 0.6 ml optimem for final concentration:**	
		50 nM	**100 nM**
MNK1 (i)	20 mM	3.75 μl	3.75 μl
MNK1 (ii)	20 mM		3.75 μl
MNK2 (i)	20 mM	3.75 μl	3.75 μl
MNK2 (ii)	20 mM		3.75 μl

Table 3:2 Transfection mix for siRNA transfections.

Apoptosis assay using Annexin V and propidium iodide (PI) staining

Cells were plated in 6 well plates at 0.2 x 10^6 cells per well in 2 ml medium. 24 h after plating cells were treated with CGP57380 at a final concentration of 20 μM in 0.5% DMSO or 0.5% DMSO vehicle control alone. Cells were assayed for apoptosis at 8 h and 24 h time points using the following technique.

Cells were trypsinised with all washes retained and centrifuged at 1000*g* for 4 min at 4° C. The medium was aspirated and cells washed twice in 1 ml cold PBS before being resuspended in 0.5 ml 1 X Annexin V binding buffer. 1.25 μl FITC conjugated Annexin V and 2.5 μl propidium iodide (1mg/ml) was added to each sample and incubated for 15 min at room temperature in the dark. Cells were analysed for Annexin V expression (FL1) and PI staining (FL2) using a FACScaliber (Becton Dickinson).

Fluorescence microscopy

Two coverslips cleaned with 100% ethanol were placed in each well of a 6 well plate. Cells were plated to 6 well plates at 0.1 x 10^6 cells in 2 ml medium. 24 h later the medium was removed from each well and the wells washed with cold PBS. Cells were fixed in the wells with 1 ml per well 4% paraformaldehyde in PBS for 15 min. A further wash with PBS was performed and the paraformaldehyde quenched with 1 ml per well 100 mM glycine for 10 min. Following a further wash with PBS cells were permeabilised with 1 ml per well 0.2% Triton-X/PBS for 10 min. 50 μl 1 μg/μl 4',6-diamidino-2-phenylindole (DAPI) was added to each coverslip which were incubated in the dark for 10 min. Coverslips were washed twice with PBS and once with water before being mounted to microscope slides with fluorescence mounting solution (Dako). Slides were kept for at least 12h at 4 °C before being visualised with a fluorescence microscope (Zeiss Axiovert 200). Images were captured using an Orca-ER digital camera (Hamamatsu) and Openlab 3.5.1 software (Improvision).

3.2.2. Protein analysis

Immunoblotting

Total Protein Extraction

Cell pellets were lysed with the addition of an equal volume of urea lysis buffer to frozen pellet on ice. The pellet was vortexed to disperse, and incubated on ice for 15 minutes. The lysate underwent centrifugation for 10 minutes at 10500*g* at 4° C and the supernatant was aspirated and kept on ice. Protein quantification was performed using the Bio-Rad Bradford reagent and normalised to a known standard curve. Lysate concentrations were normalised to 20 mg/15 ml in SDS sample loading buffer.

SDS PAGE and Protein Transfer

Lysates were heated to 95° C for 4 min before being loaded onto a 12% polyacrylamide gel. Proteins were separated by electrophoresis using a Bio-Rad Mini-gel apparatus with SDS running buffer at 150 v.

Proteins were transferred to Hybond nitrocellulose membrane (Amersham UK) using transfer buffer (1X TG, 20%v/v ethanol) at 100 v for 1 h. Protein transfer was verified using India ink staining (1:1000 India ink with 0.1% Tween / PBS) for 10 min.

Immunoblotting

Membranes were blocked by incubating in 5% non fat dried milk / 0.1% Tween / TBS for 1 h at room temperature or overnight at 4° C. Primary antibodies were diluted in 3% non fat dried milk / 0.1% Tween / PBS and membranes incubated for 1 h at room temperature or overnight at 4° C except for phospho-antibodies which were dissolved in 5% Bovine Serum Albumin (Fraction V) / 0.1% Tween / TBS and incubated overnight at 4° C. Membranes were then washed three times for five minutes in the appropriate wash buffer. HRP conjugated secondary antibodies were diluted in 3% non fat dried milk / 0.1% Tween / TBS and incubated for 1 h at room temperature. Three further washes in the appropriate wash buffer were performed for fifteen, ten and ten min. Immunocomplexes were identified using

West Pico Supersignal Chemiluminescent Reagent and a chemiluminescent imager (Fluor S Max, Bio-Rad).
Unless otherwise indicated membranes were not stripped or re-probed. Quantification of western blots was performed with Quantity One software (BioRad). Equal sized areas of interest (AOI) were created for each band analysed and the pixel density calculated for each area. A representative background AOI was calculated and subtracted from each band. To confirm the accuracy of this technique serial dilutions of quantified protein were run on a 12% polyacrylamide gel and separated by electrophoresis. MNK1 protein was identified by western blotting at each protein dilution and bands quantified. Band intensity was plotted against protein loaded (fig 2:1).

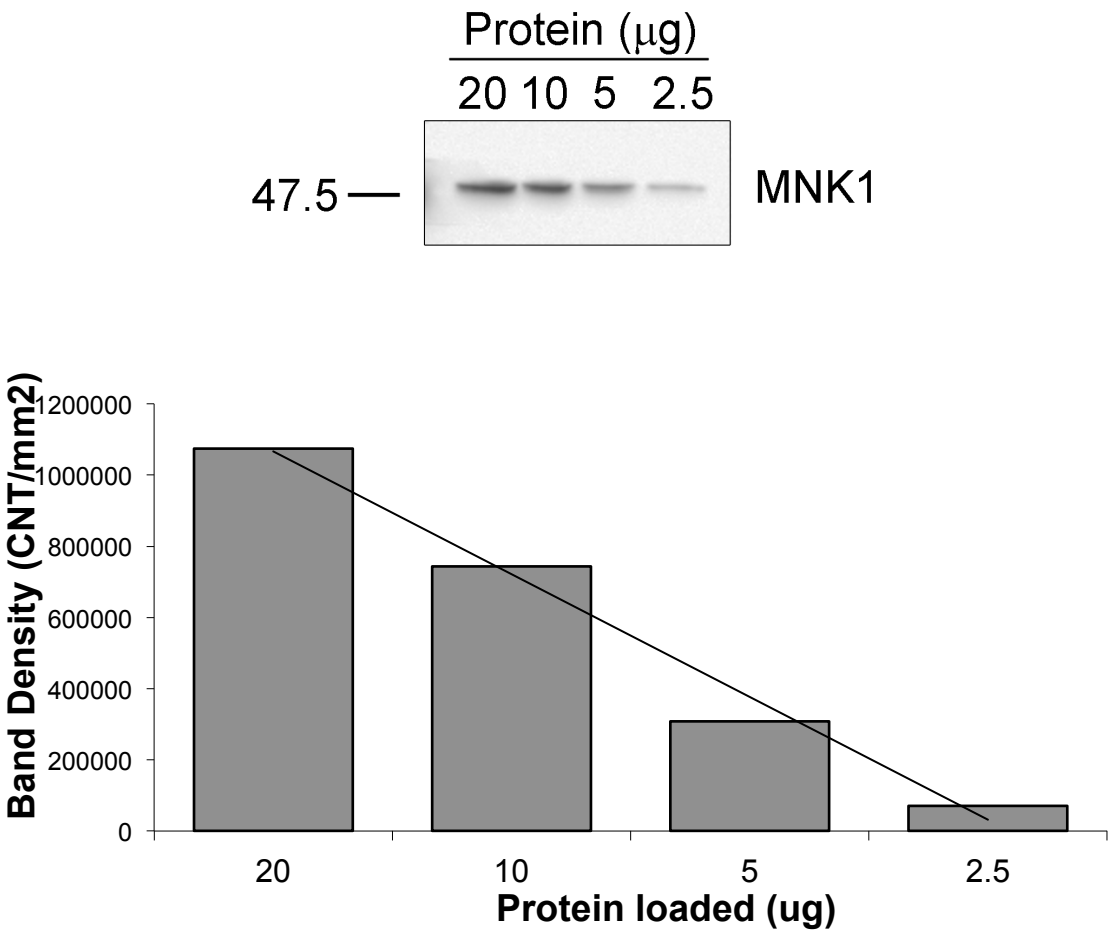

Figure 3:3 Quantification of immunoblotting

Untreated SKBr3 cells were lysed with urea lysis buffer and clarified by centrifugation. Proteins were quantified with Bradford reagent and serial dilutions made with SDS loading buffer. Protein quantities as shown were loaded to 12% polyacrylamide gel and separated by PAGE. MNK1 protein was identified by immunoblotting and band intensity quantified using Quantity One 2D gel analysis software (BioRad). Graph shows band density plotted against amount of protein loaded for the immunoblot above.

3.2.3. Nucleic acid analysis

Taqman qRT-PCR

Cells were plated at 0.5 X 10^6 cells per dish in 60mm dishes, and treated with CGP57380 or transfected with siRNA as above. Cells were harvested by washing once in PBS, scraped in PBS and pelleted by centrifugation at 1000*g* for 4 min at 4° C. Pellets were snap frozen in liquid nitrogen.

RNA extraction

RNA was extracted at room temperature by solid phase extraction using a RNeasy Mini Kit (Qiagen).

Cell pellets were homogenised and disrupted by vortex in 350 μl buffer RLT to which 1% β mercaptoethanol had been added. Buffer RLT contains high salt and guanidine-thiocyanate and results in disruption of cells and denaturing of proteins including inactivation of ribonucleases. β mercaptoethanol is added for its reducing capacity to further inhibit ribonuclease function. 350 μl 70% ethanol was then added and mixed by pipetting to establish optimum column binding conditions for RNA. 700 μl of the above lysate was then added to a spin column and centrifuged at 8000*g* for 15 s at room temperature to allow binding of RNA to the silica column. This binding occurs due to the high salt conditions allowing formation of a salt bridge between the negatively charged ribonucleic acid and silica. The column was then washed with 350 μl high salt buffer RW1 and centrifuged at 8000*g* for 15 s. An on-column DNA digestion was then performed. 10 μl DNase I was added to 70 μl buffer RDD and mixed by inversion. 80 μl of the DNase I mix was then added directly to the column and incubated for 15 min at room temperature. A further high salt wash with 350 μl buffer RW1 was performed followed by being centrifuged at 8000*g* for 15 s. Two washes were then performed with 500 μl buffer RPE to which 4 volumes of ethanol had been added. Following the first wash, samples were centrifuged at 8000*g* for 15 s, and at 8000*g* for 2 min following the second. The column was then put in a new collection tube and the RNA eluted with 30 μl ribonuclease free water and centrifuged at 8000*g* for 1 min. The eluate was then re-applied to the column and a further centrifugation at 8000*g* for 1 min was performed.

The RNA was quantified by photospectroscopic absorbance at 260 nm using a Nanodrop 1000 Spectrophotometer (Thermo Scientific), using the 260:280 nm absorbance ratio to confirm purity. Samples were stored at -80° C.

cDNA synthesis

Complementary DNA (cDNA) was synthesised using SuperScript II reverse transcriptase (Invitrogen).

0.5 μg total RNA was added to a mixture containing 1 μl Olio dt primer (0.5 μg/ml Invitrogen), 1 μl dNTP mix (10mM Invitrogen) and deionised water to a final volume 12 μl. This mixture was heated to 65° C for 5 min before being cooled on ice and pulse centrifuged at 8000*g*. A mixture of 4 μl 5X first strand buffer (Invitrogen), 2 μl 0.1M dithiothreitol (DTT) and 1 μl ribonuclease inhibitor RNaseOut (40 units / μl Invitrogen) was added, mixed by pipetting and incubated at 42° C for 2 min. 1 μl (200 units) of SuperScript II reverse transcriptase (Invitrogen) was added and mixed by pipetting, followed by incubation at 42° for 50 min. The reaction was inactivated at 70° C for 15 min and the samples stored at -20° C.

Taqman qRT-PCR

Cyclin D1 reactions were performed in triplicate with GAPDH in duplicate. Standard curves were carried out for both genes using five known quantities of cDNA from T47D cells, starting at 15 ng with serial 1:5 dilutions. No cDNA negative controls were also performed in duplicate for each gene. All reactions were performed at a final volume of 20 μl and set up as follows.

A mastermix for each reaction was made containing 10 μl 2 X Taqman Universal PCR Mastermix (Applied Biosystems), 1 μl GAPDH or Cyclin D1 20X primer/probe mix (Applied Biosystems), and 4 μl deionised water. The Universal PCR Mastermix contains AmpliTaq gold DNA polymerase, dNTPs and optimised buffers. 15 μl of the above mastermix was added to each well in a MicroAmp Optical 96 well reaction plate (Applied Biosystems). 5 μl cDNA at a concentration of 1 ng/μl was added to each well. The plate was then pulse centrifuged to 200*g* on a benchtop centrifuge (Sorvall Legend RT). PCR was performed using the ABI PRISM 7500 Sequence Detection System (Applied Biosystems) using parameters as follows:

94°C 10 min, 40 cycles 94°C for 15 s and 60°C for 1 min. Ct values were normalised to GAPDH, and absolute values obtained from the standard curve.

Cell fractionation and polyribosome purification

ACHN cells were plated at 1.5 x 10^6 cells in 10 ml medium in each of eight 90mm dishes. 24 h later cells were treated with CGP57380 at a final concentration of 20 μM in 0.5% DMSO, or 0.5% DMSO vehicle control for 6h. Cells were washed once in cold serum free medium and then scraped into 2 ml cold serum free medium containing 10μg/ml cycloheximide with cells pooled from each treatment. A 1 ml aliquot was taken from each pooled cell suspension, centrifuged at 1000*g* for 4 min at 4 °C and snap frozen for total cellular RNA. The remaining cells were centrifuged at 1000*g* for 4 min at 4 °C and resuspended in 1 ml Fractionation buffer A before being incubated on ice for 5 min. Cells were homogenized using a dounce homogeniser with 20 strokes of the loose pestle before being incubated on ice for a further 5 min. Cells were then homogenized with 20 strokes of the tight pestle of the dounce homogeniser and once again incubated for 5 min on ice. A further 20 strokes of the tight pestle were then used and the cells checked for lysis by microscopy. The cell suspension was then transferred to a 1.5 ml tube and centrifuged at 12,000*g* for 10 min at 4 °C. The supernatant was transferred to a fresh 1.5 ml tube as the cytoplasmic fraction. The pellet was resuspended in 200 μl fractionation buffer A and once again centrifuged at 12,000*g* for 10 min at 4 °C. The supernatant was removed and the pellet was snap frozen in liquid nitrogen as the nuclear fraction. The protein concentration of the cytoplasmic fraction was measured using Bio-Rad Bradford reagent.

1.5 ml fractionation buffer A with 30% sucrose (w/v) was placed in each of two 2 ml Beckman centrifuge tubes. 0.5 ml of the cytoplasmic fraction with the lowest protein concentration was carefully layered over a sucrose cushion. A volume of the other cytoplasmic fraction to give equal protein was carefully layered over the other sucrose cushion, and the volume made up to 0.5 ml with fractionation buffer A. The remaining cytoplasmic fraction for each sample was snap frozen in liquid nitrogen. The samples were centrifuged at 130,000*g* for 2.5 h at 4 °C on a Beckman-Coulter Optima Max Ultracentrifuge using a TLS-55 rotor. All but the last

100 μl sucrose cushion was removed and discarded. The final 100 μl was snap frozen in liquid nitrogen as the polyribosome fraction.

RNA was extracted by phenol extraction using RNA Bee reagent (AMSbio) as follows:
For the total and nuclear pellets 750 μl RNA Bee reagent was added and mixed by vortex. For the cytoplasmic and polysome fractions 1 ml RNA Bee reagent was added to 100 μl cell fraction and mixed by vortex. 0.1 vol chloroform was added to each sample and mixed thoroughly by vortex for 15 s and then incubated in ice for 5 min. Samples were centrifuged at 10,500*g* for 15 min at 4 °C and the upper aqueous layer removed to a fresh 1.5 ml tube. RNA was precipitated by the addition of an equal volume of isopropanol and incubated on ice for 15 min. Samples were centrifuged at 10,000*g* for 10 min at 4 °C and the isopropanol aspirated to waste. The pellet was washed in 1 ml 75% ethanol, vortexing to break up the pellet. Samples were centrifuged at 7,500*g* for 8 min. The ethanol was aspirated to waste and the pellet allowed to air dry until semi-clear. The pellet was re-suspended in 40-100 μl RNAse free water and the RNA quantified using a Nanodrop 1000 Spectrophotometer (Thermo Scientific), using the 260:280 nm absorbance ratio to confirm purity. Samples were stored at -80° C.
cDNA was synthesized as described above with the addition of 1 μl of oligonucleotide primer (table 2:3).
Semi-quantitative reverse transcriptase PCR was used to assess fractionation using primers for small nuclear RNA U6 and GAPDH. Each reaction was set up in ice as follows, with 2 quantities of input cDNA to ensure reactions were within logarithmic range:

5 x GoTaq buffer (Promega)	10 μl
25 mM $MgCl_2$	5 μl
10 mM dNTPs (ATGC)	1 μl each nucleotide
20 pmol primer	1 μl of each
GoTaq polymerase (Promega)	0.1 μl (0.5 units)
Water	to 48 μl
cDNA	2 μl

Target	Primers	Product size	Input cDNA (pg)	Cycles
snRNA U6	F_CGC TTC GGC AGC ACA TAT AC R_TTC ACG AAT TTG CGT GTC AT	100 bp	300/100	28
GAPDH	F_GAA GGT GAA GGT CGG AGT R_GAA GAT GGT GAT GGG ATT TC	200 bp	3000/1000	28

Table 3:3 PCR conditions for cellular fractionation

Reactions were run on a thermal cycler with the following parameters:

94 °C 3 min
94 °C 30 s
57 °C 30 s } cycles as per table
72 °C 30 s
72 °C 3 min

4-thiouracil RNA labeling and pull down

0.5 x 10^6 cells were plated to 60 mm dishes in 3 ml medium. 24 h later CGP57380 was added to a final concentration of 20 μM in 0.5% DMSO, or 0.5% DMSO vehicle control alone. After 1 h 4-thiouracil (Sigma) was added to a final concentration of 50 mM and cells incubated for a further 6 h. Cells were then harvested by scraping and pelletted by centrifugation at 1000*g* for 4 min at 4 °C. RNA was extracted using RNA Bee as described above and quantified using a Nanodrop photospectrometer.

4-thiouracil containing RNA was biotinylated as follows. A 1 mg/ml solution of EZ Link Biotin HPDP (Pierce) in dimethylformamide (DMF) was prepared. The following mixture was prepared with addition of Biotin-HPDP last, and incubated in the dark for 2 h at room temperature:

RNA (total)	10 μg
1M Tris (pH7.4)	0.5 μl
0.5M EDTA	0.1 μl
Biotin-HPDP	10 μl
RNAse free water	up to final volume of 50 μl

Labelled RNA was precipitated by the addition of 5 μl 5M NaCl and 50 μl isopropranol followed by vortexing and incubation at room temperature for 5 min. Samples were then centrifuged at 10,500*g* for 20 min and the supernatant aspirated. The pellet was rinsed with 250 μl 75% ethanol and the samples once again centrifuged at 10,500*g* for 10 min. The ethanol was aspirated and the pellet allowed to air dry until semi-clear. The RNA was resuspended in 40 μl RNAse free water.

Biotinylated 4-thiouracil labeled RNA was then purified as follows. Streptavidin beads (Dynabeads MyOneStreptavidin C1, Invitrogen) were first blocked with yeast tRNA (Invitrogen). Two aliquots of 40 μl beads were each blocked with 2 μg tRNA by rotating in a 1.5 ml tube for 20 min at room temperature. Tubes were then placed in a magnetic stand and the beads collected at the side of the tube for 2 min. Beads were washed 3 times in 300 μl MPG buffer, collecting beads between washes by standing in a magnetic stand for 2 min, and then resuspended in 40 μl MPG buffer. The biotinylated RNA was added to the beads and mixed with rotation at room temperature for 30 min. The beads were then collected in a magnetic stand for 2 min. The supernatant was removed to a fresh tube and snap frozen in liquid nitrogen as unbound, non-4-thiouracil labeled RNA. The beads were then washed in MPG buffer as follows with pipetting to mix; twice in 250 μl MPG buffer at room temperature, once in 250 μl MPG buffer at 65 °C and once in 50 μl MPG buffer at room temperature, retaining the final wash to check flow through of unbound RNA.

The bound, 4-thiouracil containing RNA was eluted by adding 40 μl of freshly prepared β-mecaptoethanol to the beads and incubating at room temperature for 20 min with rotation, flicking the tube at 10 min to mix well. The beads were then collecting by placing the tube in a magnetic stand for 2 min and transferring the supernatant containing bound, 4-thiouracil to fresh tubes.

RNA was precipitated from each fraction. An equal volume of isopropanol was added to each of the fractions. For the 4-thiouracil RNA fraction 1/10 volume of 5 M NaCl was also added. 5 μg glycogen (Fermentas) was added to each sample followed by incubation at room temperature for 5 min. The samples were centrifuged at 10,500*g* for 20 min. The supernatant was discarded and the precipitated RNA pellet washed in 250 μl 75% ethanol before being centrifuged at

10,000*g* for 5 min. The pellet was air-dried until semi-clear and resuspended in 10 μl RNAse free water. RNA was quantified using a Nanodrop photospectrometer. cDNA was made as above, and cyclin D1 RNA measured using Taqman qRT-PCR as described above.

Luciferase reporter assay

100,000 cells were plated to each well of a 24 well plate in 500 μl medium. 24 h later cells were transfected with 20 ng pRLSV40 renilla luciferase reporter vector together with 1 μl of firefly luciferase reporters containing either the complete CyclinD1 promoter (-1745CD1Luc)[155], a kind gift from Dr Richard Pestell, or pgl3 basic control containing firefly luciferase with no promoter. Transfections were performed by the addition of vectors as above to 50 μl Opti-MEM serum free medium (Invitrogen). 2 μl Lipofectamine 2000 transfection reagent (Invitrogen) was added to 50 μl Opti-MEM per transfection and incubated at room temperature for 5 min. 50 μl Lipofectamine mix was added to 50 μl plasmid mix, mixed by pipetting and incubated at room temperature for 20 min before being added dropwise to the cells. At 4 h post transfection the transfection mix was removed and replaced with 1 ml complete medium containing either 20 μM CGP57380 in 0.5% v/v DMSO, or 0.5% DMSO vehicle control.

24 h post transfection renilla and firefly luciferase activity was assayed using the Dual-Glo luciferase assay system (Promega). Medium was removed from each well to leave 100 μl remaining. 100 μl Dual-Glo luciferase reagent was added to each well. Once cells had lysed 100 μl cell lysate was transferred to a white OptiPlate 96 well plate (Perkin Elmer) and firefly luminescence measured using a Varioskan Flash plate reader (Thermo Electron Corporation). 100 μl Dual-Glo Stop & Glo reagent was then added to each well to quench firefly luciferase activity and act as a substrate for renilla luciferase. After 10 min incubation renilla luciferase activity was measured using a plate reader as above. Results were expressed as firefly luciferase relative to renilla luciferase for each transfection.

Site directed mutagenesis

A plasmid vector encoding EYFP-eIF4E was mutated to give a positively charged aspartic acid at serine 209, the phosphorylation site of the MNK kinases in eIF4E.

The EYFP-eIF4E plasmid was constructed by Mr Matthew Darley in Dr Blaydes laboratory using EYFP-C1 and the coding sequence for murine eIF4E which has close homology to human eIF4E.

Oligonucleotide primers were designed such that the sequence of the forward primer matched that of the sequence of eIF4E at least 12 base pairs either side of the codon coding for serine 209. The S209 codon was changed to encode an aspartic acid giving the following primers:

Forward – 5'-ACA AAG AGC GGC GAT ACC ACT AAA AAT AGG-3'

Reverse – 3'-CCT ATT TTT AGT GGT ATC GCC GCT CTT TGT-5'

A PCR Reaction was set up as follows using a Stratgene Quickchange SDM kit.

5 μl 10x pfu turbo reaction buffer

50 ng EYFP-eIF4E double stranded DNA template

1 ng forward primer

1 ng reverse primer

1 μl dNTP nucleotide mix

double distilled water to a final volume 50 μl

1 μl Pfu turbo DNA polymerase was added immediately prior to running the following reaction in a thermal cycler:

Segment 1	1 cycle	95 °C 30 sec
Segment 2	18 cycles	95 °C 30 sec
		55 °C 1 min
		68 °C 18 min

A Dpn1 digestion was then performed to digest the template plasmid DNA as follows:

1 μl Dpn1 (Promega) restriction enzyme (10U/μl) was added to the amplification reaction above and mixed by pipetting before being spun for 1 min in a microcentrifuge. The mixture was then incubated at 37 °C for 1 h and subsequently stored at -20 °C.

The resulting plasmid DNA was then transformed into XL1-Blue supercompetent bacteria (made in the Blaydes lab by Mr Matthew Darley) as follows:

XL1-Blue cells were thawed on ice

15 μl cells were placed in a pre-chilled 15 ml Falcon tube (Becton-Dickinson)

1 μl plasmid DNA was added to the cells, gently mixed and incubated in ice for 30 min.
The cells were placed in a waterbath at 42 °C for 45 s and then returned to ice for 2 min.
0.5 ml Luria-Bertani (LB) broth was added and incubated at 37 °C for 1 h shaking at 220 rpm.
250 μl LB broth was then plated to each of 2 agar plates containing kanamycin at 10 μg/ml and incubated overnight at 37 °C.
5 colonies were picked from each plate and each placed in 5 ml LB broth containing 10 μg/ml kanamycin. These were subsequently incubated overnight at 37 °C with shaking at 220 rpm.
Plasmid DNA was isolated using a QIAprep spin miniprep kit (Qiagen) as follows:
Bacterial cells were pelletted by centrifugation at 6000*g* for 15 min at 4 °C and the supernatant discarded to waste.
The cells were resuspended in 250 μl buffer P1 to which RNase A had been pre-added.
The cell suspension was transferred to a 1.5 ml microcentrifuge tube to which 250 μl buffer P2 (sodium hydroxide and SDS) was added and mixed by inverting, allowing the mixture to form a slightly viscous clear solution for a maximum of 5 min. The alkaline buffer denatures the cell contents released following lysis of the cell though solubilisation of the membrane phospholipids by SDS.
350 μl buffer P3 was added and once again mixed by inverting. This high salt buffer causes the precipitation of cellular proteins and chromosomal DNA.
The suspension was centrifuged at 18,000*g* for 10 min following which the supernatant was placed in a QIAprep spin column. This was centrifuged at 18,000*g* for 60 s and the flow through discarded.
The spin column was washed by the addition of 0.75 ml buffer PE followed by centrifugation at 18,000*g* for 60 s. The flow through was discarded and the column spun for a further 1 min at 18,000*g* to dry the column. The QIAprep column was then placed in a clean 1.5 ml microcentrifuge tube and 50 μl DNAse free water applied directly to the membrane at the centre of the column. The column was allowed to stand for 1 min and then spun at 18,000*g* for 1 min to elute the plasmid DNA.

3 samples were sent for sequencing (Geneservice) using the EGFR-CR primer. Alignment of the sequencing data was checked and the mutation confirmed.
The plasmid DNA was then amplified using tranformation of XL-1 Blue supercompetent bacteria and DNA extraction using a QIAfilter plasmid maxi kit (Qiagen).
XL-1 Blue supercompetent bacteria were transformed as described above, plated to kanamycin-agar plates and colonies picked. Bacterial cultures were grown up to 125 ml in LB broth by incubation overnight at 37 °C with shaking at 220 rpm. The bacterial cells were then pelletted by centrifugation at 6000*g* for 15 min at 4 °C. The pellet was resuspended in 10 ml buffer P1 following which 10 ml buffer P2 was added and mixed by inverting the tube 4-6 times. The cell suspension was then incubated at room temperature for 5 min. 10 ml chilled buffer P3 was added and the suspension mixed by inverting 4-6 times after which the suspension was poured into a QIAfilter cartridge and incubated at room temperature for 10 min. During this time a QIAGEN-tip was equilibrated by the addition of 10 ml buffer QBT which was allowed to drain through completely. A plunger was placed in the QIAfilter cartridge and the cell lysate filtered into the equilibrated QIAGEN-tip and allowed to pass into the resin. The resin was then washed twice with 30 ml buffer QC. The DNA was eluted into 10.5 ml isopropanol using 15 ml buffer QF. The eluted DNA was then precipitated by centrifugation at 6000*g* for 30 min at 4 °C. The supernatant was removed and the pellet re-suspended in 1 ml 70% ethanol to wash before being transferred to a 1.5 ml microcentrifuge tube. The DNA was once again precipitated by centrifugation at 10500*g* for 10 min at 4 °C and the supernatant removed. The DNA pellet was allowed to air dry, resuspended in 350 μl 10% TE in RNase free water and quantified using a photospectrometer.

Stable transfection

For stable transfection of A498 cells with the EYFP-eIF4ESD209 vector and EYFP empty vector control, cells were first cultured in increasing concentrations of G418 to establish the minimum concentration to kill all growing cells. This was established at 62.5 μg/ml.
Cells were plated at 0.4 x 10^6 cells in 2 ml medium in 60 mm dishes. 24 h later cells were transfected using 2 μg vector DNA as follows.

A plasmid mix was prepared by adding 2 μg plasmid vector to 0.5 ml Optimem serum free medium (Invitrogen). For each transfection a mix of 0.5 ml Optimem and 6 μl Lipofectamine 2000 transfection reagent (Invitrogen) was prepared, mixed thoroughly by vortex and incubated at room temperature for 5 min. The Lipofectamine mix was then added to the plasmid mix and vortexed thoroughly before incubation at room temperature for 20 min. The transfection mix was then added dropwise to the cells. The medium was replaced at 4 h after transfection. 48 h after transfection the cells were trypsinised and replated to 90 mm dishes with 10% of the trypsinised cells to one plate and 50% to another. 24 h later the medium was changed for complete medium containing G418 at 62.5 μg/ml. The medium was changed on alternate days until untransfected cells were seen to die and colonies of transfected cells form. Vector expression was confirmed by imaging the cells with a fluorescence microscope (Zeiss Axiovert 200) using excitation at 490 nm and an EYFP emission filter.

Expressing colonies were picked from the 10% plates using cloning rings to selectively trypsinise individual colonies and transfer them to 96 well plates. Colonies were maintained in medium containing G418 at 62.5 μg/ml and grown up to 25cm^2 tissue culture flasks at which point pellets were frozen in liquid nitrogen for subsequent use, and protein lysates made for western blotting to confirm vector expression.

Pooled transfectants were made from the 50% plates by serial trypsinisation and replating of all colonies on the plate in medium containing G418 at 62.5 μg/ml.

M^{7}GTP pulldown of eIF4E

To confirm the functionality of the transfected EYFP-eIF4ESD209 vector, synthetic m^{7}GTP linked to sepharose beads was used as a cap analogue to pull down the transfected eIF4E protein as follows.

Transfected cells were plated to 90mm dishes in 10 ml medium and harvested 24 h later by scraping. Cell pellets were snap frozen. Proteins were extracted using 40 μl extraction buffer for 15 min on ice. Lysates were clarified by centrifugation at 10500*g* for 15 min at 4 °C and proteins quantified using Bradford reagent (BioRad). 25 μl m^{7}GTP-sepharose beads (Amersham) were added to 1 ml extraction buffer, then pelleted by centrifugation at 1000*g* for 30 s and the supernatant removed. 180

μg protein extract was added (with the volumes equalized to at least 100 μl with extraction buffer) and mixed by rotating for 1 h at 4 °C. The beads were then extracted by centrifugation at 1000*g* for 30 s and washed twice with 1 ml extraction buffer.

18 μl of 100 μM m^7GTP (Amersham) was then added and incubated on ice for 15 min, mixing every 2 min. The beads were then centrifuged at 1000*g* for 30 s and the supernatant retained.

5 μl of 4 x SDS sample buffer was added to 15 μl pulldown supernatant and heated at 95 °C for 4 min before loading to wells on a 12% polyacrylamide gel and proteins separated by PAGE and western blotting as described above.

3.3. Statistical Analysis

Statistical analysis was performed using GraphPad Prism software Version 4.0c. For comparing multiple groups of results, analysis of variance (ANOVA) was used with Tukey's post test for subsequent comparison between single pairs of groups when $p<0.05$ for the overall analysis. For comparisons of pairs of groups Student's t test was used.

For microarray analysis GenePattern software was used for data processing and primary analysis. The database for annotation, visualisation and integrated discovery (DAVID) bioinformatics database was used to identify functional groups over-represented in the regulated genes.

4. MNK kinase inhibition in breast cancer cell lines

4.1. Introduction

Approximately 25% of breast cancers are known to over-express the receptor HER2. HER2 over-expression can result in homo-dimerisation and subsequent activation of the tyrosine kinase resulting in signalling through both the PI3K/AKT/mTOR and MAPK signaling cascades and activation of cell proliferation and survival pathways. Thus blockade of a node of signalling with input from both of these pathways such as eIF4E may be an active therapeutic target. Although a single HER2 over-expressing breast cancer cell line has been shown to be sensitive to inhibition of proliferation by the MNK inhibitor CGP57380[65], it is not clear whether this effect is limited to cells of this phenotype or whether other breast cancers may be sensitive. To investigate this, a panel of breast cancer cell lines representing a spectrum of phenotypes of clinical breast cancer cases was used to establish the significance of phosphorylated eIF4E on proliferation (table 4:1).

Cell line	**MCF7**	**ZR75.1**	**T47D**	**BT474**	**SKBr3**	**MDA-MB-231**
Oestrogen Receptor	+	+	+	+	-	-
HER2 overexpression	-	-	-	+	+	-
p53	Wildtype	Wildtype	Mutant	Mutant	Mutant	Mutant
Phenotype	Luminal	Luminal	Luminal	HER2	HER2	Basal

Table 4:1 Characteristics of breast cancer cell lines
+ overexpression, - no overexpression.

4.2. Basal levels of eIF4E phosphorylation

In order to investigate whether the presence of significant amounts of phosphorylated eIF4E in unstimulated cells varied between the different cell lines immunoblotting was performed. Protein lysates for all lines were made from exponentially growing cells, to which fresh medium had been applied 24 hours previously and analysed by immunoblotting. Bands were quantified and phosphorylated eIF4E expressed as a proportion of eIF4E, as well as being normalised to actin (fig 4.1).

There was a clear variation in the amount of phosophorylated eIF4E between cell lines, and in the ratio of phosphorylated eIF4E to unphosphorylated eIF4E. Low levels of both eIF4E and phosphorylated eIF4E were seen in MCF7 cells, with a low ratio of phosphorylated to unphosphorylated protein. The two other luminal phenotype cell lines showed higher levels of eIF4E phosphorylation which was more pronounced in ZR75.1 cells. Lower levels of unphosphorylated eIF4E in T47D cells however resulted in a higher ratio of phosphorylated to unphosphorylated protein in this cell line.

Both the HER2 phenotype cell lines, BT474 and SKBr3, showed high levels of phosphorylated eIF4E, although when normalised to actin the levels of phosphorylated eIF4E in BT474 cells was one of the lowest of the cell lines investigated. The pattern of bands for actin for this cell line, as noted previously[62], is however unusual with multiple bands seen making interpretation of normalised data for this cell line more difficult. The basal phenotype line, MDA-MB-231 showed an intermediate level of both eIF4E and phosphorylated eIF4E, with a ratio similar to that seen in the BT474 line.

In order to compare levels of phosphorylated eIF4E in breast cell lines with primary breast tissue, protein lysates from ten breast tumour tissue samples were also assessed (fig 4:2). The pathological characteristics of the breast tumours sampled, are shown in table 4:2. Again variation was seen between samples. Most samples which had measurable levels of eIF4E, also had higher levels of the phosphorylated form (samples 4,8-10), however two samples had measureable eIF4E with barely detectable levels of peIF4E (samples 4,7) and one had low levels of unphosphorylated eIF4E with higher levels of the phosphorylated form

(sample 3). Although the sample size is too small to draw any firm conclusions, there did not appear to be any relationship between those tumour samples with the highest ratio of phosphorylated eIF4E to unphosphorylated eIF4E and tumour size, grade, nodal status or ER status.

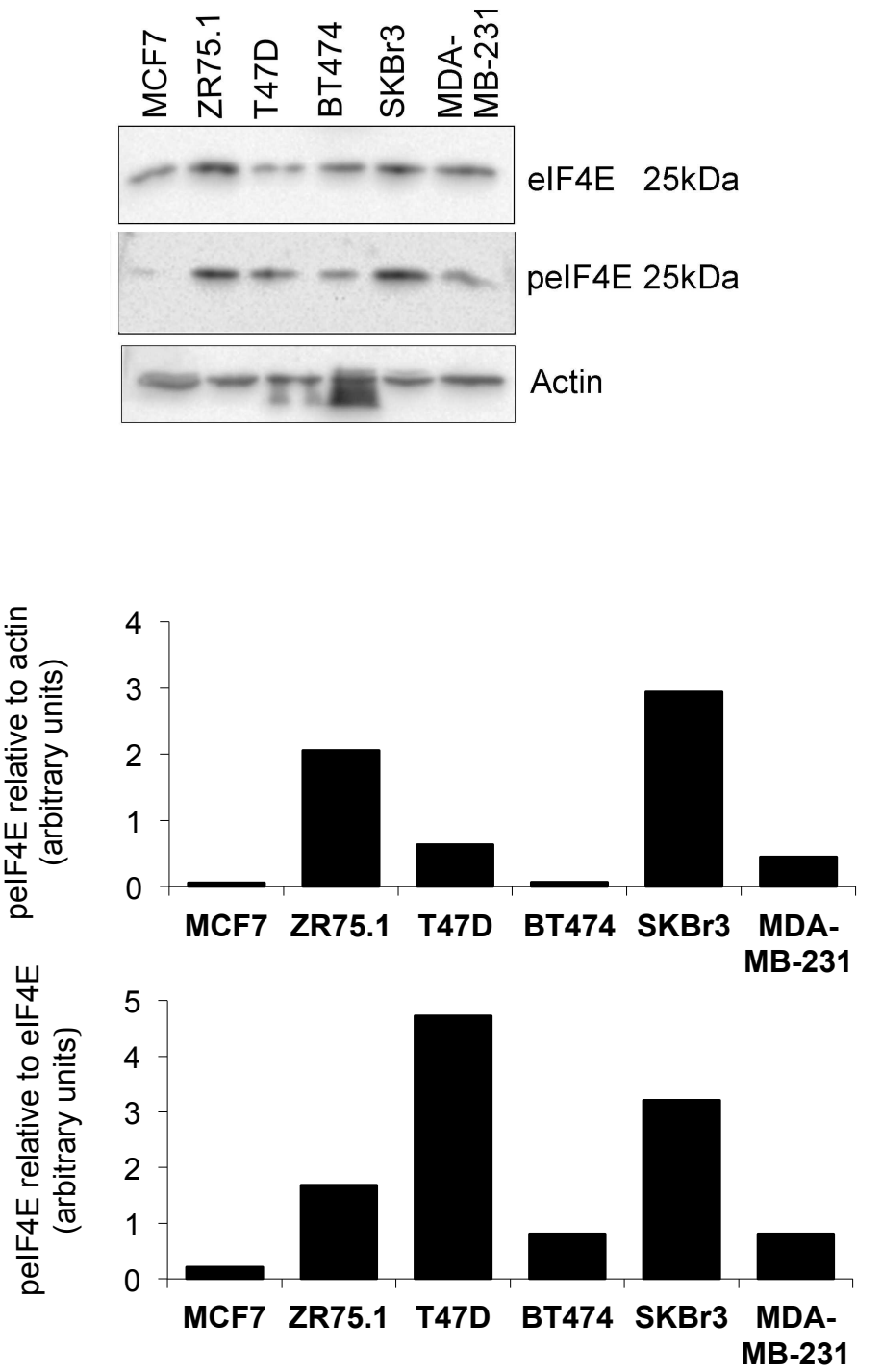

Figure 4:1 eIF4E phosphorylation in unstimulated breast cancer cells
Exponentially growing cells with fresh medium applied 24 h prior to sampling were pelleted and snap frozen. Samples were lysed by urea lysis. Equal amounts of protein were separated by PAGE, and individual proteins identified with immunoblotting. Bands were quantified with Quantity One software (BioRad) and expressed as a ratio of phosphorylated eIF4E to actin, and as a ratio of phosphorylated eIF4E to unphosphorylated eIF4E.

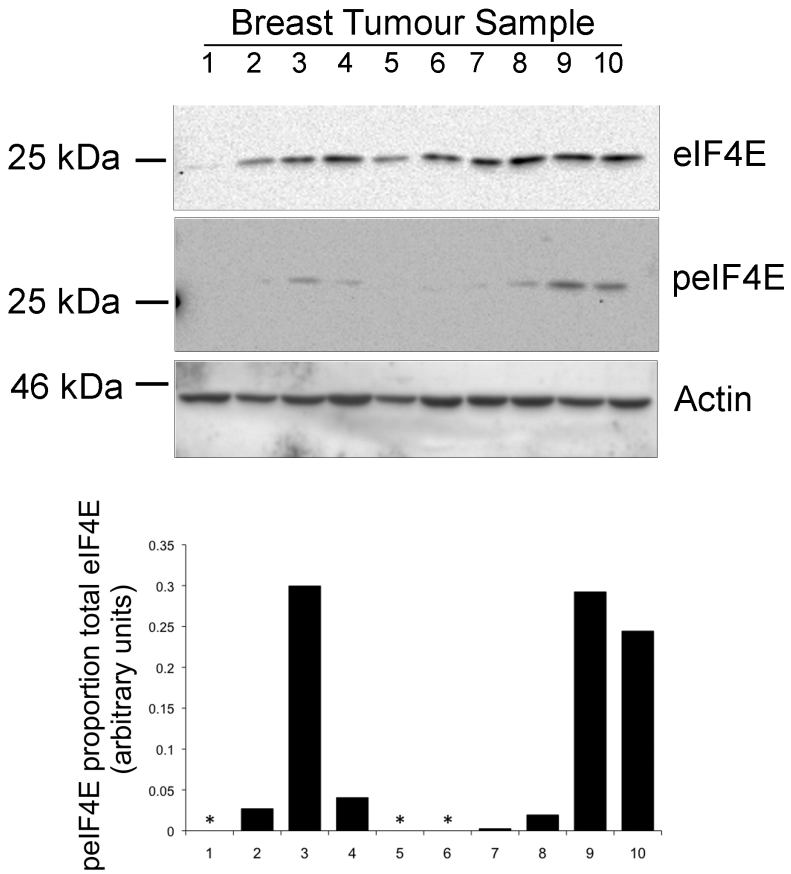

Figure 4:2 eIF4E phosphorylation in breast tissue samples
Proteins were extracted from human breast tissue samples by urea lysis and quantified. Equal amounts of protein were separated by PAGE and individual proteins identified with immunoblotting. Bands were quantified using Quantity One software (BioRad) and expressed as a proportion of phosphorylated eIF4E to total eIF4E. * no detectable phosphorylated eIF4E beyond background.

Tumour sample	Surgery	Tumour type	Tumour size	Nodal involvement	Grade	ER status
1	Mastectomy	IDC	5mm	0/8	2	++
2	Mastectomy	IDC	87mm	7/11	2	+
3	WLE	IDC	14mm	0/13	1	+
4	WLE	IDC	30mm	0/15	2	++
5	Mastectomy	IDC	40mm	1/8	3	+
6	Mastectomy	IDC	45mm	3/24	3	-
7	Mastectomy	ILC	55mm	2/7	2	++
8	Mastectomy	IDC	55mm	10/12	2	+
9	WLE	IDC	25mm	0/19	3	-
10	WLE	IDC	30mm	1/9	2	++

Table 4:2 Histological characteristics of breast tissue samples
The histological characteristics of each tumour were obtained from the diagnostic pathology report. These samples pre-date routine diagnostic testing for HER2 by either immunohistochemistry or fluorescence in situ hybridisation. WLE Wide local excision; IDC invasive ductal carcinoma; ILC invasive lobular carcinoma; nodal involvement - involved nodes/sampled nodes; ER - no expression, + weak to moderate expression, ++ strong expression by immunohistochemistry.

4.3. Effects of CGP57380 on eIF4E phosphorylation

In order to ensure CGP57380 was indeed inhibiting phosphorylation of eIF4E, cells were treated with increasing concentrations of CGP57380 or 0.5% DMSO control for 24 h and immunoblotting used to measure effects on eIF4E phosphorylation. Both SKBr3 and BT474 cell lines showed inhibition of eIF4E phosphorylation with 20 μM CGP57380 (fig 4:3).

A time course was also performed with cells treated for 72 h with CGP57380 at 20 μM, and protein lystates obtained at various time points (fig 4:4). BT474 cells were most sensitive to CGP57380, with inhibition of eIF4E phosphorylation by 15 min, which was sustained for 72 h. SKBr3 cells showed reduced levels of eIF4E phosphorylation by 4 h, however by 24 h this was starting to return, and had returned to baseline levels by 72 h. MDA-MB-231 cells were less sensitive to CGP57380 with partial loss of eIF4E phosphorylation at 1 h, which persisted to 72 h, when both eIF4E and phosphorylated eIF4E levels were almost undetectable. T47D cells showed a rapid loss of eIF4E within 2 hours. Although phosphorylated protein was visible at 24 h, it otherwise remained inhibited until 72 h.

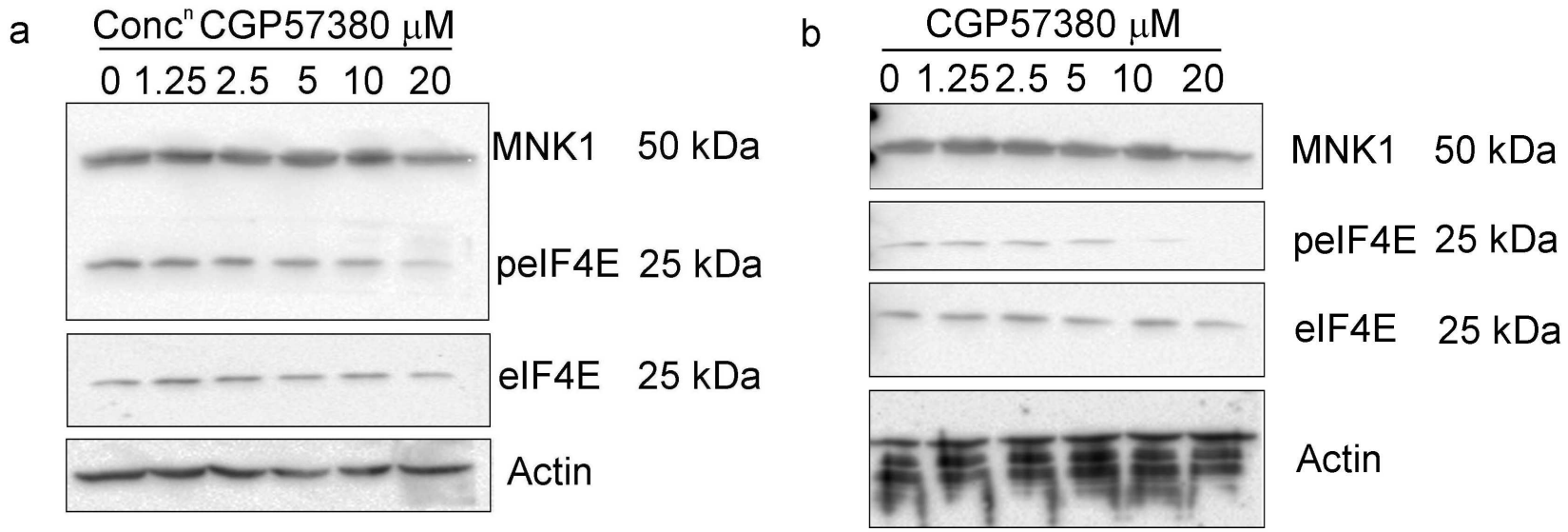

Figure 4:3 eIF4E phosphorylation following treatment with CGP57380
0.5 X 10^6 SKBr3 (a), and BT474 (b) cells were plated to 60mm dishes. 24 h later cells were treated with CGP57380 at the concentrations as indicated in DMSO vehicle control 0.5% v/v for 24 h. Cells were pelleted and lysed with urea lysis buffer. Equal amounts of protein were separated by PAGE. Individual proteins were identified by Immunoblotting.

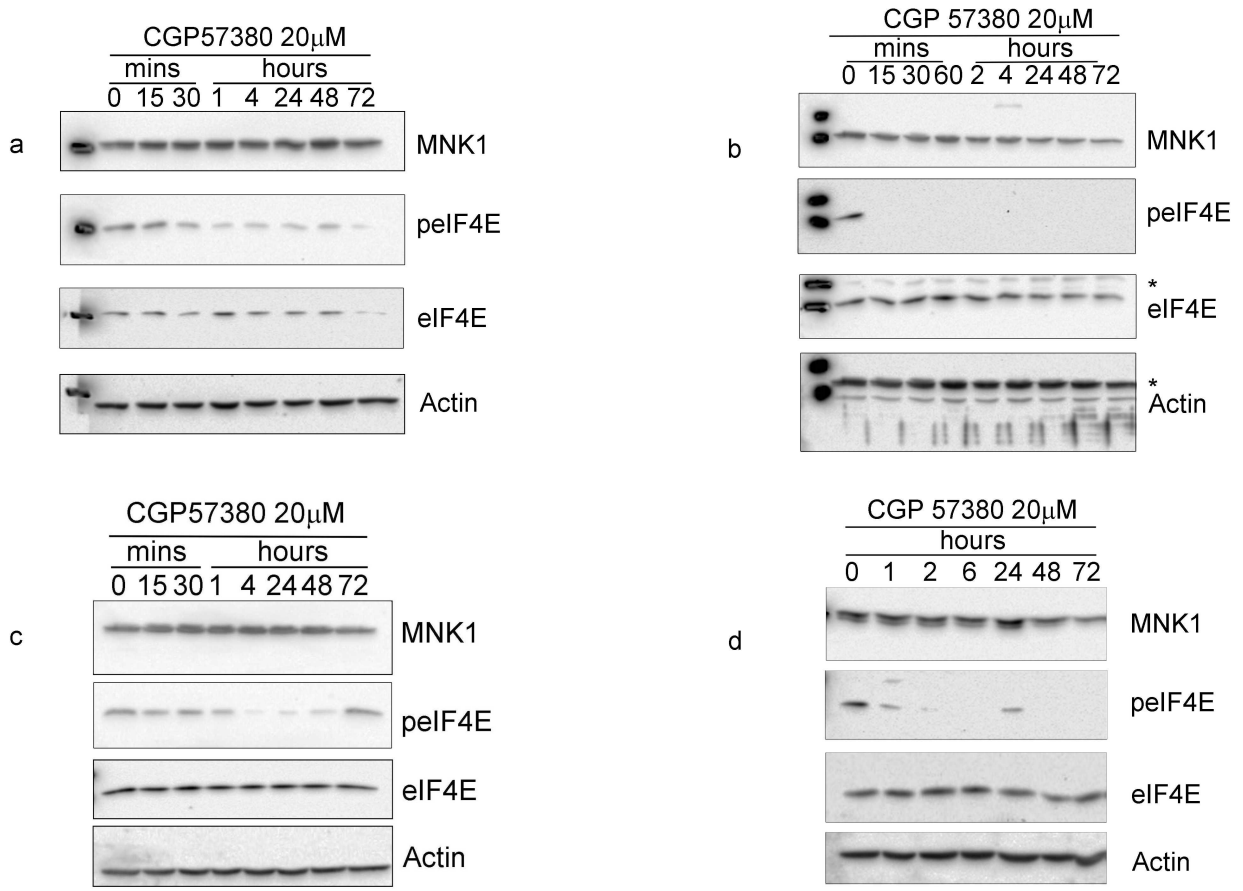

Figure 4:4 eIF4E phosphorylation following treatment with CGP57380
MDA-MB-231 (a), BT474 (b), SKBr3 (c) and T47D (d) cell lines were treated with CGP57380 at 20 μM for times as indicated. Equal amounts of protein were loaded and separated by PAGE. Individual proteins were identified by immunoblotting. Time 0 represents 0.5% DMSO vehicle control.

4.4. Effects of CGP57380 on proliferation

Having established that variation exists between the unstimulated level of eIF4E phosphorylation between cell lines, and that CGP57380 is able to inhibit eIF4E phosphorylation at a concentration of 20 μM, the effects of CGP57380 were investigated on the proliferation of the panel of breast cancer cell lines.

Initially the MTS assay of cell proliferation was used to assess proliferation over a 72 h time period. Initial escalating cell number experiments in each cell line, using the MTS assay to assess proliferation, revealed differences in the effect of proliferation dependent on the cell number plated. It was shown that beyond a certain number of cells plated, no further increase in output from the MTS assay, and no effect on proliferation was seen, whatever the dose of CGP57380 with which the cells were treated. Equally if too few cells were plated then little effect on proliferation was seen. Therefore a point on the cell number plating graph just before the curve plateaued was taken to assess the effects of proliferation (fig 4.5). Three experiments were performed for each cell line, with wells plated in triplicate. The mean MTS result was obtained for each triplicate plating, and the background MTS result for medium only was subtracted. Results for each experiment were normalised by adding the total MTS results for each experiment and dividing by the number of wells. This value was used to generate a correction factor to apply to each result for that experiment. At the cell number used to define proliferation, the results from three experiments were combined, and normalised to DMSO vehicle control (fig 4.6).

With this experiment no effect on proliferation at any cell number or dose of CGP57380 was seen in MCF7 cells. This was consistent with the low levels of unstimulated eIF4E phosphorylation seen in this cell line. Surprisingly no effect was seen in T47D cells either, which was not expected on the basis of the relatively high unstimulated levels of eIF4E phosphorylation in this line. More surprising was an apparent increase in proliferation seen in ZR75.1 cells at all doses of CGP57380 tested. Both of the cell lines with a HER2 phenotype showed a trend to reduction in proliferation compared to control, consistent with previously published data[73]. The MDA-MB-231 cell line which has a basal phenotype, and does not express estrogen receptor or the HER2 receptor also showed a response to CGP57380. This cell line is known to harbour an activating mutation of k-RAS[156],

and therefore may be expected to have increased signaling through MNK1 and be sensitive to its inhibition.

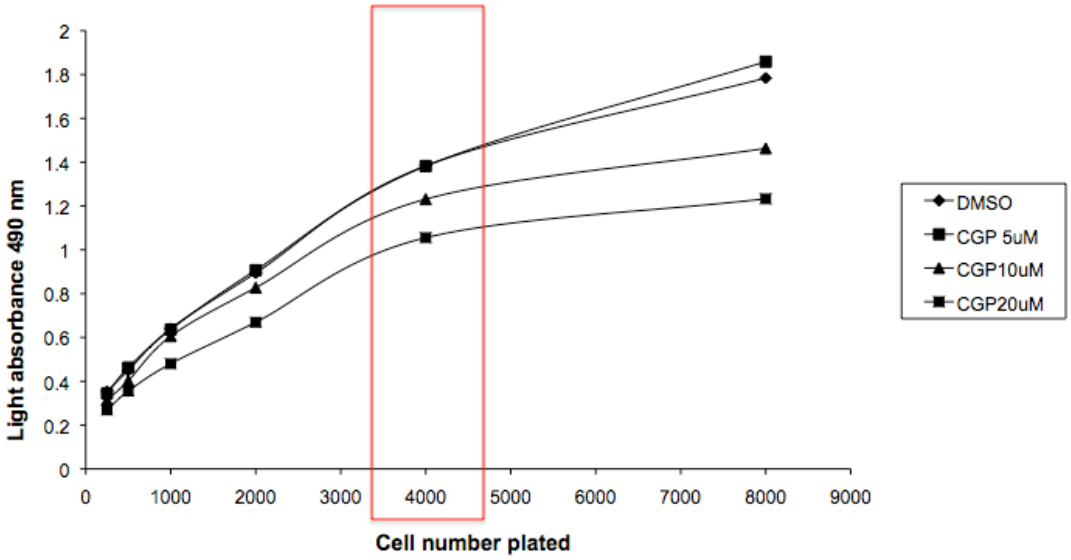

Figure 4:5 Proliferation in response to CGP57380
BT474 cells were plated at the numbers shown in 120 μl medium. 24 hours later 110 μl medium was removed from each well and DMSO or CGP57380 added to give a final concentration as shown with 0.5% v/v DMSO vehicle control. 100 μl medium was returned to the well, and proliferation assessed 72 h later by the MTS assay. Results represent the mean of three separate experiments performed in triplicate. Highlighted results are those used for subsequent statistical analysis.

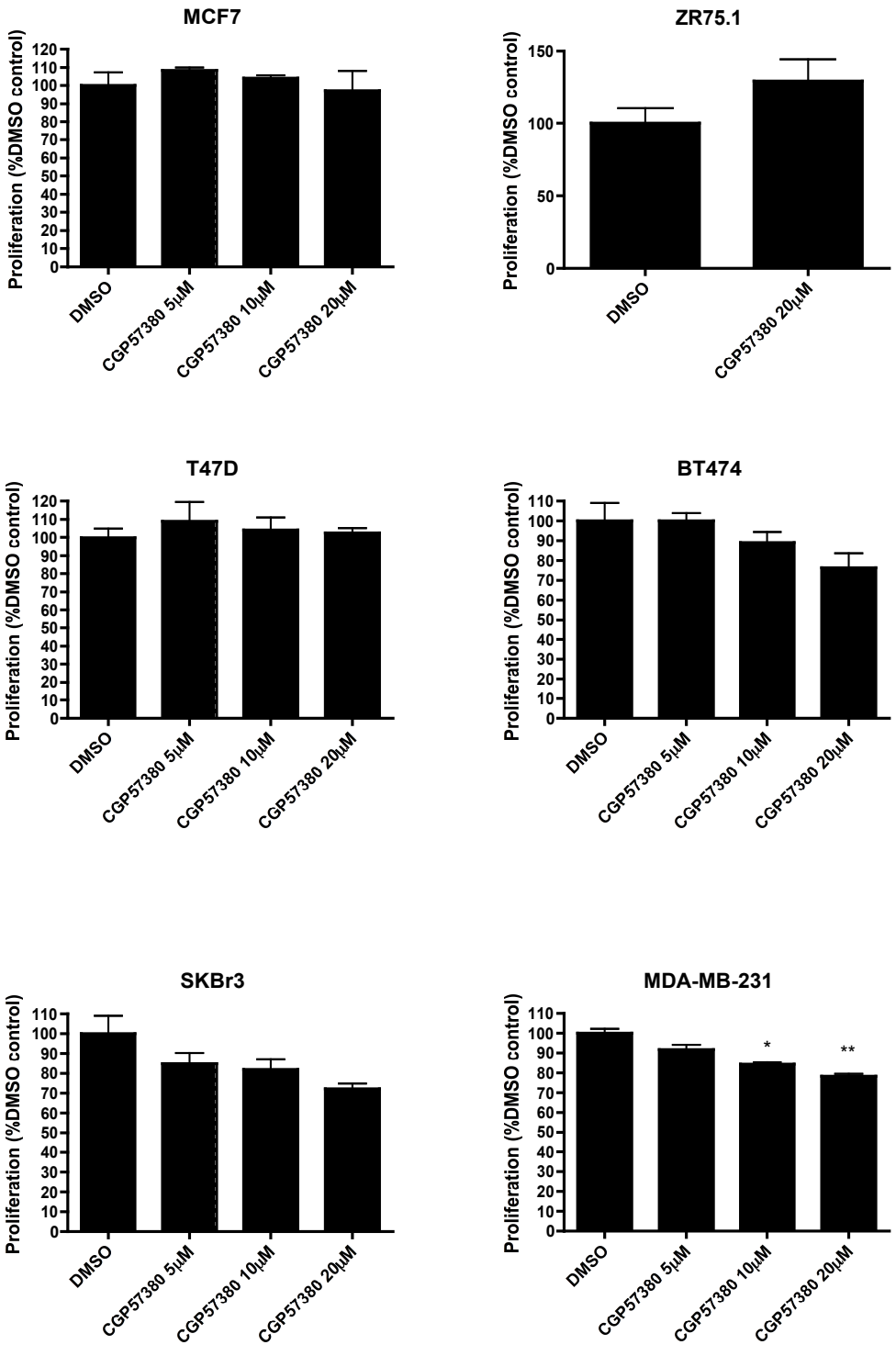

Figure 4:6 Proliferation in response to CGP57380
Cells were plated to 96 well plates in 120 μl medium. 24 h later 110μl medium was removed and CGP57380 added to give a final concentration as shown in 0.5% v/v DMSO vehicle. Proliferation was assessed using the MTS assay 72 h later. Results represent the mean of 3 experiments at plating cell numbers immediately below peaking of the MTS/cell number response curve. Statistical analysis: ANOVA with Tukey post test *=$p<0.05$ **=$p<0.001$

The effects seen on proliferation in the HER2 cell lines were relatively modest with this assay and did not reach statistical significance.

In order to assess the effects of CGP57380 on proliferation under conditions of cellular stress, CGP57380 was combined with etoposide in SKBr3 cells. A dose response curve to etoposide was performed with and without CGP57380. This showed that CGP57380 was in fact protective from the effects of etoposide, rather than showing increased sensitivity (fig 4:7) with more growth inhibition seen in those cells treated with etoposide combined with DMSO vehicle control, than seen in combination with CGP57380.

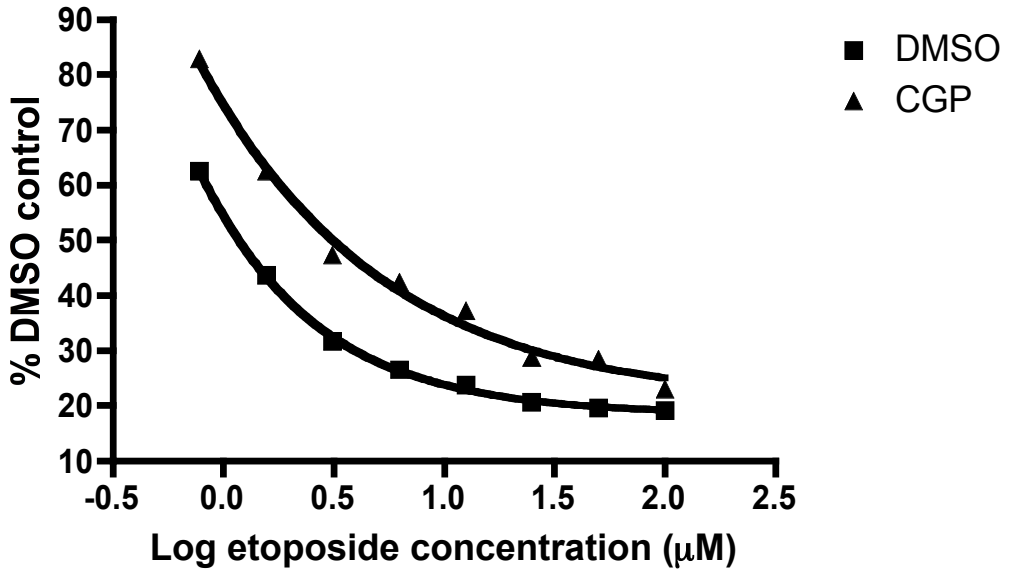

Figure 4:7 Proliferation in response to CGP57380 with etoposide
SKBr3 cells were plated at 4000 cells/well in 120 μl medium in 96 well plates. 24 h later 110 μl medium was removed from each well and pooled for triplicate repeats. Concentrations of etoposide were added as shown, with CGP57380 20 μM or 0.5% DMSO vehicle control, and 100 μl added to each well. Proliferation was measured at 72 h using the MTS assay.

Given the surprising results of the MTS assay with respect to the ZR75.1 and T47D cell lines, a colony-forming assay of proliferation was performed (fig 3:8). This assay also puts the cells under additional stress by creating a single cell environment. It investigates the long term survival capacity of a single cell with both senescence and death giving a definitive result.

Using this assay, once again MCF7 cells showed little response to CGP57380 at 20 μM with a similar number of colonies grown with both treatment and control. All of the three lines showing a response in the MTS assay, also showed a response in the colony assay with almost complete inhibition of growth in the treated cells. Contrary to the MTS assay, T47D cells, which had not previously shown a response, showed a marked reduction in colony forming ability in the treated cells. In addition the ZR75.1 cell line, which showed an apparent proliferative effect in the MTS assay, also showed a reduction in colony number with the colony assay.

One possible explanation for the discrepancy between the two assays in the ZR75.1 cell line may lie in the way in which the MTS assay measures cellular proliferation. This assay uses the reducing ability of cells as a measure of metabolic activity, and therefore as a surrogate for proliferation. Multiple cytoplasmic and mitochondrial enzymes are able to achieve this[157]. It is conceivable that applying a compound to the cell which has effects on cellular metabolism may lead to differential effects on the readout of the MTS assay compared to actual cellular proliferation as measured by the colony forming ability of the cells.

Using the colony assay as the main readout for proliferation it therefore becomes apparent that all the cell lines with higher constitutive levels of eIF4E phosphorylation, which includes lines of luminal, HER2 and basal phenotype, have their growth inhibited by CGP57380.

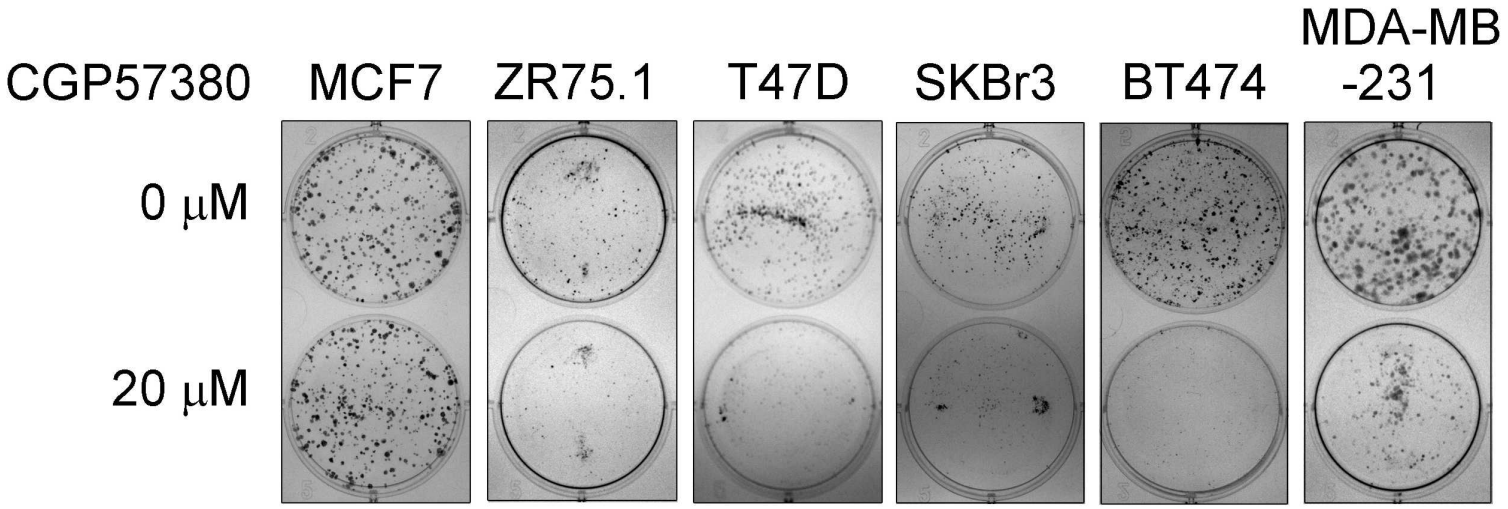

Figure 4:8 Colony forming assay in response to CGP57380
0.5 X 10^6 cells were plated in 3 ml complete medium. At 24 h cell lines as indicated were treated with 0.5% DMSO vehicle control (upper wells) or CGP57380 20 μM (lower wells) for 24 h. Cells were then trypsinised, counted and re-plated at 1000 cells/well in 6 well plates, in medium containing CGP57380 20 μM or 0.5% DMSO as previously. At 9-12 days colonies were fixed in methanol and stained with Geimsa. Pictures are representative of triplicate wells.

4.5. Effects of CGP57380 on targets of eIF4E phosphorylation

As the BT474 breast cancer cell line appeared the most sensitive to CGP57380, both in terms of inhibition of eIF4E phosphorylation, and inhibition of proliferation, this cell line was chosen to examine the effects of CGP57380 on downstream targets of eIF4E phosphorylation. Following exposure of cells to CGP57380 at 20 μM for 72 h, immunoblotting was used to probe protein lysates for cyclin D1 and Mcl-1. A sustained inhibition of cyclin D1 protein was seen from 24 hours onwards, however no change in levels of the anti-apoptotic Mcl-1 was seen. In a repeat experiment examining intermediate time points from 1-8 h, once again an immediate and sustained inhibition of eIF4E phosphorylation was seen, however there was a less marked effect on cyclin D1 at the time points examined (fig 4:9).

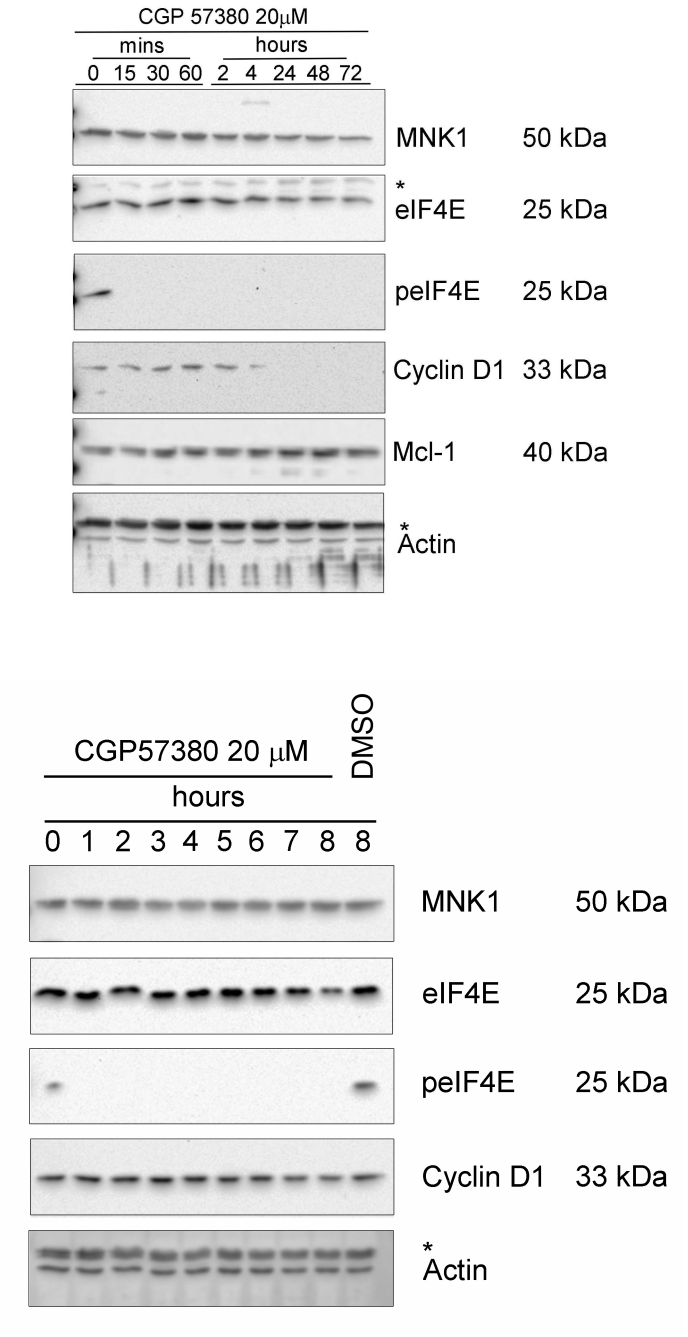

Figure 4:9 Downstream targets of phosphorylated eIF4E
BT474 cells were treated with CGP57380 at 20 μM for times as indicated. Time 0 represents untreated control. Equal amounts of protein were separated by PAGE. Immunoblotting was used to identify individual proteins. *These blots were re-probed. The lower bands represent eIF4E/actin respectively.

4.6. Mechanisms of inhibition of proliferation

The marked effect on proliferation seen in the colony forming assay may be due either to senescence or cell death in those cells exposed to CGP57380. To investigate this, live cell imaging was used to assess changes in mitotic and apoptotic events over a time period of exposure to either CGP57380 or DMSO control. Using this technique SKBR3 and MDA-MB-231 cell lines were investigated. Cells were imaged for 24 h after 24 h pre treatment with CGP57380. Images were recorded every 15 min. Cells undergoing mitosis and apoptosis were identified by reviewing sequential images, and the number of events counted over the 24 h period.

A differential effect was seen between cell lines. Over the 24 h time period SKBr3 cells showed a reduction in mitotic events from 33.3±1.9 per 100 cells in the DMSO treated cells to 13.4± 1.5 per 100 cells in the CGP57380 treated cells ($p<0.0001$). Apoptotic events were low in both treated and untreated samples, however there was an increase from 0.4±0.3 events per 100 cells in the DMSO treated cells to 2.1±0.5 events per 100 cells the CGP57380 treated over 24 h in the CGP57380 treated cells compared with the DMSO controls ($p=0.01$).

In MDA-MB-231 cells there was also a reduction in mitoses in the CGP57380 treated cells. There was a reduction in mitotic events from 36.0±1.2 events per 100 cells in the DMSO treated cells, to 21.9± 0.7 events per 100 cells in the CGP57380 treated cells ($p=0.009$). Again there were low numbers of apoptotic events with a small increase from 3.3±0.4 events per 100 cells in the DMSO treated cells to 3.8±0.5 events per 100 cells in the CGP57380 treated cells ($p=0.5$) (fig 4:10).

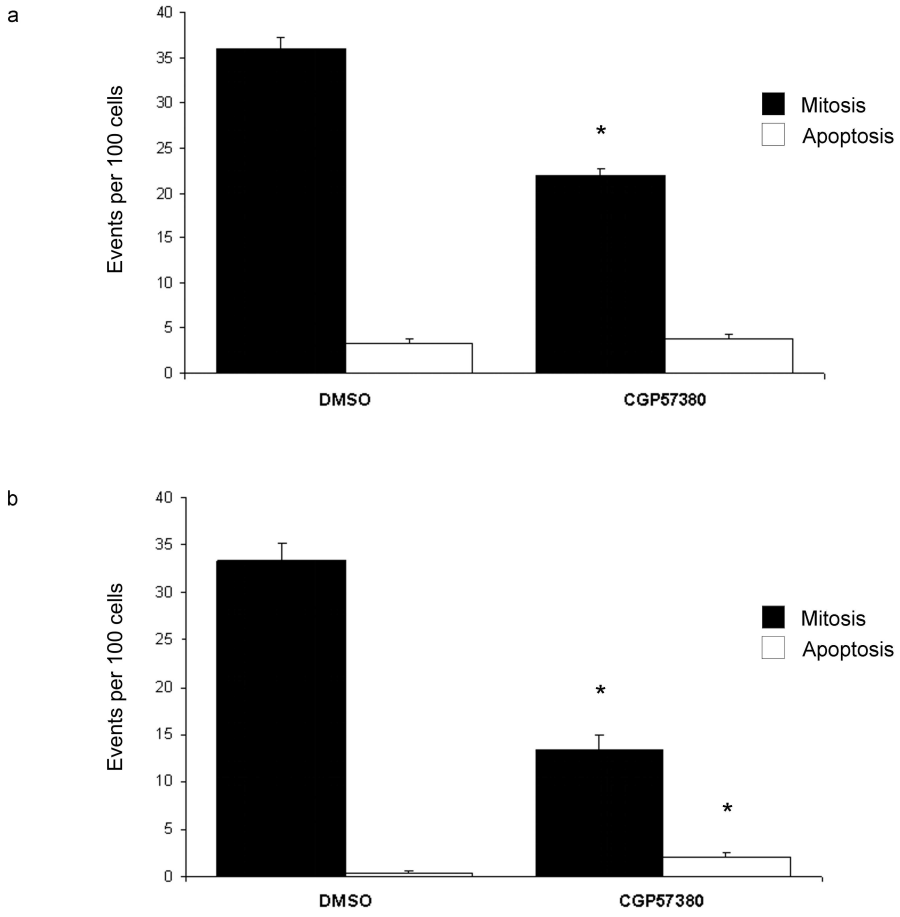

Figure 4:10 Live cell imaging following treatment with CGP57380
MDA-MB-231 cells (a) and SKBr3 cells (b) were assessed with live cell imaging. Cells were treated with 0.5% DMSO control or CGP57380 20μM for 24 h prior to imaging for 24 h with micrographs taken at 15 min intervals. The number of cells at the beginning and end of the time period, as well as the number of mitotic and apoptotic events were counted. Statistical analysis by Student's t test *=$p<0.05$.

The above results would suggest that cell cycle control may be involved in the response of breast cancer cells to MNK inhibition by CGP57380. To further investigate this as the underlying mechanism of inhibition of proliferation, cell cycle analysis using DNA staining with propidium iodide was used. A flow cytometry plot of fluorescence against events shows two peaks of fluorescence representing 2n and 4n DNA content, and hence cells and G1 and G2/M of the cell cycle respectively. Those events falling between the two peaks represent cells in S phase. Following 24 hours treatment with CGP57380 at 20 μM, MDA-MB-231 cells showed an accumulation in G1 compared with DMSO treated controls (Fig 4:11). Cells were lost from both S phase and G2/M. This result is consistent with immunoblotting of BT474 cells, showing a reduction in one of the key regulators of the transition from G1 to S phase; cyclin D1.

a

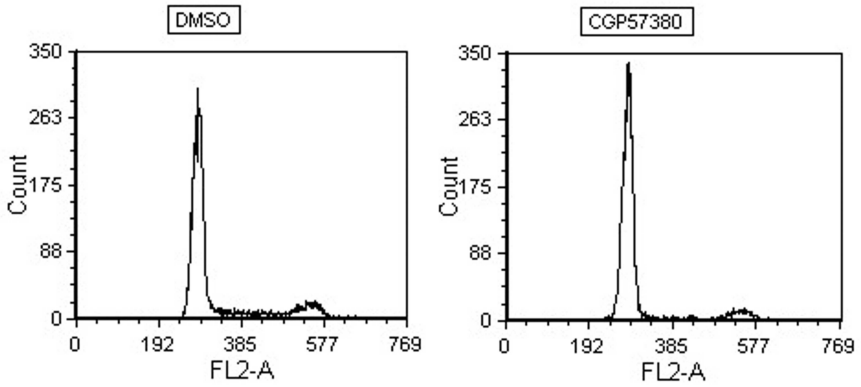

b

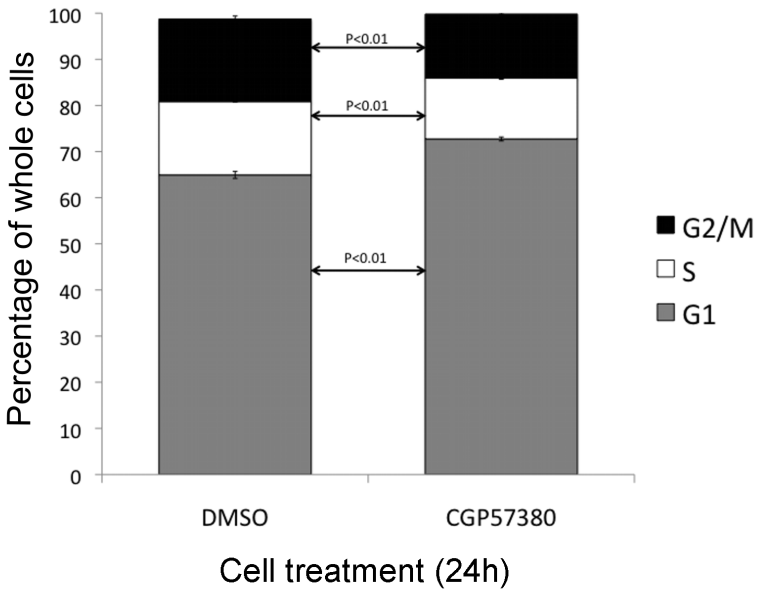

Figure 4:11 Cell cycle analysis following treatment with CGP57380
MDA-MB-231 cells were treated with CGP57380 20 μM, or DMSO vehicle control for 24 h. Cells were trypsinised with all washes retained and fixed in cold ethanol. Cells were resuspended in PBS, stained with propidium iodide and analysed by flow cytometry. a Example flow cytometry plots of fluorescence (FL2-A) against events. b quantification of cell cycle distribution from triplicate repeat experiments. Error bars represent standard error of the mean. Statistical analysis by Student's t-test.

4.7. Discussion

These results have shown that CGP57380 can inhibit the proliferation of a range of breast cancer cell lines, including those of luminal, HER2 and basal phenotypes. This both supports the results of Chrestensen et al[73], and extends the findings of sensitivity to inhibition of the MNK proteins in breast cancer cells to include additional phenotypes. Within the relative limitations of the number of cell lines investigated it appears that the presence of the target of CGP57380, phosphorylated eIF4E, predicts for sensitivity to MNK inhibition, rather than an individual phenotype *per se*. This also supports the assertion that the growth inhibitory effects of CGP57380 are specific to its inhibition of the MNK kinases[60], despite the concerns that additional kinases may be targeted by this reagent[124].

The effect of proliferation is modest when using the MTS proliferation assay, which also appears to be misleading in certain cell lines, showing an apparent proliferative effect in ZR75.1 cells. This may be related to the use of an assay which measures metabolic activity as a surrogate for proliferation, which may be inappropriate in the context of inhibition of pathways which regulate critical cellular functions.

A more marked effect was seen using a colony forming assay. This may be due to the increased cellular stress involved in re-plating the cells at low density through anoikis. It is recognised that lack of cell-matrix interaction has the ability to induce apoptosis in a specific manner through the process termed anoikis[158]. Many intracellular signaling pathways are involved in the maintenance of cell survival via interactions with the extra-cellular matrix. These include both the MAPK[159] and PI3K/AKT[160] signaling pathways both of which interact through eIF4E. It may be therefore that intact signaling through one or both of these pathways is required to maintain cell integrity during periods of cellular stress due to lack of either cell-cell interaction or contact with extra-cellular matrix, conditions which may be mimicked by plating at extreme low density. Thus interruption of normal eIF4E function through inhibition of the MNK kinases may result in increased sensitivity to anoikis. This may manifest as a more marked effect on proliferation when using an assay such as the colony forming assay investigated in the experiments described above.

The combination of CGP57380 with a cytotoxic chemotherapy drug shows a protective effect, with less effect on growth inhibition from the combination of

etoposide and CGP57380 than seen with etoposide alone. This result would be consistent with CGP57380 having a cytostatic rather than a cytotoxic effect. If CGP57380 were to cause cell cycle arrest, then this may protect the cells from the effects of etoposide, a topoisomerase II inhibitor, which increases in cytotoxicity as cells progress through S and G2/M phases of the cell cycle[161].

These findings are consistent with both live cell imaging experiments and cell cycle analysis which show a dominant effect on mitotic events and cell cycle arrest, rather than an increase in apoptosis.

Immunoblotting confirmed inhibition of eIF4E phosphorylation at the dose of CGP57380 used. The kinetics of inhibition of eIF4E phosphorylation varied between cell lines with BT474 cells showing inhibition of phosphorylation within 15 min, whereas MDA-MB-231 cells showed a gradual inhibition over the 72 h time period investigated. Several mechanisms may explain this difference, for example variation in intracellular handling of CGP57380, either through degradation, or export. The recent identification of the phosphatase for eIF4E, protein phosphatase 2A[76], may provide an alternative explanation for the difference with differential expression of this phosphatase between cell lines representing another possible explanation for the varying kinetics of dephosphorylation. These experiments additionally confirmed inhibition of cyclin D1 protein, a key regulator of the cell cycle. Other groups have shown eIF4E phosphorylation to be critical in cyclin D1 regulation through promoting mRNA nuclear export[12,13]. In these experiments inhibition of eIF4E phosphorylation has been linked to both a reduction in cyclin D1 protein, and subsequent G1 cell cycle arrest.

5. MNK kinase inhibition in renal cancer cell lines

5.1. Introduction

Renal cancer is an attractive target in which to investigate sensitivity to inhibition of the MNK proteins. The majority of clear cell renal cancers harbour mutations, deletions or hypermethylation of the VHL gene, causing a constitutive up-regulation of HIFα[137,138]. This is already a therapeutic target in clinical use via inhibition of mTOR with temsirolimus[17] and everolimus[18], however inhibition of mTOR can lead to increased eIF4E phosphorylation in cell culture model systems[20]. Of note, the rapalog mTOR inhibitors such as those described above are allosteric inhibitors of mTOR function and not ATP competitive inhibitors of mTOR kinase. As such they have specific activity against mTORC1 (Rictor) with no activity against mTORC2. S6kinase, a target of activated mTOR has a negative feedback role in inhibiting insulin receptor substrate 1 activity, however when inhibited with agents such as the rapalogs this feedback is lost. As a result increased signalling through mTORC2 can result in increased AKT activity, and may explain the relatively modest activity of the rapalogs in advanced renal cancer. mTOR kinase inhibitors currently in pre-clinical development have a dual effect on both mTORC1 and mTORC2 and thus may have more promising activity in the clinical setting. Stabilisation of disease rather than measurable reductions in disease burden are usually seen with currently available mTOR inhibitors, and the impact on survival is modest. Temsirolimus has shown an increase in survival from 7.3 to 10 .9 months when compared with interferon alpha in patients with poor risk advanced renal cancer[17].

HIFα mRNA has been identified as being regulated by eIF4E phosphorylation[74]. In addition a screen for novel agents showing inhibition of HIF1α revealed a quassinoid compound able to inhibit HIF1α protein via translation control though eIF4E phosphorylation[162]. Thus inhibition of the MNKs may also inhibit proliferation in kidney cancer cell lines.

Clear cell renal cell cancers exhibit high levels of VEGF[163], a gene regulated by HIF activity. Inhibition of VEGF is a current therapeutic strategy with the monoclonal antibody bevacizumab[154], which binds circulating VEGF, preventing binding to the VEGF receptor. Sunitinib, a multi targeted kinase inhibitor has

activity against the kinase domains of both VEGF and PDGF receptors and as such is another proven therapeutic strategy targeting VEGF signaling[164]. Sorafenib, a multi-targeted agent with activity against VEGF also has activity against RAF and is active in advanced renal cancer in patients who have failed first line interferon therapy[165]. Additional agents are in development including pazopanib, a multi targeted agent active against VEGF, PDGF and c-KIT[166], and axitinib which has an increased potency specifically for the VEFG receptors 1, 2 and 3[167].
Following activation of VEGF receptors, signaling occurs through both the MAPK and PI3K pathways. As such targeting kinases such as the MNKs which act at a node of convergence of these cascades is an attractive therapeutic strategy.

Growth inhibition of CGP57380 was investigated in a panel of kidney cancer cell lines representing VHL wild-type and VHL mutant tumours.

Cell line	ACHN	CAKI 2	786-O	769-P	A-498
VHL status	WT	WT	Null	Null	Null
Mutation			1 bp deletion	Promoter hypermethylation Point mutation	4 bp deletion
Effect			Stop codon	Inhibition of transcription Proline-Serine codon 2	Stop codon

Table 5:1 Characteristics of renal cancer cell lines
VHL Von Hippel Lindau, WT Wild type, bp base pair[168]

5.2. Effects of CGP57380 on eIF4E phosphorylation

To confirm the activity of CGP57380 on inhibiting eIF4E phosphorylation, ACHN and A498 cell lines were chosen as examples of VHL wild-type and null cancers respectively. Immunoblotting was used to investigate the effects of CGP57380 on eIF4E phosphorylation, and known downstream targets. ACHN cells showed a rapid reduction in eIF4E phosphorylation after 1 hour of treatment with CGP57380 at 20 μM which was sustained for 8 hours, with no change in eIF4E phosphorylation in control cells assessed untreated at baseline, and with DMSO vehicle control at 4 and 8 h. A reduction in both cyclin D1 and Mcl-1 was seen after

4 h of treatment. This was sustained for both proteins to 8 h by which time there was almost complete loss of Cyclin D1 protein (fig 5:1).
A498 cells were less sensitive to inhibition of eIF4E phosphorylation. eIF4E phosphorylation was inhibited after 1 h, and remained undetectable for 8 h. A reduction in Cyclin D1 was seen by 3 h, but was less pronounced than that seen in ACHN cells. An apparent increase in cyclin D1 protein is seen in the three control samples and as such when each control time point is compared with the treated sample at the same time point, a reduction in cyclin D1 is indeed noted. A more marked reduction in Mcl-1 was seen, first apparent by 3 h and then sustained until 8h. (fig 5:2).

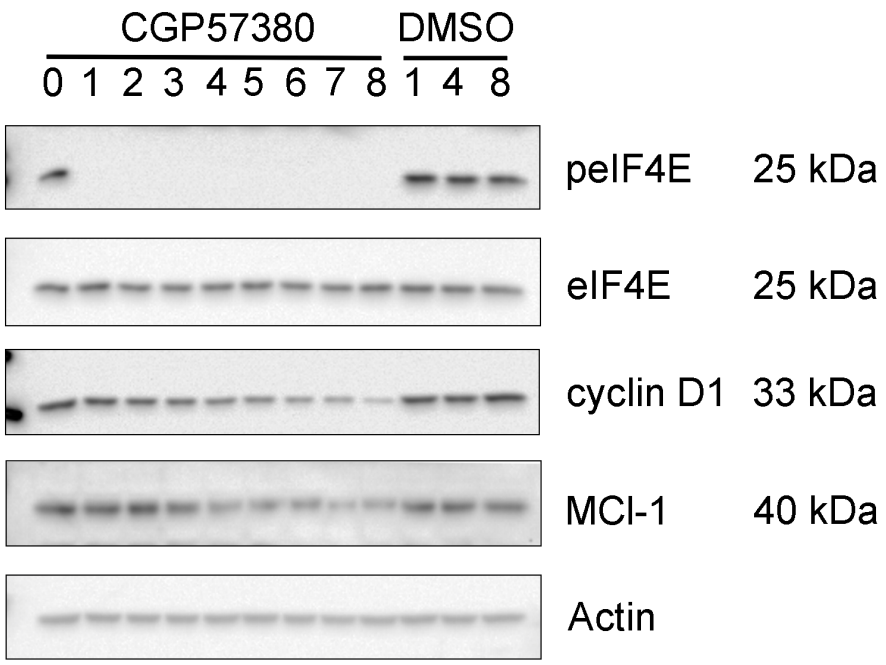

Figure 5:1 Phosphorylated eIF4E and downstream targets
ACHN cells were treated with CGP57380 at 20 μM or 0.5% DMSO vehicle control for times as indicated. Time 0 represents untreated control. Cells were lysed with urea lysis buffer and proteins quantified. Equal amounts of protein were separated by PAGE. Immunoblotting was used to identify individual proteins as indicated.

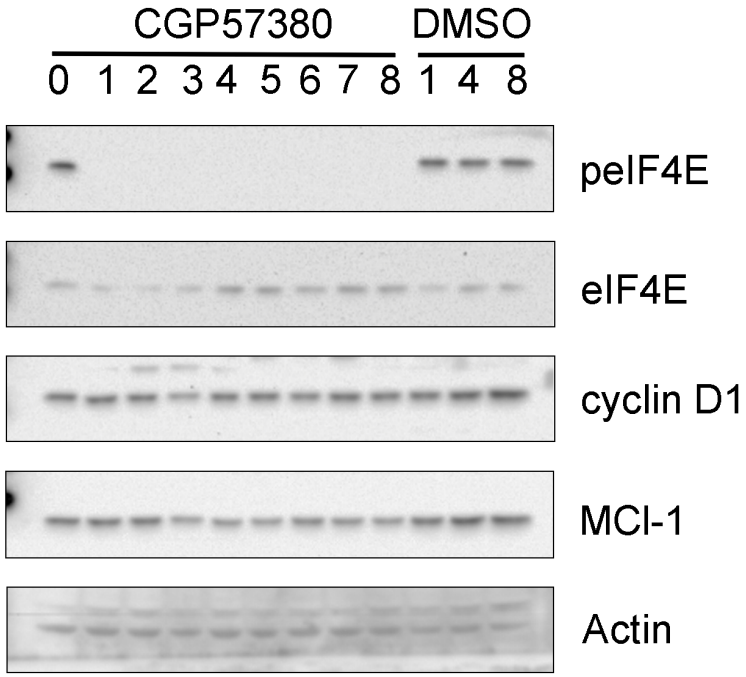

Figure 5:2 Phosphorylated eIF4E and downstream targets
A498 cells were treated with CGP57380 at 20 μM or 0.5% DMSO vehicle control for times as indicated. Time 0 represents untreated control. Cells were lysed with urea lysis buffer and proteins quantified. Equal amounts of protein were separated by PAGE. Immunoblotting was used to identify individual proteins as indicated.

5.3. Effects of CGP57380 on proliferation

Having demonstrated an effect on the cell cycle regulatory protein cyclin D1, and the anti-apoptotic protein MCl-1, the effect of MNK inhibition with CGP57380 on proliferation was assessed. As with the breast cancer cell lines, increasing numbers of cells were plated in 96 well plates and treated with CGP57380 at a variety of concentrations. The MTS assay was used to assess proliferation at 72 h (fig 5:3). Pre-confluent cell numbers were chosen for statistical analysis (fig 5:4). Although an apparently greater response was seen in all renal cancer lines than the breast cancer lines, statistically significant differences were only seen in the two VHL null lines, 786-O and 769-P.

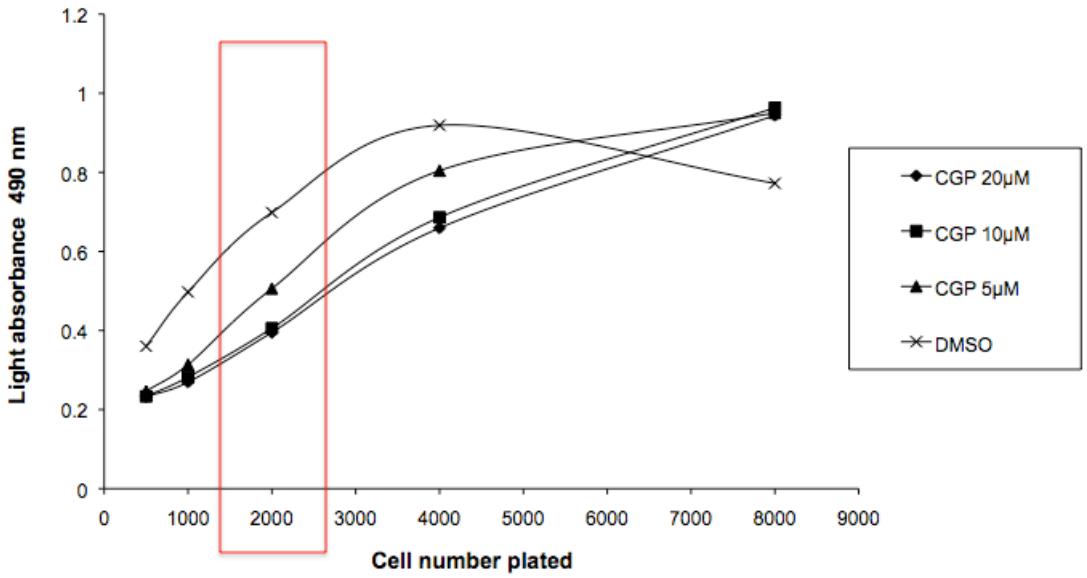

Figure 5:3 Proliferation in response to CGP57380
ACHN cells were plated at the numbers shown in 120 μl medium. 24 h later 110 μl medium was removed from each well and DMSO or CGP57380 added to give a final concentration as shown with 0.5% v/v DMSO vehicle control. 100 μl medium was returned to the well, and proliferation assessed 72 h later by the MTS assay. Results represent the mean of three separate experiments performed in triplicate. Highlighted results are those used for subsequent statistical analysis.

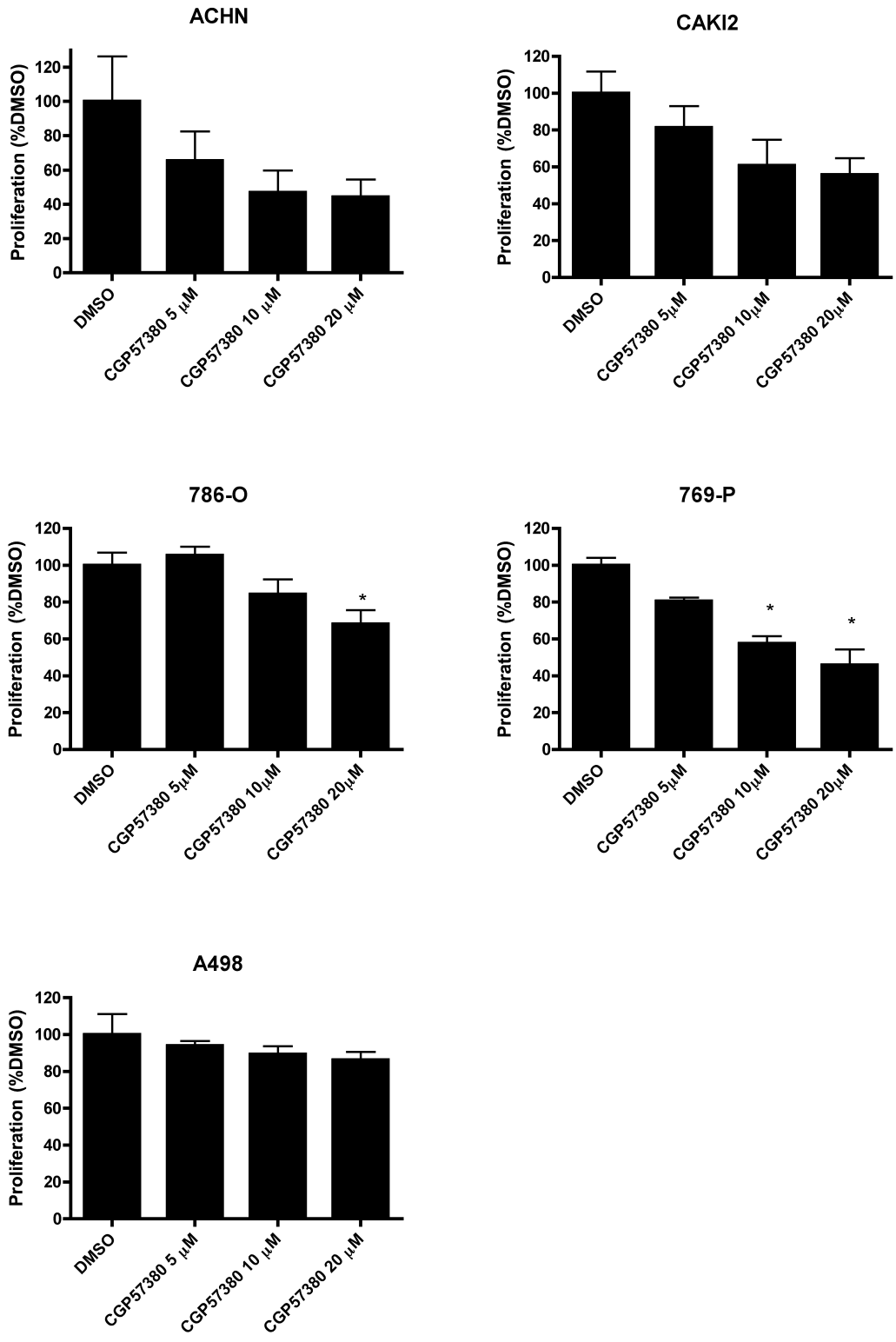

Figure 5:4 Proliferation in response to CGP57380
Cells were plated to 96 well plates in 120 μl medium. 24 h later 110μl medium was removed and CGP57380 added to give a final concentration as shown in 0.5% v/v DMSO vehicle. Proliferation was assessed using the MTS assay 72 h later. Results represent the mean of 3 experiments at plating cell numbers immediately below peaking of the MTS/cell number response curve. *=$p<0.05$. Statistical analysis was by ANOVA with Tukey post test.

Due to uncertainty about the results obtained with the MTS assay in the context of CGP57380 an alternative proliferation assay was investigated. The CyQuant Direct assay uses a cell permeable nucleic acid stain to identify viable cells. A second quenching dye which is only permeable in dead or dying cells which have lost membrane integrity is added to exclude dead cells.

Using this assay the effects of proliferation on A498 cells was investigated in response to increasing concentrations of CGP57380. Maximal inhibition of proliferation occurred with CGP57380 20 μM with a small amount of inhibition at 10 μM but no effect on proliferation with 5 μM (fig 5:5).

Although all renal cell lines investigated with the MTS assay showed an anti-proliferative response following treatment with CGP57380, once again a colony forming assay was used as a more sensitive measure of proliferation. All of the cell lines investigated, both VHL wildtype (CAKI2 and ACHN) and VHL null (A498, 769-P and 786-0) showed a marked anti-proliferative response to CGP57380 with either a reduction in, or complete absence of, colony formation in the CGP57380 treated cells (fig 5:6).

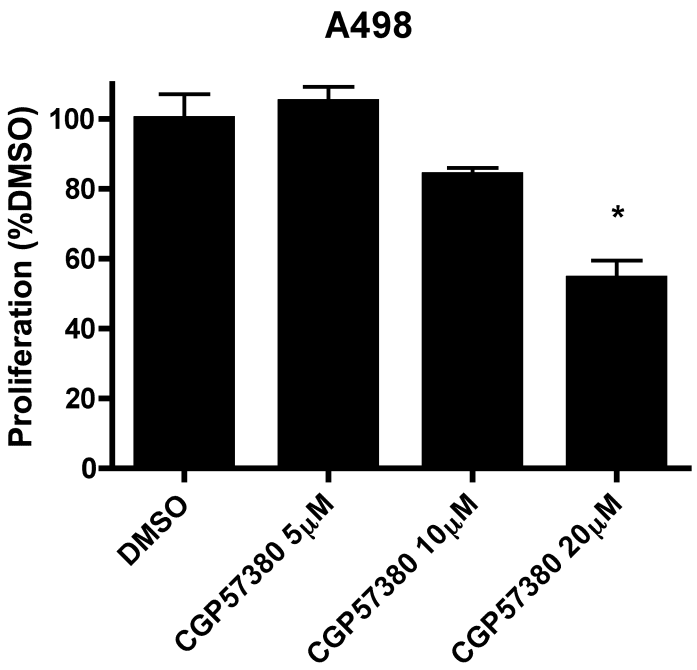

Figure 5:5 Proliferation in response to CGP57380. A498 cell line
A498 cells were plated at 1000 cells per well in 120 μl medium in 96 well plates. 24 h later 110 μl medium was removed from each well and pooled for triplicate repeats. CGP57380 was added to the medium to give a final concentration as indicated with 0.5% v/v DMSO. 100 μl was returned to each well. At 72 h proliferation was analysed using the CyQuant assay. Results represent triplicate repeats in a single experiment. Statistical analysis by ANOVA with Tukey post test.

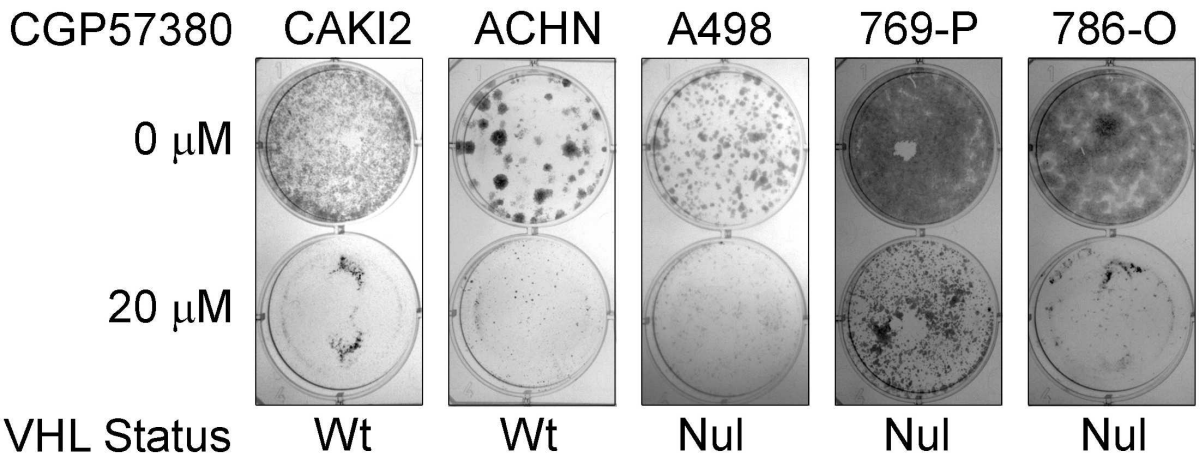

Figure 5:6 Colony assay in response to CGP57380
0.5 X 10^6 cells were plated in 3 ml complete medium. At 24 h cell lines as indicated were treated with 0.5% DMSO vehicle control or CGP57380 20 μM for 24 h. Cells were then trypsinised, counted and re-plated at 1000 cells/well in 6 well plates, in medium containing CGP57380 20μM or 0.5% DMSO as previously. At 9-12 days, according to growth kinetics between lines, colonies were fixed in methanol and stained with Giemsa. Pictures are representative of triplicate wells.

5.4. Mechanisms of inhibition of proliferation by CGP57380

As both the short term proliferation assays (MTS and CyQuant) and the colony assay may represent effects of either cell cycle arrest, or apoptosis, cell cycle analysis using flow cytometry was used to assess the predominant mechanism of growth inhibition. Both ACHN and A498 cell lines were investigated. Cells were plated and subsequently treated for 24 h with either CGP57380 at 20 μM, or DMSO control. Cells were then assessed for cell cycle distribution by harvesting, fixing in ethanol and staining with propidium iodide. DNA content was assessed by flow cytometry. In both cases cells accumulated in G1 with no significant change in the sub-G1 fraction, representing fragmented, apoptotic cells (fig 5:7 and fig 5:8). The accumulation in G1 is consistent with the results of immunoblotting in these cell lines, showing a reduction in the cell cycle regulatory protein cyclin D1. Both ACHN and A498 cells showed a reduction in Mcl-1 protein on immunoblotting in response to CGP57380, however this was not associated with an accumulation of cells in the sub-G1 fraction on cell cycle analysis.

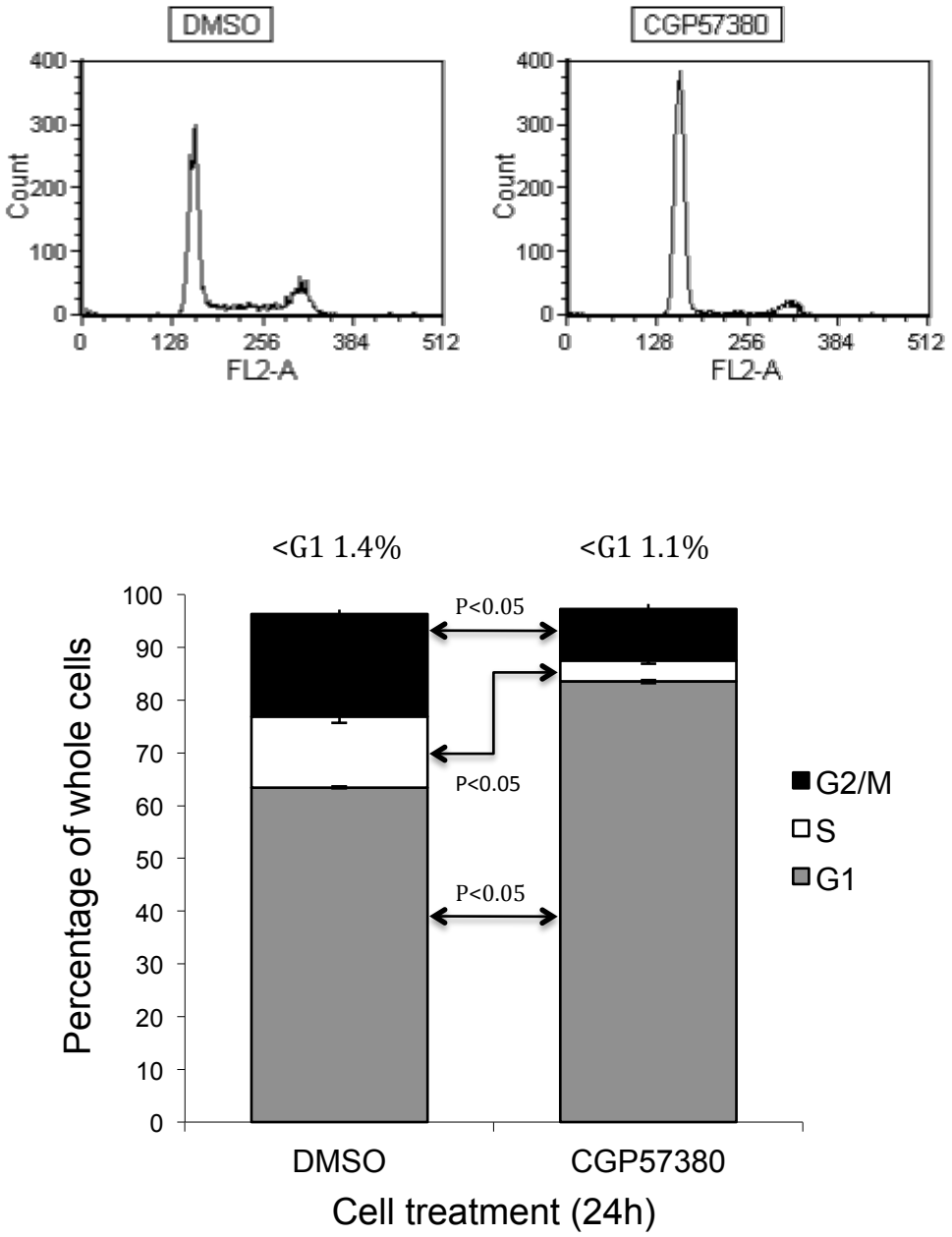

Figure 5:7 Cell cycle analysis following treatment with CGP57380
ACHN cells were treated with CGP57380 20 μM, or DMSO vehicle control for 24 h. Cells were trypsinised with all washes retained and fixed in cold ethanol. Cells were resuspended in PBS, stained with propidium iodide and analysed by flow cytometry. Upper panel shows representative flow cytometry plots from single experiment. Results are mean of triplicate repeat experiments. Statistical analysis by Student's t test.

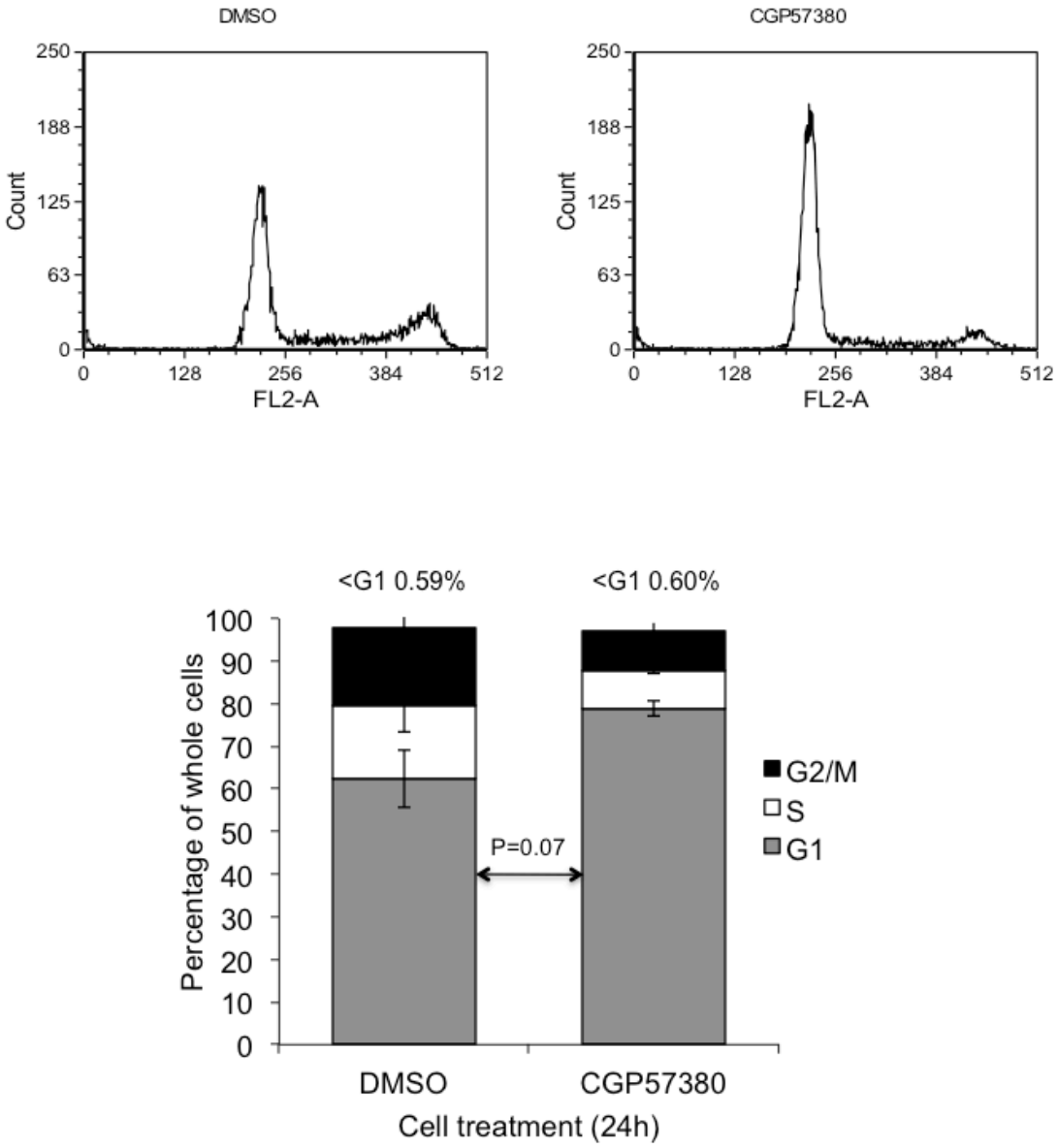

Figure 5:8 Cell cycle analysis following treatment with CGP57380
A498 cells were treated with CGP57380 20 μM, or DMSO vehicle control for 24 h. Cells were trypsinised with all washes retained and fixed in cold ethanol. Cells were resuspended in PBS, stained with propidium iodide and analysed by flow cytometry. Statistical analysis by t-test. No comparisons reached statistical significance.

Although no accumulation in the sub G1 fraction was seen during cell cycle analysis, a more specific assay for the investigation of apoptosis was used. Cells were treated with either CGP57380 or DMSO vehicle control and then co-stained with FITC conjugated Annexin-V and propidium iodide (PI). During early apoptosis phosphotidylserine translocates from the inner to the outer cell membrane. Annexin-V has a high affinity for phosphotidylserine and therefore stains cells in early apoptosis. Cells in later apoptosis, and those undergoing necrosis, lose membrane integrity and become permeable to the DNA binding dye propidium iodide. Thus when stained with both compounds, live cells stain with neither annexin-V or propidium iodide, early apoptotic cells stain with Annexin V alone, and cells in late apoptosis or undergoing necrosis stain with both Annexin-V and PI.

Both A498 and ACHN cells were treated with either CGP57380 at 20 μM or DMSO vehicle control for 8 h and 24 h. Staurospaurine was used as a positive control. In both cell lines no increase in either early or late apoptosis was seen at either time point, confirming the predominant mechanism of inhibition of proliferation as cell cycle arrest (fig 5.9).

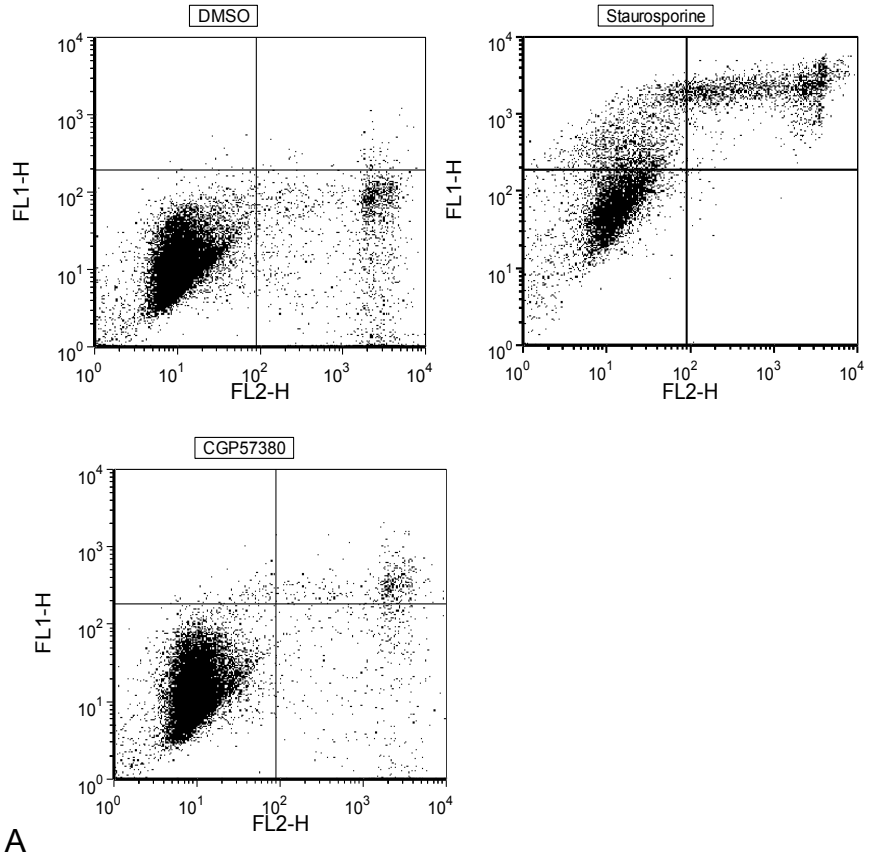

A

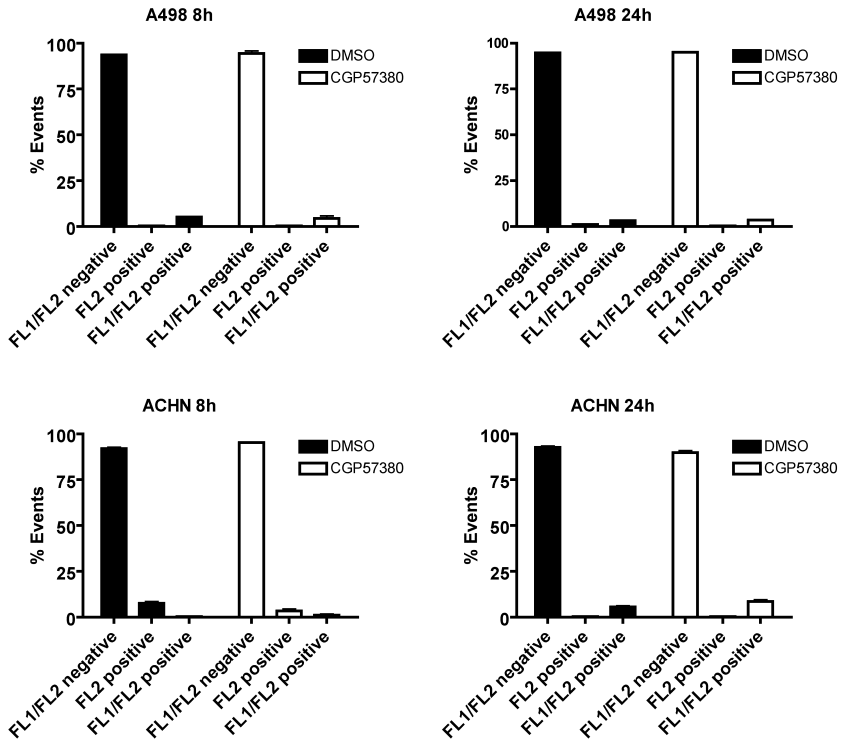

B

Figure 5:9 Effects of CGP57380 on induction of apoptosis
A498 and ACHN renal cancer cells were treated with CGP57380 20 μM, 0.5% DMSO vehicle control or staurosporine 20nM. Following harvesting by trypsinisation and dual staining with Annexin V and propidium iodide, cells were analysed by flow cytometry at time points as indicated. A) example FACS plots following 8 h treatment. B) percentage of cells alive (FL1/FL2 negative), early apoptosis (FL2 positive only) and late apoptosis (FL1/FL2 positive). Bars represent mean and standard error of triplicate samples.

5.5. CGP57380 in combination with mTOR inhibition

Previous work has shown an increase in eIF4E phosphorylation in lung cancer cells following inhibition of mTOR with rapamycin[20]. mTOR inhibition is now an established therapeutic strategy in renal cancer with the rapalogue mTOR inhibitors temsirolimus[17] and everolimus[18]. It is possible that the increase in eIF4E phosphorylation induced by mTOR inhibition could attenuate the anti-proliferative effects of mTOR inhibition in renal cancer cells, and as such the combination of mTOR inhibition with inhibition of the MNKs may induce enhanced antiproliferative effects in renal cancer cells.

A498 and CAKI 2 renal cancer cells were investigated following treatment with the mTOR inhibitor rapamycin, or CGP57380 or both compounds in combination. Western blot analysis was used to investigate the effect of each compound on eIF4E phosphorylation, and 4E-BP phosphorylation (fig 5:10). In A498 cells there was no increase in eIF4E phosphorylation seen in response to treatment with rapamycin, however eIF4E phosphorylation was inhibited by both CGP57380 alone and in combination with rapamycin. Loss of 4E-BP phosphorylation was seen in response to treatment with rapamycin both alone and in combination with CGP57380 as indicated by loss of the higher molecular weight bands, suggesting that rapamycin was inhibiting mTOR at the concentration used. In CAKI 2 cells there was an increase in eIF4E phosphorylation seen following treatment of cells with rapamycin, however this was inhibited by the addition of CGP57380. Once again loss of 4E-BP phosphorylation was seen in response to treatment with rapamycin, both alone and in combination with CGP57380.

Subsequently the antiproliferative effects of treatment with rapamycin and CGP57380 were investigated in these cell lines (fig 5:11). Both lines showed an inhibition of proliferation in response to CGP57380 as previously documented. A498 cells were sensitive to treatment with rapamycin with a similar anti-proliferative effect to that seen with CGP57380. When cells were treated with both compounds in combination a modestly enhanced effect was seen on proliferation compared to either compound used alone.

CAKI 2 cells showed no effect on proliferation when treated with rapamycin alone, however when treated with both rapamycin and CGP57380 an anti-proliferative

effect at least as substantial as that seen with CGP57380 alone was seen with the suggestion of an enhanced effect.

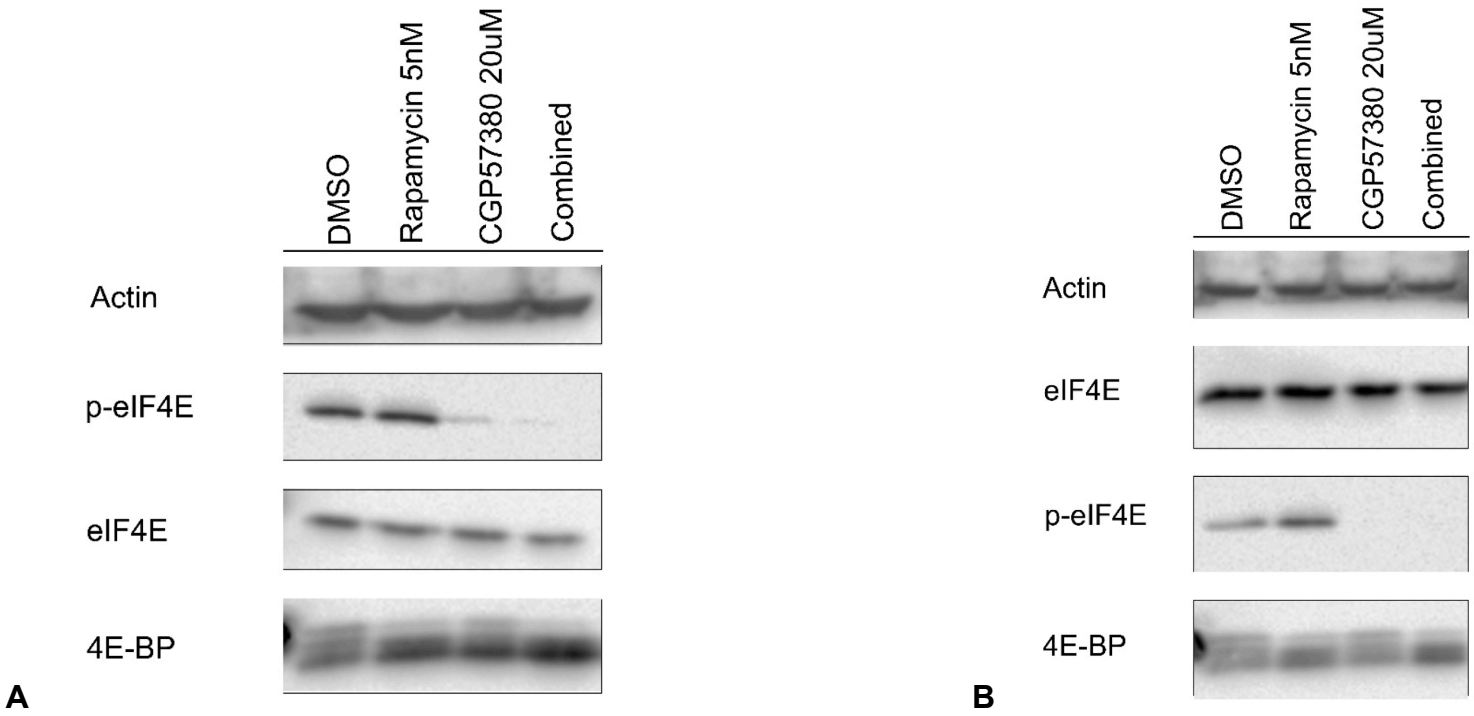

Figure 5:10 A498 and CAKI 2 cells treated with rapamycin and CGP57380
A498 (A) and CAKI 2 (B) cells were treated with 0.5% DMSO vehicle control, rapamycin, CGP57380, or both in combination for 24 h at concentrations as indicated. Cells were harvested and proteins extracted by urea lysis. Equal amounts of protein were separated by PAGE and individual proteins identified by western blotting. 4E-BP was probed with a non-phospho antibody. The upper two bands represent higher molecular weight phosphorylated protein and the lower band un-phosphorylated 4E-BP (Experiment performed by GB)

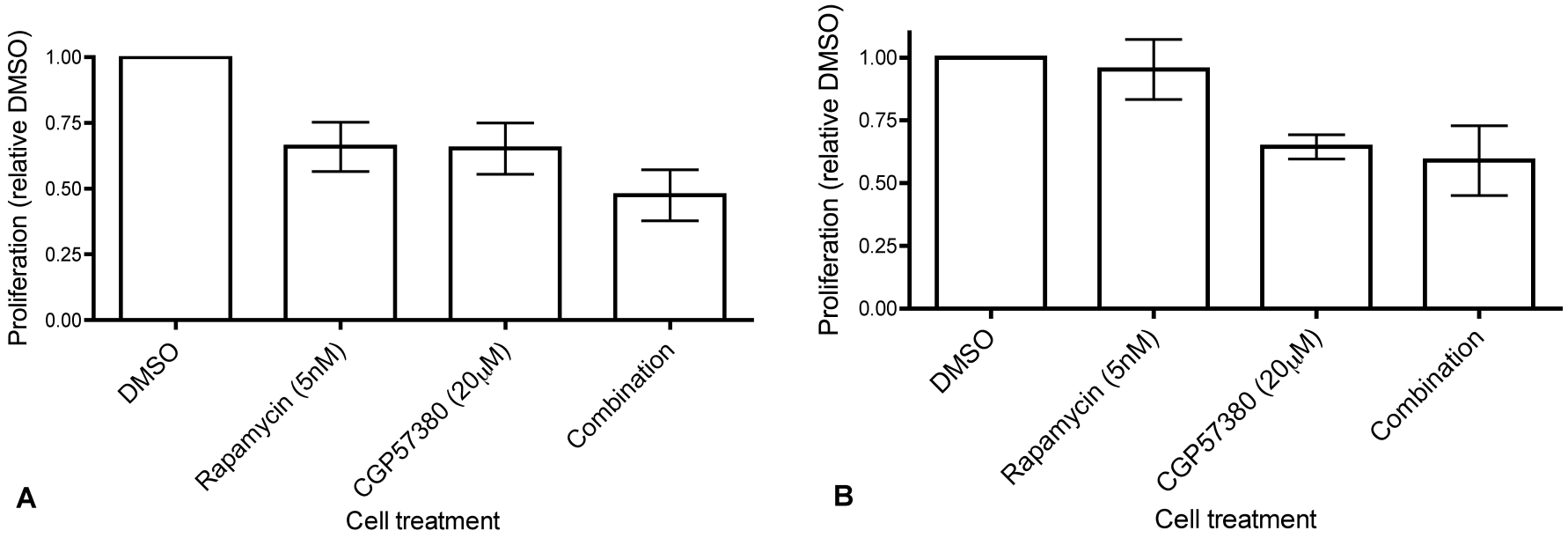

Figure 5:11 Proliferation following treatment with rapamycin and CGP57380
A498 (A) and CAKI 2 (B) cells were treated with 0.5% DMSO vehicle control, rapamycin, CGP57380 or the combination at concentrations as indicated. Proliferation was measured at 72 h using the CyQuant assay. Results are mean and standard error of triplicate wells normalised to DMSO control. (Experiment performed by GB)

5.6. Specificity of CGP57380

MNK inhibition with siRNA

Bain et al have investigated the specificity of a panel of protein kinase inhibitors, including CGP57380, and have raised concerns about the specificity of the compound for the MNK proteins[124]. With this in mind alternative strategies of inhibiting the MNK proteins, and thus eIF4E phosphorylation have been sought in order to demonstrate that the specificity of the effects of CGP57380 are through inhibition of eIF4E phosphorylation.

One strategy to achieve this is the use of RNA interference with siRNA duplexes. By inhibiting the MNK proteins at the RNA level and repeating the assays described above it may be possible to confirm that the growth inhibitory effects of CGP57380 are indeed through inhibition of eIF4E phosphorylation by the MNKs. Two siRNA duplexes were obtained for each of MNK1 and MNK2. ACHN cells were transfected with a final concentration of siRNA of 50nM. Initially a time course was performed to confirm the effects of the siRNA both on their target molecules and eIF4E phosphorylation. Using a combination of a single MNK1 and single MNK2 duplex, partial inhibition of MNK1 was seen by 24 h which was complete at 48 h and persisted to 120 h (fig 5.12). A MNK2 antibody was obtained from Santa Cruz biotechnology, however despite attempts to optimise the antibody, multiple bands were seen throughout the membrane. A band at the predicted size of 50kDa was however identified which showed a reduced intensity at 24 h and 48 h, but less than that seen for MNK1 (fig 5:12). eIF4E phosphorylation was reduced at 48 h, but never reduced to the extent of that seen through MNK kinase inhibition with CGP57380.

In order to clarify the specificity of the MNK2 antibody, HEK293 human embryonal kidney cells were transfected with a MNK2 vector (pCMVMNK2-HA) or control vector (pCMV) at two vector concentrations, and MNK2 protein measured at 48 h by western blotting. Two clear bands were identified close to the expected size for MNK2, with the band intensity proportional to the concentration of vector transfected. It would be anticipated that the band seen would be slightly larger than the size of endogenous MNK2 (50 kDa) due to the HA tag. The upper of the two

bands correlates with that seen in the cells treated with MNK1 and MNK2 directed siRNA and would suggest that this does indeed represent MNK2.

In order to generate maximal inhibition of the MNK proteins, all four siRNA duplexes were combined in a single experiment to give a final concentration of siRNA of 100 nM. ACHN cells were transfected and samples were assessed at 72 h for inhibition of MNK1 with no band detected in the MNK1/2 transfected cells. No eIF4E phosphorylation was seen in the MNK1/2 transfected cells and a reduction in cyclin D1 protein was also identified, although this was not as marked as that seen with CGP57380 (fig 5:14).

ACHN cells transfected with this combination of four siRNA duplexes were assayed for both proliferation, and cell cycle distribution. Using the CyQuant assay, a small but non-significant effect on proliferation was seen following siRNA transfection (fig 5.15).

Using the colony assay, which was a more sensitive marker of proliferation in both the renal and breast cancer cell lines following treatment with GGP57380, no change in colony forming ability was seen following transfection with siRNA (fig 5:16). Equally the accumulation of cells in G1 of the cell cycle seen with CGP57380 was not seen following siRNA transfection (fig 5:17).

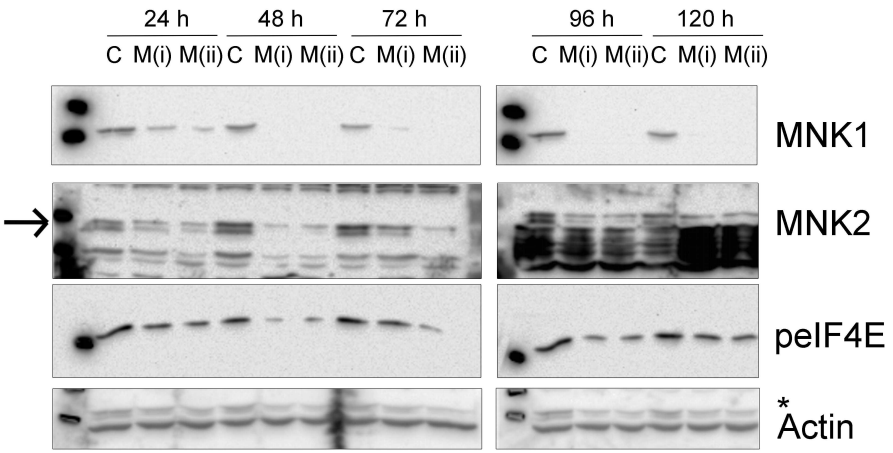

Figure 5:12 ACHN cells transfected with MNK siRNA
0.25 X 10^6 ACHN cells were plated in 6 well plates. 24 h later cells were transfected with a pair of MNK1 and MNK2 siRNA duplexes to a final concentration of 50 nM in 2 combinations (i and ii). Cells were harvested every 24 h, pelleted and snap frozen. Proteins were extracted by urea lysis and quantified. Equal amounts of protein were separated by PAGE and individual proteins identified with immunoblotting. Lanes represent control siRNA (C), MNK1 and MNK2 siRNA combination 1 (M(i)) and MNK1 and MNK2 siRNA combination 2 (M(ii)). Arrow indicates expected size for MNK2.

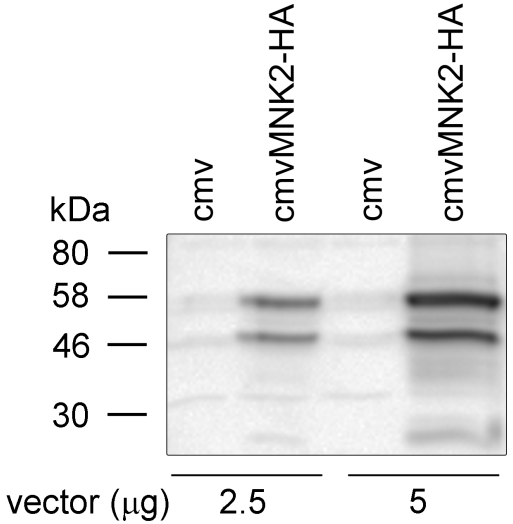

Figure 5:13 HEK293 cells transfected with MNK2 vector
HEK293 cells were transfected with pcmvMNK2-HA or pcmv parent vector using Lipofectamine 2000 transfection reagent (Invitrogen) at vector quantities as shown. Cells were harvested at 48 h and proteins extracted with urea lysis buffer and quantified. Equal quantities of protein were separated by PAGE and transferred to a nitrocellulose membrane. The membrane was probed for MNK2 (expected size 50kDa).

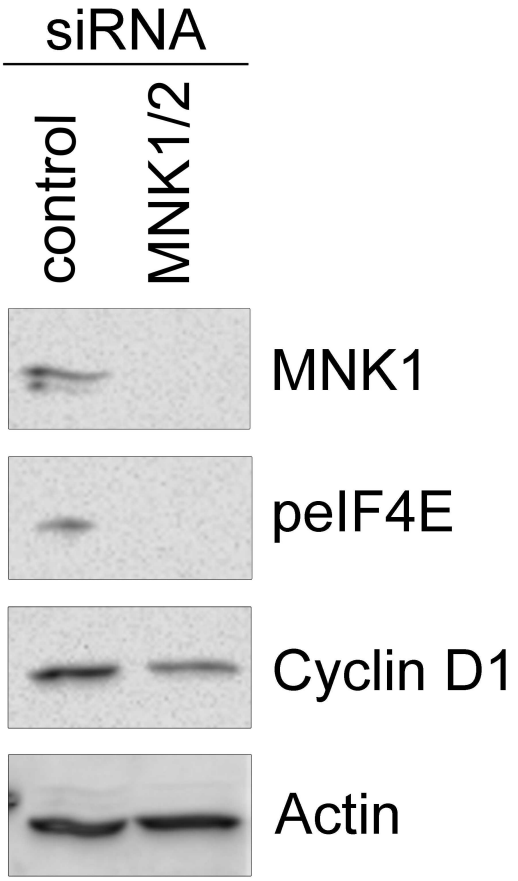

Figure 5:14 ACHN cell line transfected wtih MNK siRNA
siRNA transfection of ACHN cell line at final concentration 100 nM.
0.5 X 10^6 ACHN cells were plated to 60mm dishes. At 24 h cells were transfected with 2 MNK1 and 2 MNK2 siRNA duplexes to a final concentration of 100 nM. 72 h later cells were harvested and proteins extracted by urea lysis. Equal amounts of protein were separated by PAGE and individual proteins were identified with immunoblotting.

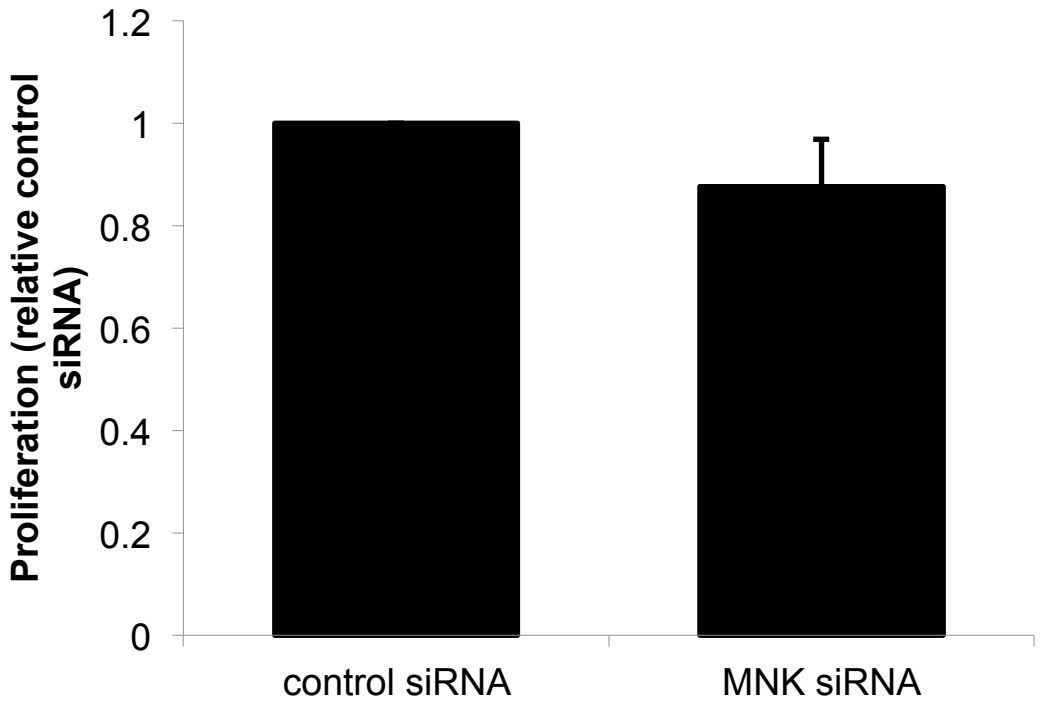

Figure 5:15 Proliferation in ACHN cells following MNK siRNA transfection
Cells were transfected in 6 well plates with 2 siRNA duplexes targeting each of MNK1and MNK2 to a final siRNA concentration of 100 nM. 48 h post transfection cells were trypsinised, counted and replated in 120 μl fresh medium at 1000 cells per well in 96 well plates. 72 h later proliferation was assessed using the Cyquant assay. Results represent mean and standard error of triplicate experiments, each performed with triplicate wells.

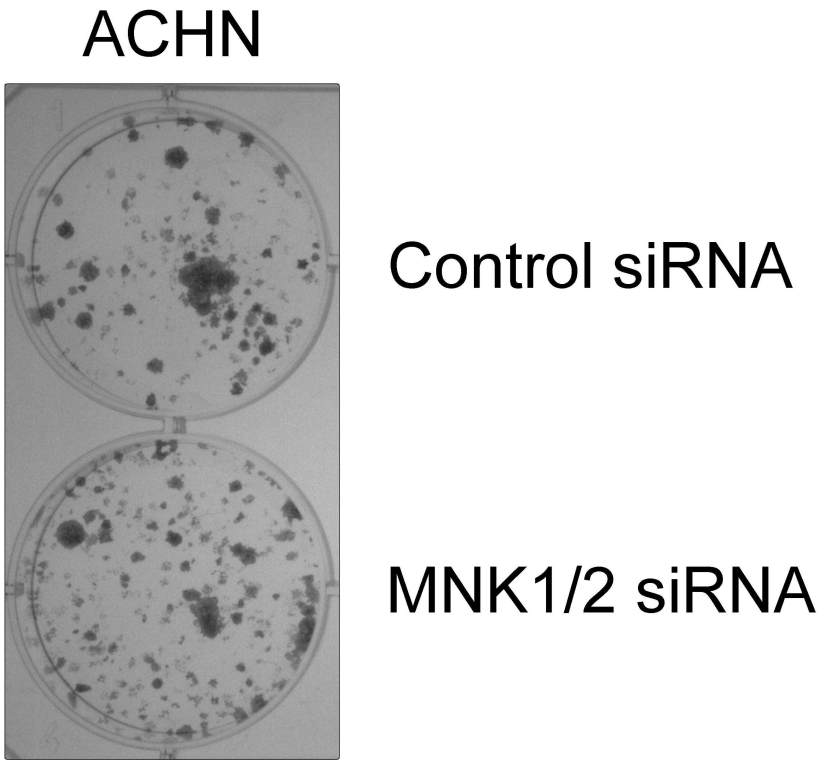

Figure 5:16 Colony assay following MNK1/MNK2 siRNA
0.5 X 10^6 ACHN cells were plated to 60mm dishes. At 24 h cells were transfected with 2 MNK1 and 2 MNK2 siRNA duplexes to a final concentration of 100 nM. At 48 h post transfection cells were trypsinised, counted and re-plated at 1000 cells/well in 6 well plates. At 10 days colonies were fixed in methanol and stained with Giemsa. Pictures are representative of triplicate wells.

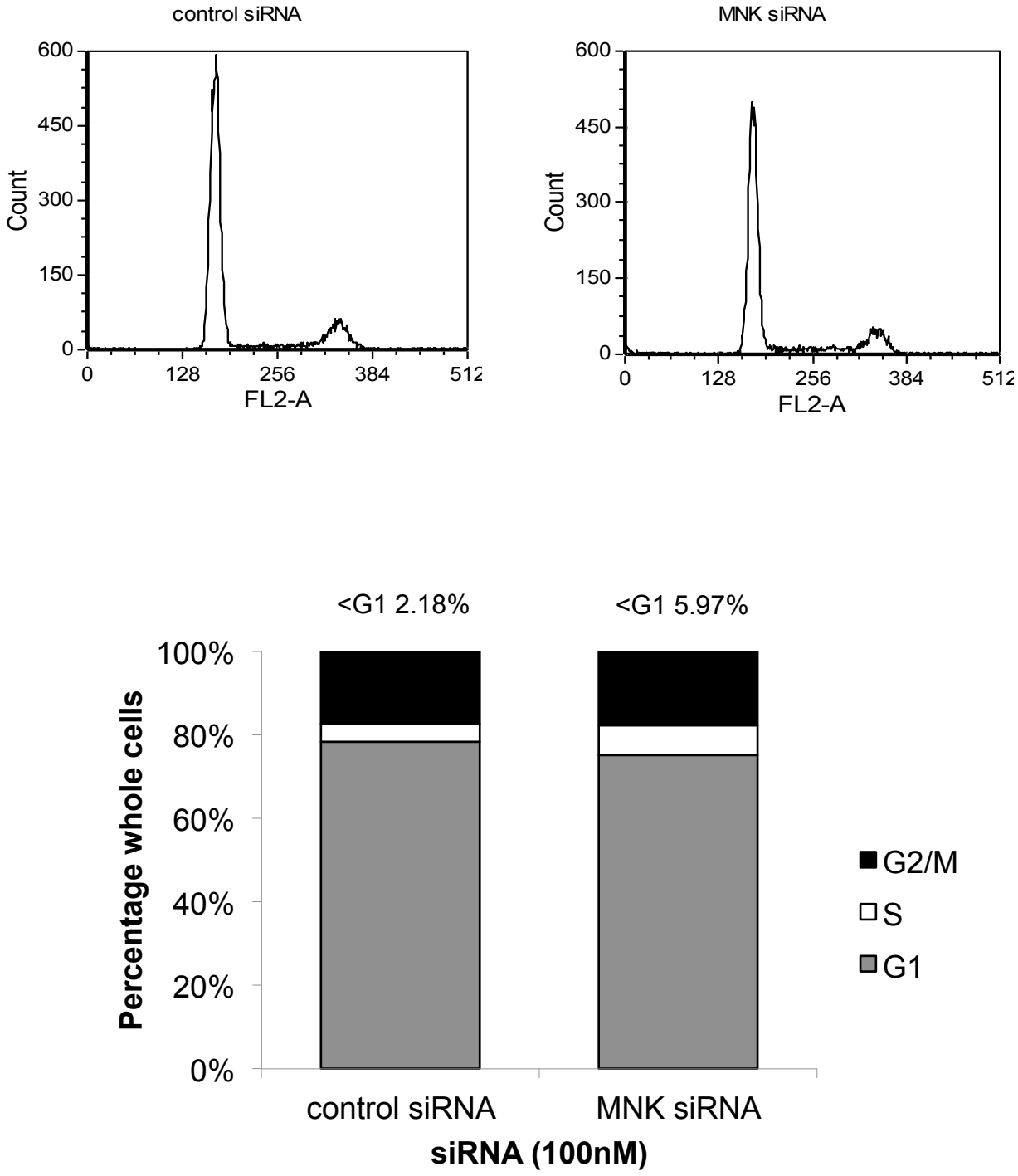

Figure 5:17 Cell cycle analysis following MNK1/MNK2 siRNA
ACHN cells were transfected with 2 duplexes of each of MNK1 and MNK2 siRNA, or control siRNA at a final concentration of 100 nM. At 72 h cells were trypsinised with all washes retained and fixed in cold ethanol. Cells were resuspended in PBS, stained with propidium iodide and analysed by flow cytometry.

Combination of CGP57380 with MNK1 and MNK2 directed siRNA

CGP57380 alone has shown significant effects on the proliferation of kidney cancer cell lines, however siRNA targeted at the MNK proteins has failed to replicate these results. A series of experiments was therefore performed in which the siRNA duplexes were combined with CGP57380, the hypothesis being that removal of the target for CGP57380 might abrogate its effect on proliferation. Cells were transfected with either control siRNA or a combination of four siRNA duplexes targeted at MNK1 and MNK2 at a final concentration of 100 nM. Following this cells were treated with increasing concentrations of CGP57380, and cell pellets harvested at 24 h for protein extraction. Western blotting was used to assess levels of eIF4E phosphorylation in the treated cells. Lower levels of eIF4E phosphorylation were seen in the MNK siRNA treated cells such that no eIF4E phosphorylation could be detected in cells treated with CGP57380 at 5 μM. This was compared with control transfected cells where low levels of eIF4E phosphorylation were still detected following treatment with CGP57380 at 10 μM. (fig 5:18).

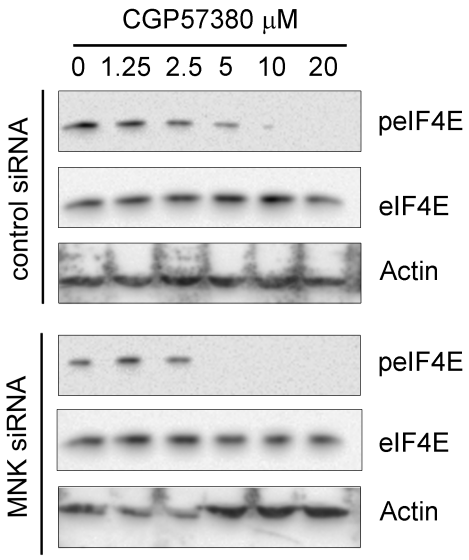

Figure 5:18 eIF4E phosphorylation in response to CGP57380 in MNK directed siRNA transfected cells
Cells were transfected in 6 well plates with a combination of 2 MNK1 directed, and 2 MNK2 directed siRNA duplexes to a final concentration of 100 nM. 48 h post transfection cells were harvested and replated to 6 well plates. 24 h later cells were treated with concentrations of CGP57380 or DMSO vehicle control as shown. At 24 h cells were harvested and proteins extracted by urea lysis. Lysates were quantified and proteins separated by PAGE. Individual proteins were identified by immunoblotting.

Similar experiments were performed to assess the effect on proliferation of adding CGP57380 to control or MNK1 and MNK2 directed siRNA transfected cells. Following transfection with either control, or a combination of 2 MNK1 directed and 2 MNK2 directed siRNA duplexes, cells were re-plated and treated with CGP587380 at increasing concentrations. No differential effect on proliferation was seen between either transfection, either without the addition of CGP57380, or at any of the treated concentrations (fig 5:19)

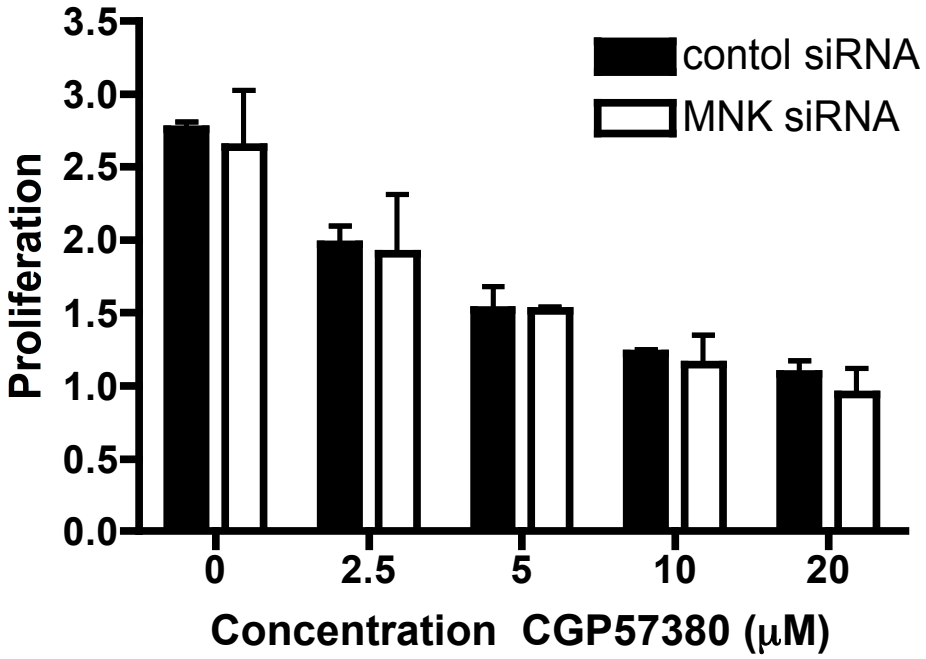

Figure 5:19 Proliferation in ACHN cells transfected with MNK directed siRNA and treated with CGP57380
Cells were transfected in 60mm dishes with either control siRNA at 100 nM, or a combination of 2 MNK1 and 2 MNK2 siRNA duplexes at a final concentration of 100 nM. After 48 h cells were trypsinised, counted and re-plated to 96 well plates at 1000 cells/well. 24 h later cells were treated with CGP57380 at concentrations as shown, or DMSO vehicle control. Proliferation was assessed at 72 h using the CyQuant assay. Results indicate mean and standard error of triplicate wells.

Stable transfection with mutated eIF4E

An alternative strategy to demonstrate the specificity of the CGP57380 compound was to generate stable transfectants of one of the renal cancer cell lines in which the phosphorylation site of eIF4E, serine 209, was mutated to an aspartic acid. The negatively charged aspartate is able to act as a phosphomimetic; in a murine lymphoma model transfection with either wild-type or S209D mutated eIF4E resulted in formation of tumours with a similar latency, whereas mutation of serine 209 to a phosphoresistant alanine resulted in impaired tumour formation[69]. Stable transfection of cancer cells with the eIF4E S209D mutant should make them at least partially resistant to the effects on proliferation of CGP57380.

A498 cells were stably transfected either with parent vector (EYFP-C1) or EYFP-eIF4ES209D and clones selected with G418. Initial screening was performed using fluorescence microscopy to identify EYFP expressing clones. Subsequently cell pellets were lysed for each clone, and eIF4E expression analysed with western blotting (Fig 5:20).

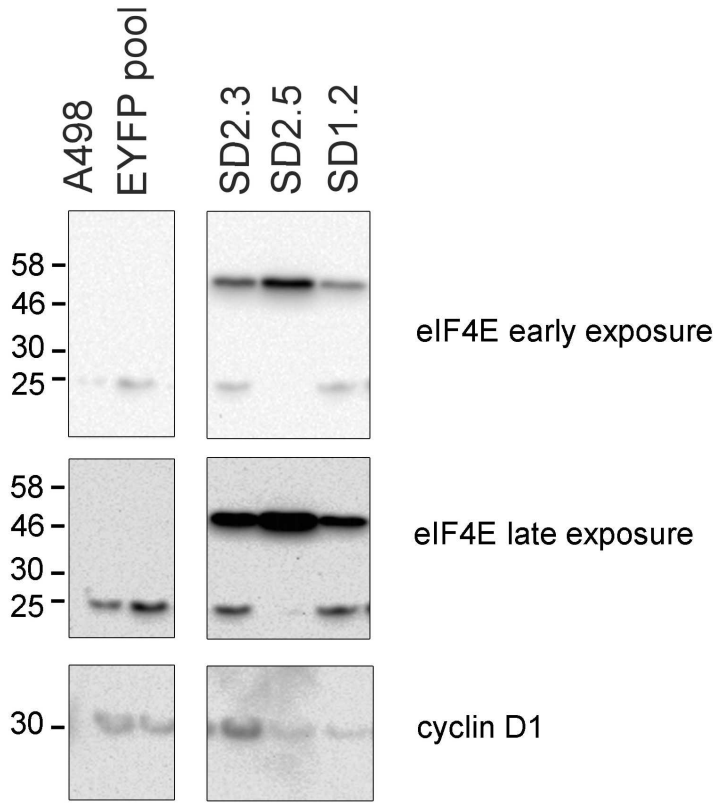

Figure 5:20 Immunoblotting of A498 eIF4E stable clones

A498 cells were stably transfected with EYFP-C1, or an EYFP-eIF4E construct in which serine 209 had been mutated to aspartate (SD). Clones were selected with G418 and individual colonies picked from EYFP-eIF4E-SD transfected cells. For EYFP transfected cells colonies were pooled. Parental cells (A498), pooled transfectants with EYFP, and clones SD2.3, 2.5 and 1.2 were harvested and proteins extracted by urea lysis and quantified. Equal protein was loaded to polyacrylamide gels and separated by PAGE. Individual proteins were identified by immunoblotting.

Both endogenous eIF4E at the expected size of 25 kDa, and the EYFP-eIF4E construct at a predicted size of approximately 50 kDa were detected. There was variation in both expression of the construct and endogenous eIF4E between the clones. Two clones eIF4ESD2.5 and eIF4ESD1.2 had lower levels of cyclin D protein than either another clone, eIf4ESD2.3, or untransfected parental controls. Pooled transfectants with both the EYFP parent vector and EYFP-eIF4ES209D vector were also made. Of interest when the eIF4ESD pool was assayed for eIF4E expression, no second band at the expected size for the construct was seen. When the expression of EYFP was measured in these cells, the size of the band detected with an EYFP antibody was slightly smaller than that seen with the parent EYFP vector. This would suggest not only that the vector had been cut when incorporated stably into the transfected cells, but also a negative selection pressure against the full length eIF4ESD vector, leading to absence of expression in the pooled population (Fig 5:21).

eIF4E is predominantly cytoplasmic in its localisation[12]. To ensure that the EYFP-eIF4E construct was distributed in the expected fashion within the cell, stable tranfectants of EYFP-eIF4ES209D, and EYFP parent were fixed and EYFP subcellular distribution assessed with fluorescence microscopy. Cells expressing the EYFP parent vector showed equal distribution of fluorescence through both nuclear and cytoplasmic compartments, however cells expressing the mutated eIF4E construct showed clear evidence of nuclear exclusion of the fluorescence signal (fig 5:22).

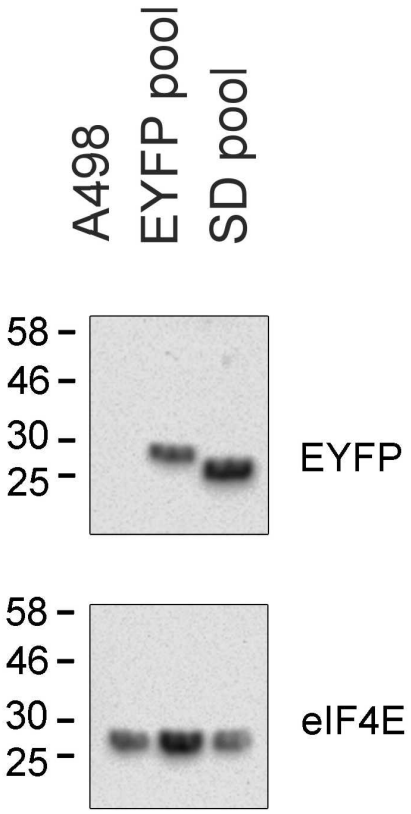

Figure 5:21 Immunoblotting of pooled stable transfectants from A498 cells
A498 cells were transfected with parent EYFP-C1 vector or eIF4E-EYFP with mutation of serine 209 to aspartate (SD). Colonies were selected with G418 and pooled. Cells were harvested and proteins extracted by urea lysis and quantified. Equal protein was loaded to polyacrylamide gels and separated by PAGE. Individual proteins were identified by immunoblotting.

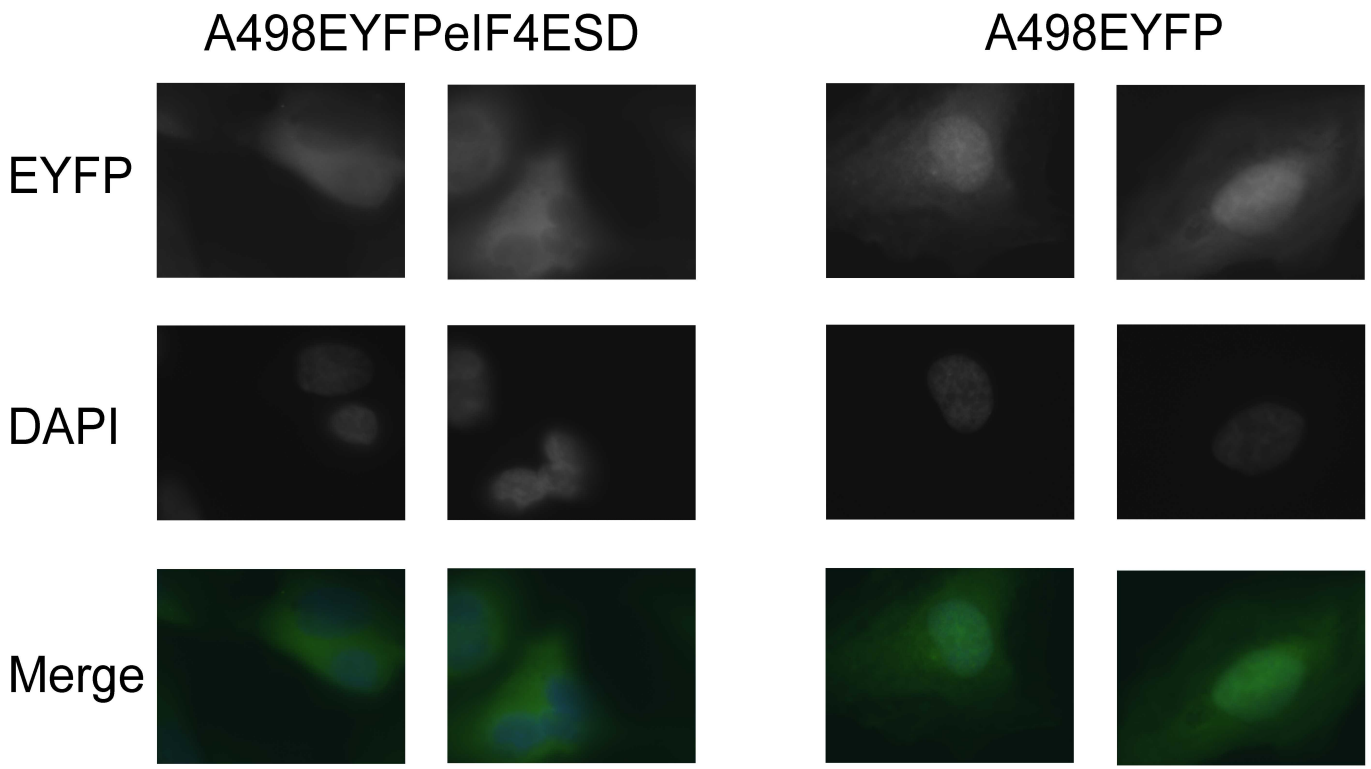

Figure 5:22 Cellular distribution of eIF4ESD protein in stable transfected cells
Stable transfectants of A498 cells were fixed with methanol and counterstained with the nuclear stain DAPI. 2 fields of cells at 100 X magnification were visualised for each tranfectant using fluorescence microscopy, and imaged using a greyscale camera. Green and blue colour was superimposed and merged images created.

The functionality of the construct was additionally investigated using m^7GTP pull down. Functional eIF4E is able to bind the cap analogue m^7GTP, and thus m^7GTP beads were used to extract eIF4E from clarified protein lysates from parent cells, and cells expressing the EYFP-eIF4ES209D construct. Following pulldown the lysates were separated by PAGE and membranes probed with antibody directed at eIF4E. Endogenous eIF4E could be detected in both parent and transfected cells, however in transfected cells the construct at the predicted size of 50 kDa could also be detected confirming the ability to bind the m^7GTP cap. The lack of actin in the pulled down lysates confirms the specificity of the pulldown (fig 5:23).

To investigate the impact of variable eIF4E expression on the growth characteristics of the clones, cells were plated to 96 well plates in triplicate, and growth assessed at 24 h, 48 h, and 96 h using the CyQuant assay. Variability in growth characteristics was seen such that the eIF4ESD2.3 clone in which higher baseline levels of cyclin D1 was seen, grew more quickly than either the untransfected parent cells, or the eIF4ESD2.5 and eIF4ESD1.2 clones. In addition these latter two clones grew more slowly than the untransfected parent cells, in keeping with the lower baseline levels of cyclin D1 protein in these clones (fig 5:24).

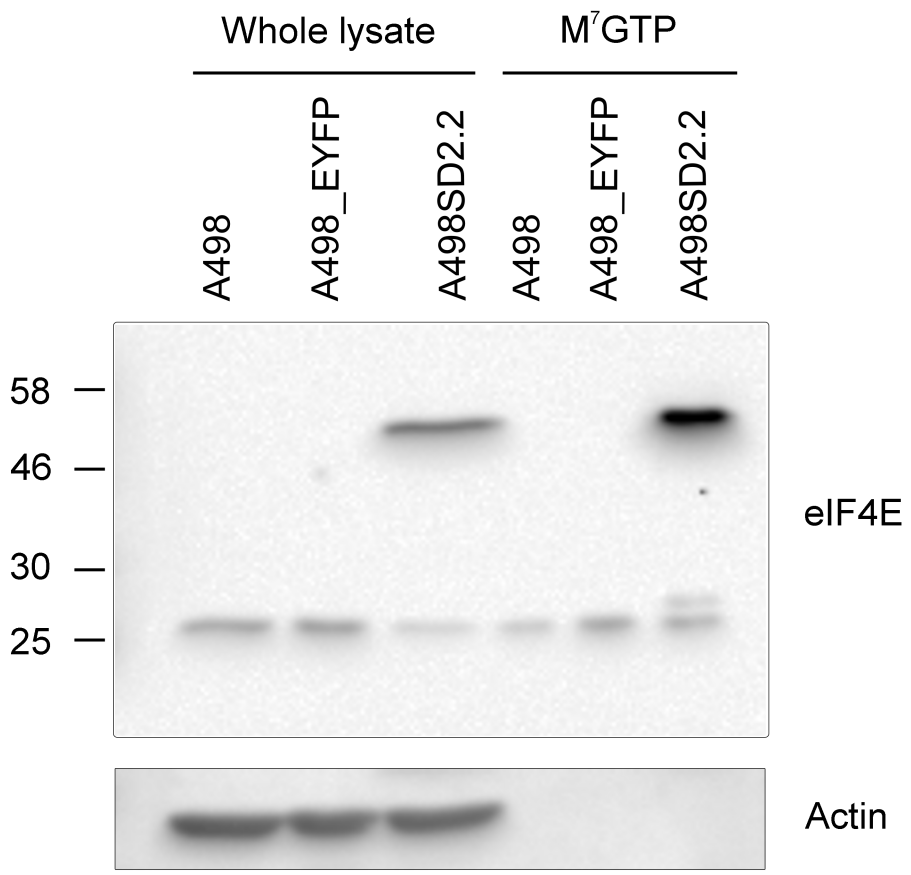

Figure 5:23 m^{7}GTP pulldown of eIF4ESD mutant clones
A498 parental cells, A498_EYFP pooled clones and A498SD2.2 clone cells were harvested, pelleted and snap frozen. Proteins were extracted with extraction buffer, clarified by centrifugation and quantified. Equal amounts of protein were mixed with m^{7}GTP-sepharose. Beads were extracted by centrifugation and washed. m^{7}GTP was used to elute the bound proteins, and the beads pelleted by centrifugation. Equal volumes of supernatant were separated by PAGE, and individual proteins identified with immunoblotting. Whole cell lysates were run as a comparison.

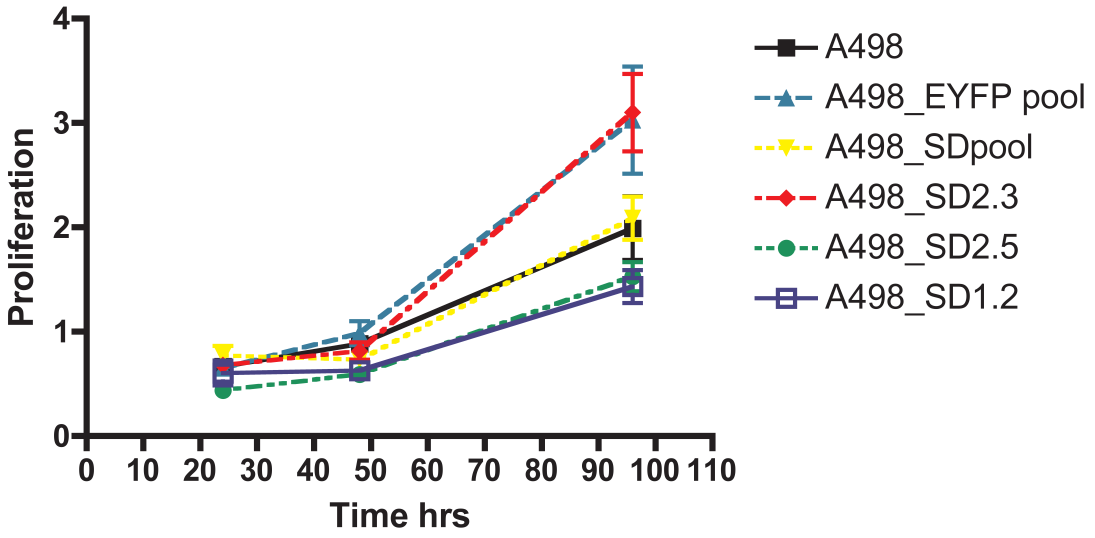

Figure 5:24 Proliferation in A498 stable transfectants
A498 parental cells, pooled stable transfectants transfected with either EYFP alone (A498_EYFP pool) or EYFPeIF4ES209D (A498_SD pool), and stable clones transfected with EYFPeIF4ES209D (A498_SD2.3, A498_SD2.5, A498_SD1.2) were plated to 96 well plates at equal densities. Proliferation was assessed at 24, 48 and 96 h using the CyQuant proliferation assay. Error bars represent standard error of the mean for triplicate wells.

The effect of CGP57380 on proliferation was investigated for each of the eIF4ESD clones using the CyQuant short term proliferation assay, the hypothesis being that stably transfected cells would be at least partially insensitive to CGP57380. Following 72 h treatment of the EYFP pooled population, a reduction in proliferation was seen with treatment at both 10 μM and 20 μM concentrations. In the two stable clones eIF4ESD1.2 and eIF4ESD2.5, although inhibition of proliferation was seen with CGP57380 at 20 μM, no inhibition was seen with CGP57380 at 10 μM. The third clone however, which differed both in growth characteristics and baseline levels of cyclin D1 protein, responded in the proliferation assay in a similar way to control cells at both CGP57380 10 μM and 20 μM (fig 5:25).

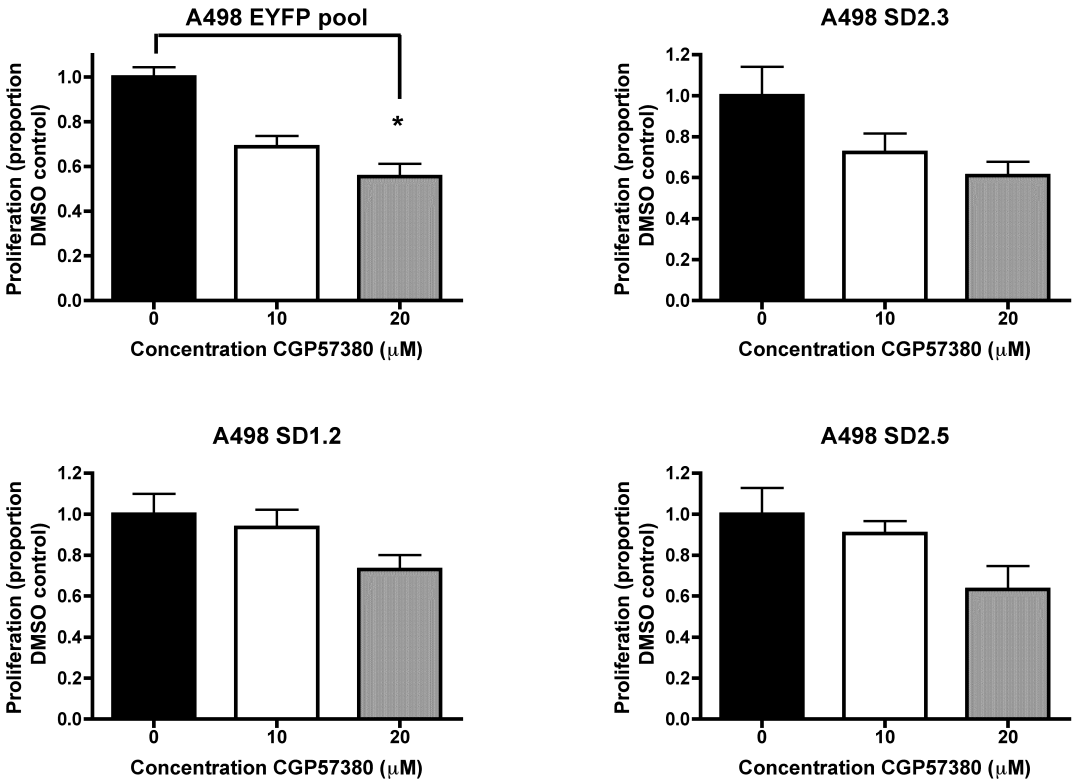

Figure 5:25 Proliferation in A498 stable transfectants exposed to CGP57380
Stable transfectants were plated to 96 wells plates and 24 h later treated with CGP57380 at concentrations as indicated, or 0.5% DMSO vehicle control. Proliferation was assessed at 72 h using the CyQuant assay. Error bars represent standard error of the mean for three experiments each performed in triplicate wells. Statistical analysis was with ANOVA with Tukey's post test.

The results of the above experiment using proliferation as an output to assess the effects of CGP57380 on the stable transfected clones would suggest that in clones SD1.2 and SD2.3 then some resistance to the effects of CGP57380 exists. Further experiments were performed in which cell cycle analysis was used as the endpoint, to see if this would correlate with the proliferation experiments, providing additional weight to the conclusion that mutating serine 209 to aspartate does indeed provide some resistance to the effects of CGP57380. Thus stable transfectants were treated with CGP57380 at 10 and 20 μM or 0.5% DMSO vehicle control. 24 h later cell cycle distribution was assessed using flow cytometry. Both A498 and A498_EYFP showed an accumulation in G1 following treatment with both 10 and 20 μM CGP57380. In a similar pattern to the proliferation experiment, A498SD2.5 cells remained sensitive to CGP57380 at both concentrations of CGP57380, however no effect on cell cycle distribution was seen with the A498SD1.2 and A498SD2.3 clones when exposed to either 10 μM or 20 μM CGP57380 (fig 5:26).

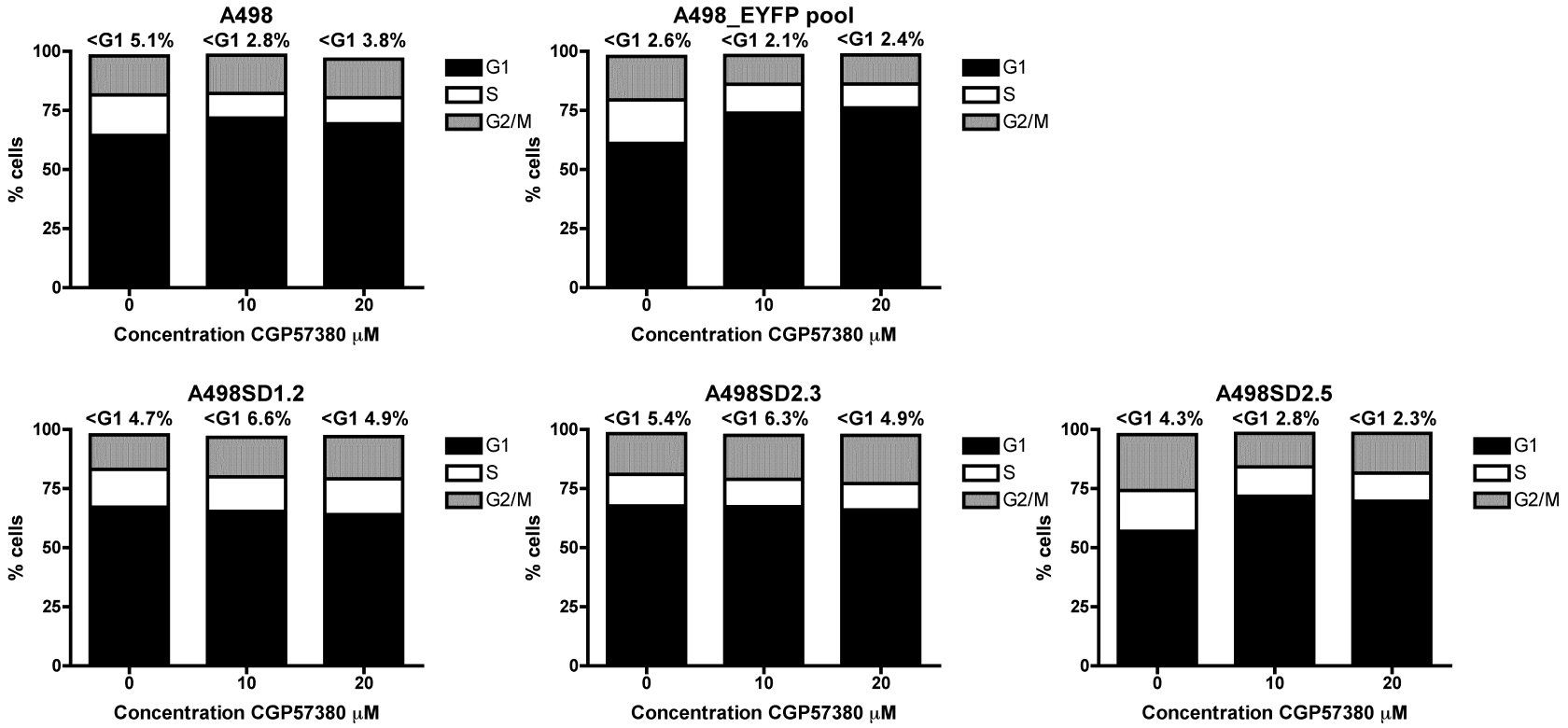

Figure 5:26 Cell cycle analysis in A498 clones treated with CGP57380
Parental A498 cells, control A498_EYFP pooled transfectants and A498 clones (A498SD1.2, A498SD2.3 and A498SD2.5) were plated to 6 well plates. At 24 h cells were treated with CGP57380 at concentrations as indicated or 0.5% DMSO vehicle control. At 24 h cells were harvested by trypsinisation, washed once in ice cold PBS, and fixed in ice cold ethanol. Cells were stained with propidium iodide staining solution and cell cycle analysis performed by flow cytometry.

5.7. Discussion

Investigation of the effects of CGP57380 on the proliferation of renal cell lines has shown inhibition of proliferation in all of the cell lines studied. This includes cell lines of both VHL null and VHL wildtype phenotype, with those of null phenotype including cell lines with somatic mutation of VHL, and those with promoter hypermethylation, representing the spectrum of clinical phenotypes of clear cell renal cell carcinoma[137,138]. Inhibition was seen in a short-term assay, with similar results using both the MTS assay, and the CyQuant assay. Additionally a longer term assay of cell proliferation by colony formation, during which the cells undergo additional stress through low density plating, showed a marked anti-proliferative effect in response to CGP57380. This anti-proliferative effect is similar to that previously documented in other cell types including breast[73], lung[20] and prostate cancers[74], and similar to those seen in breast cancer cell lines in this work. Immunoblotting has confirmed inhibition of eIF4E phosphorylation and down regulation of known targets of eIF4E phosphorylation. Two proteins were specifically investigated which are regulated by phosphorylated eIF4E, cyclin D1 through control of mRNA export, and Mcl-1 through translation control. The changes in cyclin D1 protein were more marked in the VHL null than the VHL wildtype cell line investigated, however Mcl-1 protein was reduced following treatment with CGP57380 in both cell types.

With a reduction seen in both a cell cycle regulatory protein and an anti-apoptotic protein, it might be anticipated that either cell cycle arrest or apoptosis may be the underlying mechanism for the growth inhibitory properties of CGP57380. Subsequent investigation showed a G1 cell cycle arrest following treatment with CGP57380, with no induction of apoptosis, either as an accumulation in the sub G1 cell fraction on cell cycle analysis, or through annexin V/PI staining. Investigation of the effects of MNK inhibition in prostate cancer cells have also shown a cell cycle inhibitory rather than a pro-apoptotic effect[74]. It is possible that renal cancer cells are less dependent on Mcl-1 for survival than some other cell types where inhibition would be expected to induce apoptosis. Alternatively the time points examined may have been too early to see evidence of apoptosis. Previous studies of a Raf kinase inhibitor able to inhibit Mcl-1 through post translational control,

showed an early reduction in Mcl-1 protein as assessed by immunoblotting, but no induction of apoptosis until 4-5 days exposure to the compound[169].

Although several groups have used CGP57380 as a specific inhibitor of the MNK proteins and demonstrated anti-proliferative effects, there has been some criticism of the use of this agent on the basis of its ability to target other kinases when tested in an in vitro kinase assay[124]. Although the reduction in known targets of regulation by the MNK proteins such as cyclin D1, and an associated anti-proliferative effect mediated through cell cycle arrest, would support specificity of action of CGP57380, alternative strategies have been investigated to demonstrate the specificity of the effects seen.

Using siRNA targeted at both the MNK1 and MNK2 genes, knockdown of both proteins has been shown, with associated reduction in phosphorylated eIF4E. In order to demonstrate a reduction in downstream targets of eIF4E phosphorylation, relatively high concentrations of siRNA were required with two siRNA duplexes targeted at each gene. The reduction in cyclin D1 protein was partial, and less marked than that seen when using the kinase inhibitor CGP57380. Using this technique the reduction in cyclin D1 protein achieved did not translate into a change in either proliferation or cell cycle distribution. It therefore remains possible that the effects of CGP57380 on proliferation are not specific to its activity through the MNK proteins. Equally it may be that an insufficient reduction either in eIF4E phosphorylation, or in cyclin D1 was seen to replicate the effects of the kinase inhibitor. Alternatively the prolonged dynamics of achieving a reduction in eIF4E phosphorylation with siRNA, may lead to the induction of compensatory pathways allowing the cell to continue to proliferate and prevent cell cycle arrest.

An alternative strategy was pursued to demonstrate the specificity of the anti-proliferative effects of CGP57380 to the MNK kinases. A phosphomimetic mutation of eIF4E can be created by substitution of serine 209 to a positively charged aspartic acid[69]. It was hypothesised that cells with stable integration of mutant eIF4E would develop resistance to the effects of the CGP57380 kinase inhibitor. A498 cells with stable integration of a construct containing mutated eIF4E (serine 209 to aspartic acid) and EYFP showed expected subcellular distribution of eIF4E[12] with nuclear exclusion not seen with EYFP transfected cells. The functionality of the construct was further demonstrated with m^7GTP pulldown of the EYFP-eIF4E fusion protein confirming the ability of the transfected eIF4E to bind

the mRNA cap. Of the three mutant eIF4E expressing clones tested, two had similar proliferation patterns with similar levels of cyclin D1. Of interest a third clone had significantly higher levels of cyclin D1 and a much faster proliferation than the other two. An anti-proliferative response was still seen in the two clones with similar levels of cyclin D1 protein with 20 μM CGP57380. When cell cycle analysis was investigated, a G1 arrest following treatment with CGP57380 was seen in EYFP containing cells. No effect was seen at either 10 μM or 20 μM CGP57380 in the two similar eIF4E mutants, however the effect seen in untransfected A498 cells was not statistically significant. The third eIF4E mutant containing higher levels of cyclin D1 behaved in a similar fashion to the EYFP transfected cells in both proliferation and cell cycle assays with an effect seen at both concentrations of CGP57380. A lack of effect seen on inhibiting the effects of CGP57380 may have several explanations. The most likely may be that the effects of CGP57380 are through both inhibition of eIF4E phosphorylation, but also through other undefined pathways due to inhibition of additional kinases. Alternatively it may be that the proliferation of the clones containing mutated eIF4E is partially dependent on the transfected, mutated eIF4E, but that endogenous eIF4E also has an ongoing role. The endogenous eIF4E would continue to be sensitive to the effects of CGP57380, therefore resulting in a degree of inhibition of proliferation on treatment with the compound, but less so than that seen in parental cells due to the presence of the resistant mutated eIF4E.

Overall these results show an anti-proliferative effect of CGP57380 in a panel of renal cancer cell lines of both VHL wild-type and null phenotype covering the clinical spectrum of clear cell renal cancer. This appeared to be a cytostatic rather than a cytotoxic effect with no induction of apoptosis at the time points investigated despite a reduction in Mcl-1 protein. The induction of cell cycle arrest is however correlative with the demonstrated reduction in cyclin D1 protein, a key regulator of the G1/S transition. Although MNK directed siRNA was able to show a reduction in eIF4E phosphorylation, and a modest effect on cyclin D1 protein, this did not translate into an effect on proliferation. The generation of A498 clones with stable integration of S209D mutated eIF4E had little effect on the anti-proliferative and cell cycle inhibitory effects of CGP57380, suggesting that CGP57380 is likely to have additional targets beyond the phosphorylation of eIF4E.

6. MNK mediated control of transcription and translation

6.1. Introduction

The experimental data described so far has identified the anti-proliferative effect of CGP57380 in breast and renal cancer cell lines. This effect has been shown to be largely due to inhibitory effects on cell cycle progression, with an accumulation of cells in G1, and an associated reduction in cyclin D1 protein. The regulation of cyclin D1 protein in response to eIF4E phosphorylation has been previously described as mediated through the inhibition of cyclin D1 mRNA export with an associated reduction in translation but no effect on total cellular cyclin D1 mRNA[12]. It is proposed that the phosphorylation of eIF4E also modulates the affinity of mRNA cap binding[59], and therefore polysome recruitment of regulated mRNAs. In order to further investigate the influences of eIF4E phosphorylation on the regulation of cyclin D1 RNA a series of experiments was proposed to assess the impact of inhibition of eIF4E phosphorylation using CGP57380 on RNA abundance. Current data would support no change in total cyclin D1 RNA abundance in response to inhibition of eIF4E phosphorylation, and rather an accumulation of RNA within the nuclear compartment. With this in mind experiments were performed both to investigate the levels of total cyclin D1 RNA in response to inhibition of the MNK proteins, but also to assess the distribution of RNA within subcellular fractions.

6.2. Effects of MNK inhibition on RNA abundance

Previous work has identified RNA export to be the mechanism of control of cyclin D1 protein through eIF4E phosphorylation[12]. It may therefore be expected that there would be no change in total RNA in response to treatment with CGP57380. To confirm this to be the case, qRT-PCR was used to measure total cyclin D1 RNA normalised to GAPDH RNA following treatment with CGP57380 at 20 μM. Following treatment of ACHN cells with CGP57380, total RNA was measured at time points up to 24 h, with DMSO vehicle control samples at each time point. Unexpectedly a fall in total RNA was seen over the time course (fig 6:1). A progressive reduction in total cyclin D1 RNA was seen, with a 1.7 fold reduction compared with untreated control at 4 h, 2.5 fold by 6 h and 6.8 fold at 24 h.

Although some reduction in cyclin D1 total RNA was seen in control cells at 24 h, possibly due to the lack of new growth factors for 48 h by this time point, a much greater reduction was seen in those cells treated with CGP57380, at both earlier time points and 24 h. This would suggest additional regulation of RNA beyond simply re-distribution within the cell. Possible explanations for the changes seen might include either a change in RNA synthesis through regulation of transcription, of altered degradation of RNA, perhaps related to the movement of RNA between cell compartments.

Although no change in proliferation or cell cycle distribution was seen following siRNA transfection with MNK1 and MNK2 duplexes at 100 nM, a change in cyclin D1 protein was seen, albeit less so than in response to CGP57380. The specificity of the changes in total cyclin D1 RNA was therefore additionally investigated using siRNA to modulate eIF4E phosphorylation through knockdown of the MNK1 and MNK2 RNA transcripts. The effects of MNK1 and MNK2 siRNA on total cyclin D1 RNA was investigated using qRT-PCR. Again a fall in total cyclin D1 RNA was seen, normalised to GAPDH, suggesting that this effect is indeed specific to the activity of the MNK proteins, and therefore likely to be related to phosphorylation of eIF4E (fig 6:2).

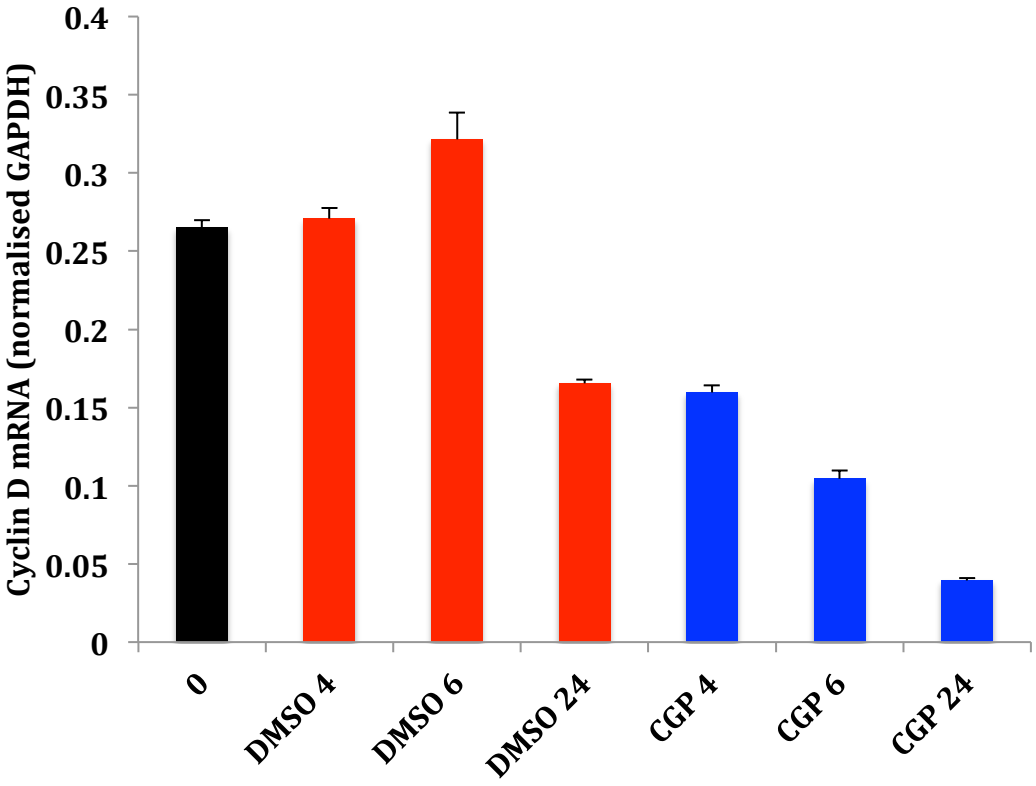

Figure 6:1 Cyclin D1 RNA following treatment with CGP57380
ACHN cells were treated with CGP57380 or DMSO vehicle control for times as indicated. Cells were harvested by pelletting and snap frozen. RNA was extracted and cDNA synthsesised as described. Cyclin D1 cDNA was measured using qRT-PCR and normalised to GAPDH. Time 0 = untreated control. Values are mean of triplicate repeat qRT-PCR reactions. Error bars represent standard error of the mean.

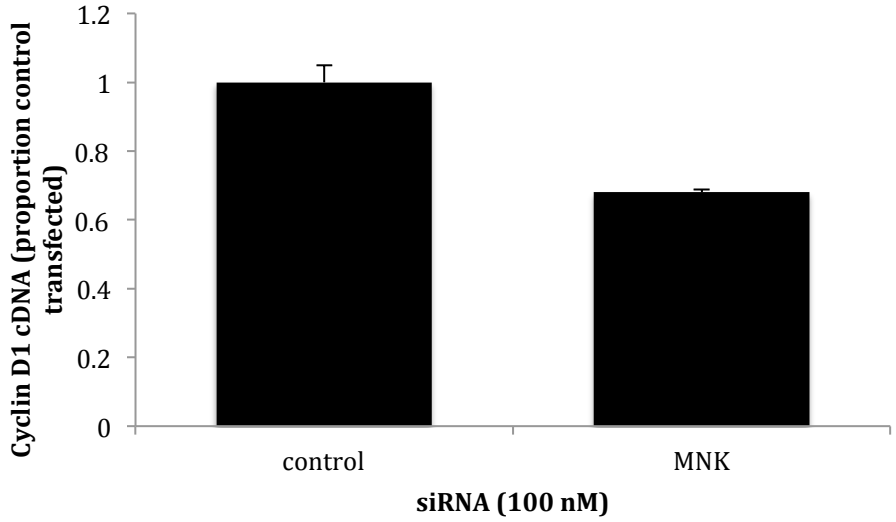

Figure 6:2 Cyclin D1 RNA following MNK1/MNK2 siRNA
ACHN cells were transfected with with 2 duplexes of each of MNK1 and MNK2 siRNA, or control siRNA at a final concentration of 100 nM. At 48 h cells were harvested by pelletting and snap frozen. RNA was extracted and cDNA synthsesised as described. Cyclin D1 cDNA was measured using qRT-PCR and normalised to GAPDH. Values are expressed as a proportion of untreated control and are mean of triplicate repeat qRT-PCR reactions.

Having established a reduction in total cellular cyclin D1 RNA following both inhibition of eIF4E phosphorylation with CGP57380, and using siRNA knockdown of the MNK proteins, experiments were performed to investigate the underlying mechanisms of this reduction. As outlined above, changes in total cellular RNA for a given transcript may be due to reduced production of new RNA through inhibition of transcription, or if transcription remains unchanged, then through enhanced degradation of an existing pool of RNA molecules.

For inhibition of transcription to cause the reduction in cyclin D1 RNA seen, the half life of the RNA transcript would have to be such that on inhibiting transcription, the existing pool of RNA would be degraded at a rate fast enough to account for the changes in total RNA seen. As such an experiment was performed to assess the stability of cyclin D1 mRNA following treatment of cells with Actinomycin D. By forming DNA adducts, Actinomycin D prevents the activity of RNA polymerase, and thus inhibits transcription. Cells were treated with either 0.5% DMSO vehicle control, Actinomycin D or CGP57380 for 6 h, and cyclin D1 RNA assessed by qRT-PCR. Whereas those cells treated with CGP57380 showed a reduction in cyclin D1 RNA as previously, those cells in which transcription was inhibited by Actinomycin D showed no reduction in cyclin D1 RNA (fig 6:3). This would indicate that the cyclin D1 RNA transcript is stable for at least 6 h, and that therefore regulation of transcription alone is not responsible for the reduction in cyclin D1 RNA seen with CGP57380.

This question was subsequently investigated by examining the effects of CGP57380 on cyclin D1 transcription using a reporter construct consisting of the cyclinD1 promoter within a luciferase reporter plasmid. It would be anticipated that should eIF4E phosphorylation be a regulator of cyclin D1 transcription, treatment of cells with CGP57380 would result in a reduction in cyclin D1 promoter activity, and thus a reduction in firefly luciferase activity.

ACHN renal cancer cells were transfected with either an empty luciferase reporter (pGl3 basic) or the cyclin D1 promoter construct[155], in each case together with the Renilla luciferase plasmid pRLSV40 as a transfection control. 4 h post transfection the cells were treated with either CGP57380 at 20 μM, or DMSO vehicle control, and luciferase activity measured at 48 h post transfection. Both firefly and Renilla luciferase activity were measured using the dualglo system (Promega) and results

expressed as firefly luciferase activity normalised to Renilla luciferase. In cells transfected with the empty firefly luciferase vector (pGl3) no luciferase activity was seen. In those cell transfected with the cyclin D1 promoter plasmid, firefly luciferase activity was seen, however subsequent treatment with CGP57380 resulted in an increase in cyclin D1 promoter activity (fig 6:4). This would indicate that regulation of transcription is not the mechanism underlying the reduction in cyclin D1 RNA seen with inhibition of eIF4E phosphorylation.

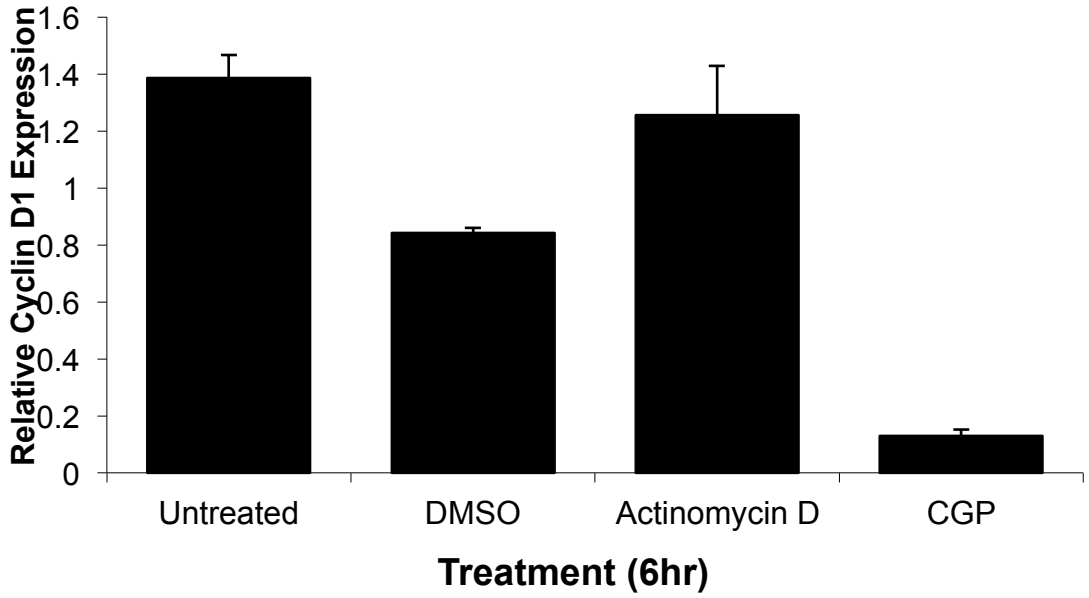

Figure 6:3 Cyclin D1 RNA expression following Actinomyin D
ACHN cells were treated for 6 h with 0.5% DMSO vehicle control, Actinomycin D (5µg/ml), or CGP57380 20µM. Cells were harvested and RNA extracted. Cyclin D1 RNA was measured by qRT-PCR and normalised to GAPDH. Results indicate mean and standard error of triplicate qRT-PCR reactions. (Experiment performed by AD)

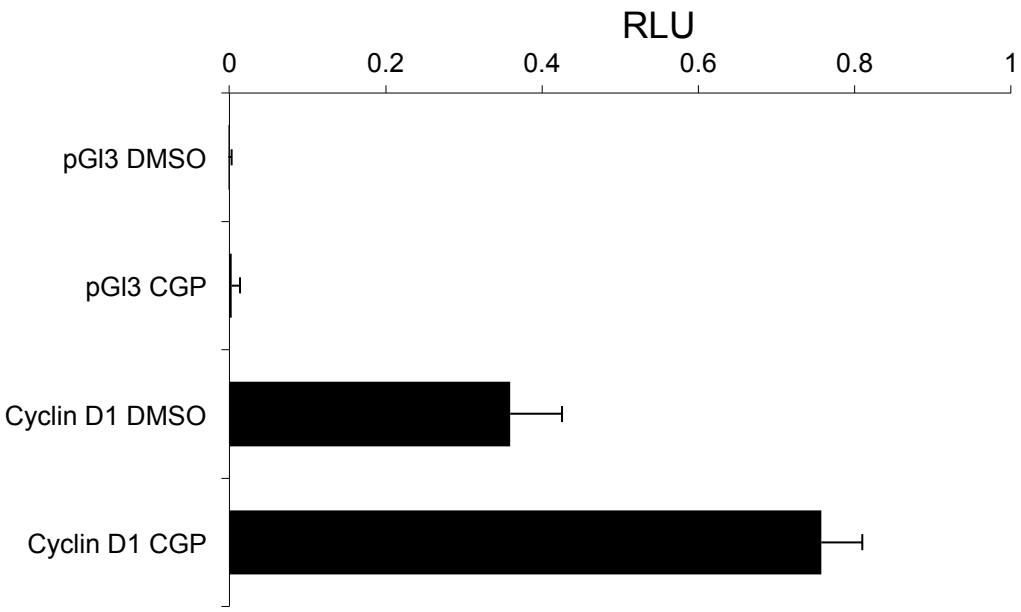

Figure 6:4 The effects of eIF4E phosphorylation on cyclin D1 transcription
ACHN renal cancer cells were transfected with the Renilla luciferase reporter vector under the control of the SV40 promoter (pRLSV40) together with the firefly luciferase vector pGl3 with no promoter (pGl3 basic) or the cyclin D1 promoter. 4h following transfection new medium was applied containing either 0.5% DMSO vehicle control or CGP57380 at 20 μM. Luciferase activity was measured 48 h post transfection using the DualGlo system. Results are expressed as firefly luciferase activity relative to Renilla luciferase activity in relative light units (RLU). Results represent the mean of triplicate transfections. Error bars represent standard error of the mean.

6.3. Effects of CGP57380 on mRNA subcellular localisation

The results from the above experiment may therefore suggest that degradation of RNA may be the mechanism for the reduction in total cellular RNA seen following both treatment with CGP57380, and transfection with MNK1 and MNK2 directed siRNA. It may be postulated that in the face of known data showing that phosphorylated eIF4E can regulate the nuclear export of a subset of RNA molecules[170], cyclin D1 RNA may accumulate in the nucleus, and then become degraded in the nuclear compartment, resulting in an overall decrease in total RNA.

An insight into the distribution of cyclin D1 RNA within the cell following inhibition of eIF4E phosphorylation may be gained by fractionating cells into nuclear, cytoplasmic and polysome fractions after treatment with CGP57380. Subsequent measurement of the amount of cyclin D1 RNA in each compartment may therefore provide an indication of the fate of transcribed RNA. Therefore ACHN cells were treated with CGP57380 or DMSO vehicle control for 6 h before undergoing fractionation. RNA was then extracted from each cell fraction, and the amount of cyclin D1 RNA measured and normalised to the housekeeping gene GAPDH. Fractionation was confirmed using semi-quantitative RT-PCR to measure the small nuclear RNA U6 in each fraction, which confirmed enrichment of the nuclear compared to the cytoplasmic fraction (fig 6:5).

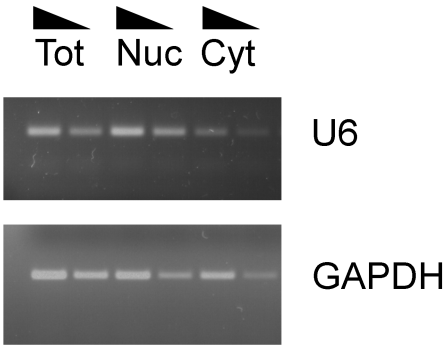

Figure 6:5 Fractionation of ACHN cell line
ACHN cells were fractionated using fractionation buffer A and a Dounce homogeniser as described. RNA was extracted from each fraction using phenol and cDNA synthesised. PCR was performed with two quantities of input cDNA for each sample, the second reaction representing one third of the input cDNA of the first. The upper bands show U6 small nuclear RNA and the lower GAPDH control for total (unfractionated) nuclear and cytoplasmic samples.

Subsequently qRT-PCR was used to measure cyclin D1 RNA in each of the fractionated samples including the polysome fraction (fig 6:6). This confirmed a reduction in the total RNA in cells treated with CGP57380 consistent with previous experiments. A global reduction was therefore also seen in all of the cell fractions from the samples treated with the MNK inhibitor. To provide a clearer indication of the relative distribution of the cyclin D1 RNA the results were normalised to the amount of total cyclin D1 RNA. This showed a relative accumulation of RNA in the nuclear fraction compared with either the cytoplasmic or polysome fractions in those cells treated with CGP58380.

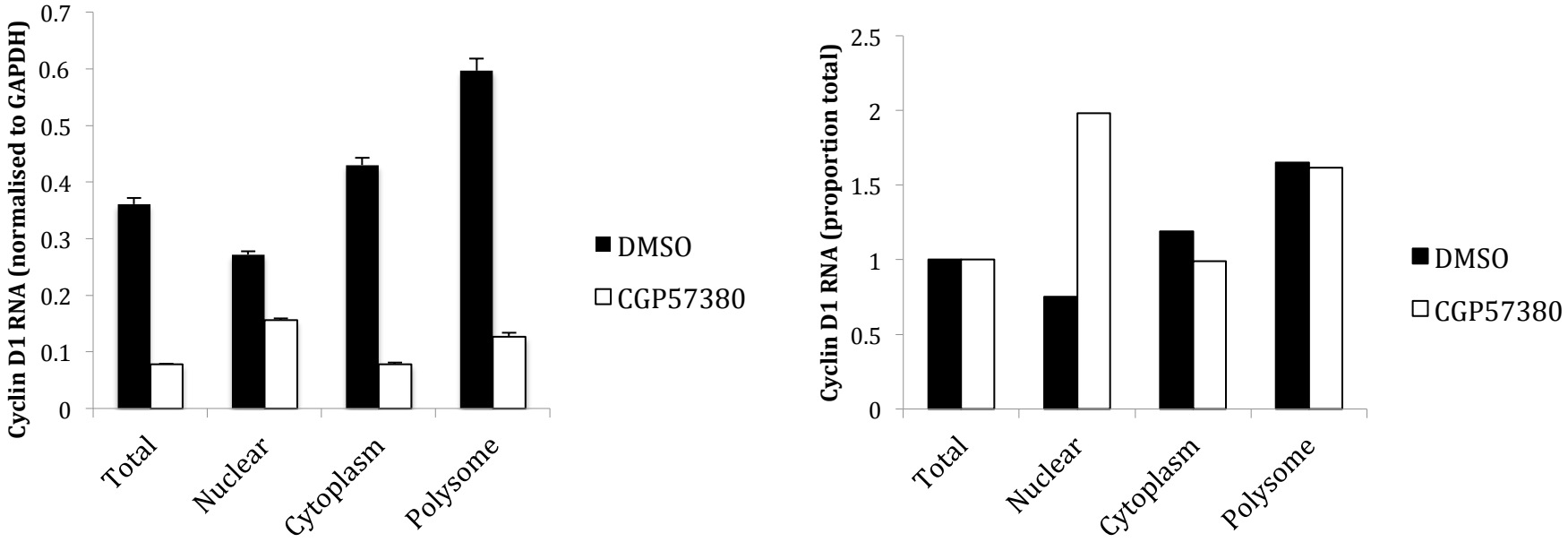

Figure 6:6 Cyclin D1 RNA in ACHN cell fractions
ACHN cells were treated with CGP57380 20 μM or 0.5% DMSO vehicle control for 6 h. Cells were harvested by scraping and fractionated as described with fractionation buffer A and a Dounce homogeniser. RNA was extracted from each fraction, cDNA synthesised and cyclinD1 RNA quantified with qRT-PCR. Left panel represents absolute cyclin D1 RNA levels in each fraction normalised to GAPDH. Bars are mean and standard error of triplicate repeat qRT-PCR reactions. The right panel represents values normalised to the levels of cyclin D1 RNA in the unfractionated (total) sample for each condition.

Together these results suggest that cyclin D1 RNA is not regulated at the transcriptional level by treatment with CGP57380, and that there is a relative accumulation of cyclin D1 RNA in the nucleus in the context of a decrease in total cellular cyclin D1 RNA. Possible explanations for these findings include either an accumulation and subsequent degradation of RNA within the nucleus, or degradation of RNA in the cytoplasm.

A further method of investigating the fate of RNA in response to inhibition of the MNK proteins with CGP57380 is to label newly synthesized RNA, and measure the effects of the compound on the relative levels of both total and newly synthesised transcripts. RNA can be labelled by incorporating 4-thiouracil, such that when RNA is extracted, the sulfhydryl groups can be biotinylated and the newly synthesized RNA extracted by binding to strepdavadin labelled magnetic beads. Thus ACHN cells were treated with CGP57380 or DMSO vehicle control for 1 h before the addition of 4-thiouracil and incubation for a further 6 h. Following this the 4-thiouracil labelled, newly synthesized RNA was extracted, and cyclin D1 RNA measured in both the newly synthesized fraction, and the unlabelled fraction using qRT-PCR. A reduction in cyclin D1 RNA was seen in the CGP57380 treated cells for both the labelled and unlabelled RNA, however the reduction seen in the unlabelled RNA was greater than that seen in the newly synthesized labelled samples (fig 6:7)

The more significant reduction in cyclin D1 RNA from the unlabelled RNA fraction would suggest that this may be the driver of the overall reduction in cyclin D1 RNA leading to a reduction in cyclin D1 protein. This would further support a hypothesis that existing RNA in the cell accumulates within the nucleus and is subsequently degraded, and that subsequently newly synthesised RNA which would also lie within the nucleus also starts to be degraded leading to a reduction in 4TU labelled RNA, but one less significant than that seen for the existing pool. This could be further investigated by performing a series of labeling experiments over a time course to identify the time points at which a reduction in 4TU labelled and 4TU unlabelled RNA are seen.

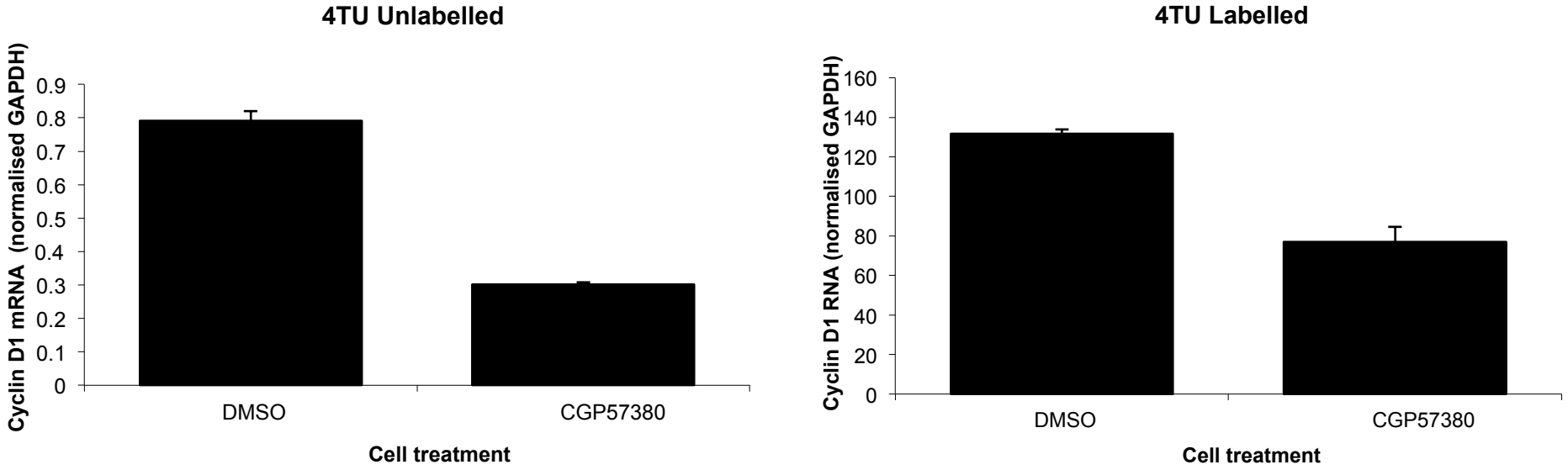

Figure 6:7 4-Thiouracil labeling of cyclin D1 RNA
ACHN cells were plated and treated with CGP57380 20 μM or 0.5% DMSO vehicle control. 1 h later 4-thiouracil was added to each dish and incubated for a further 6 h. Cells were harvested and the 4-thiouracil biotinylated. Strepdavidin beads were used to extract the biotinylated RNA. cDNA was synthsesised from the extracted biotinylated RNA (4TU Labelled), and the un-labelled RNA (4TU Unlabelled). qRT-PCR was used to measure the amount of cyclin D1 RNA in each sample normalised to GAPDH. Results represent the mean of triplicate qRT-PCR reactions from a single biotinylation experiment.

6.4. Novel targets of regulation of RNA in response to CGP57380

Studies in prostate cancer have used a microarray platform with 263 genes specific to prostate cancer to assess the impact of CGP57380 on polysome recruitment. Eight genes were identified in which polysome recruitment was down-regulated. These including cell cycle regulatory genes, the cyclin dependent kinases CDK2, CDK8, CDK9, and the CDK inhibitor KAP1[74]. Genome wide array analysis provides a platform whereby genes across the whole human genome can be investigated in a single experiment. This provides the potential to investigate additional targets of CGP57380. By measuring the effects of MNK inhibition on gene expression in total cellular mRNA extracts, additional genes in which total mRNA may be reduced might be identified.

Phosphorylation of eIF4E can play a dual role in the regulation of protein synthesis, both through regulation of RNA export and regulation of cap binding. It has been postulated through the experiments described in this work that retention of RNA within the nucleus and subsequent degradation may be the explanation for the changes in total RNA seen. Measurement of total cellular mRNA would not however directly measure the effects of CGP57380 on translation, which is rather most closely represented by the degree of polysome recruitment of mRNA molecules. Thus by additionally analysing the changes in RNA in the polysome cell fraction, those genes regulated through cap binding, and subsequently ribosome loading, might be identified.

Thus data may be obtained regarding the regulation of both cyclin D1, and other mRNAs at multiple levels. By comparing the gene expression in whole cell RNA extracts (total mRNA) following treatment with CGP57380, changes may be seen which might be accounted for either by reduced transcription or enhanced degradation. The work described so far would suggest that this is due to degradation. The closest correlate to protein expression however would be obtained from the expression of genes in the polysome cell fraction ie those RNA molecules actively undergoing translation. Changes in polysome recruitment may simply be a consequence of changes in either transcription or degradation as identified through analysis of total mRNA samples, however additionally direct regulation of translation, for example through polysome loading, would also influence this result. The combination of these two data sets may therefore provide

the most powerful analysis by indicating a shift in mRNA to or from the polysome. By examining the ratio of polysome associated to total mRNA in untreated cells, an indication of baseline translational efficacy may be obtained. Any change in this ratio seen on repeating this analysis following treatment of cells with CGP57380 may indicate a change in polysome association due to translational control, providing that an absolute decrease in expression in the polysome fractions between control and treated cell is seen. Should the change in the ratio be due to an increase in total cellular mRNA, this could be explained by enhanced transcription which has not yet affected polysome loading, but would be apparent due to an absolute change in total rather polysome associated mRNA.

ACHN cells, in which cyclin D1 protein and mRNA down regulation has been consistently identified were used for these experiments. Previous time course experiments have identified 6 h as a time by which a marked reduction in cyclin D1 mRNA was seen. Thus ACHN cells were treated for 6 h with CGP57380 at 20 μM following which cells were harvested and fractionated into nuclear, cytoplasmic and polysome fractions, with retention of whole cell samples prior to fractionation. Two independent experiments were performed, and RNA extracted from both whole cells and each cell fraction using phenol extraction. Qiagen RNeasy spin columns were then used as a clean up step to obtain purified RNA which was snap frozen and stored at -80 °C.

The Affymetrix GeneChip Human Genome U133 plus 2 array was used for these experiments. This array chip includes 38,500 characterised human genes, with 11 pairs of oligonucleotide probes for each gene. RNA samples were couriered on dry ice and array experiments were performed by the Patterson Institute Micro-array Service (Manchester).

cDNA synthesis was performed as a 2 step process using a NuGen WT Ovation Pico RNA amplification and labeling protocol. Newly synthesised cDNA was purified using RNAClean magnetic beads followed by an amplification step with a SPIA amplification protocol and a further purification step. Quantified cDNA was then fragmented and labeled with biotin using a NuGen Encore Biotin module. Biotin labeled cDNA was hybridised to the HG-U133 gene chip array during a 16 h incubation and then washed and stained with a strepdavidin-phycoerythrin

conjugate. The chip was read using a GeneChip Scanner 3000 with emission intensity at 570nm proportional to bound target cDNA.
Data manipulation was performed using Genepattern software hosted by the Broad Institute[171]. The raw data from the array experiments showing individual probe fluorescence was uploaded as cel files. Pre-processing was performed using Robust Multi-Array analysis (RMA). This three component protocol incorporates background correction to account for optical noise and low level non-specific hybridisation to probes. Normalisation between samples allows comparison between chips. Finally summarisation combines the corrected and normalised data from each probe set to give a single expresssion measure for each gene. Comparisons between treatment conditions were made using differential expression analysis. A two-sided t-test was used to assess differences in individual genes. A p value ≤ 0.05 and a greater than 2 fold absolute change in expression was used to define genes of interest.

An initial analysis was made of those genes differentially expressed in the total mRNA samples. 1791 features were identified with a significant difference in expression ($p \leq 0.05$). When this analysis was limited to those with an absolute fold change of >2 a subset of 169 features was identified (fig 6:8). Of these 61 were down regulated, representing 53 known genes, and 108 up regulated, representing 72 known genes.
Of note the list of genes which were downregulated included cyclin D1. Two probe sets for this gene are represented on the HG-U133 chip, one showing a 3.8 and the other showing a 3.5 fold reduction in expression, comparable to the data obtained from qRT-PCR.

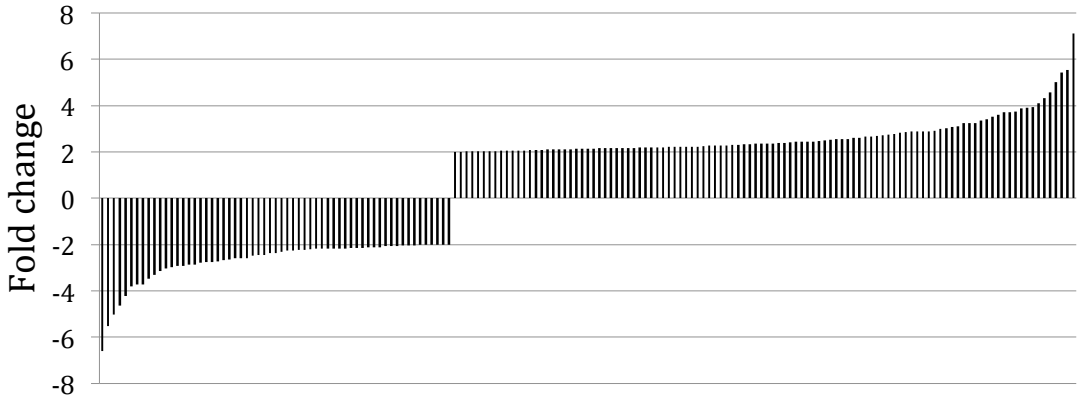

Figure 6:8 Genes differentially expressed in total RNA samples
Fold change in RNA expression for 169 features showing a significant difference ($p \leq 0.05$) in expression between CGP57380 treated and untreated cells with a fold change of at least 2.

Within the gene set showing differential expression in the total mRNA samples, several genes were identified with critical regulatory functions in cellular metabolism (table 6:1). Two genes which encode enzymes with rate limiting effects in the glycolytic pathway were identified, with a decrease in expression following treatment of cells with CGP57380. Hexokinase (HK) catalyses the conversion of glucose to glucose-6-phosphate as the initial step in the glycolysis pathway, and is associated with the outer mitochondrial membrane. Although catalysing an anaerobic metabolic pathway, it consumes ATP generated through oxidative phosphorylation within the mitochondria. It is the rate-limiting step in glycolysis in fast growing tumour cells[172]. 6-phosphofructo 2-kinase (PFKB3) catalyses the conversion of fructose-6-phosphate to fructose-2,6-bisphosphate (F2,6BP). Although not itself an intermediary in the glycolytic chain, F2,6BP is an allosteric promoter of the activity of phospho-fructokinase-1, a component of the glycolytic pathway. PFKB3 is highly expressed in tumours, and indeed shows high expression in the ACHN renal cancer cell samples examined in these experiments. It is highly inducible both by hypoxia, and its activity is induced by growth factors, and as such has been suggested as a potential anti-neoplastic target[173].
In contrast, phosphoenolpyruvate carboxykinase 2 was up regulated and has a key role in gluconeogenesis, suggesting a switch from a glycolytic metabolic pathway.

This would be supported by an increase in other genes associated with the TCA cycle including Isocitrate dehydrogenase 1 and acyl-CoA synthetase medium-chain family member 3.

Feature ID	Gene abbreviation	Gene name	Fold change	P
222305_at	HK2	Hexokinase 2	-2.9	0.04
202464_s_at	PFKFB3	6-phosphofructo-2-kinase/fructose-2,6-biphosphatase 3	-2.5	0.03
242001_at	IDH1	Isocitrate dehydrogenase 1	2.4	0.01
205942_s_at	ACSM3	acyl-CoA synthetase medium-chain family member 3	2.2	0.01
202847_at	PCK2	phosphoenolpyruvate carboxykinase 2 (mitochondrial)	3.9	0.02
205047_s_at	ASNS	asparagine synthetase (glutamine-hydrolyzing)	3.4	0.05

Table 6:1 Genes with cellular metabolic functions and altered expression following treatment with CGP57380
Genes with significant up or down-regulation of expression and at least a 2 fold change in expression following treatment of ACHN cells with CGP57380. Total RNA samples.

Online software was used to look for enrichment of particular functional categories within the regulated genes identified. The database for annotation, visualisation and integrated discovery (DAVID http://david.abcc.ncifcrf.gov) allows comparison of an uploaded geneset with the background incidence of functional groups within the genes represented on a specified array platform. By using a modified Fisher's exact test (EASE Expression Analysis Systematic Explorer) a statistical value is given to the strength of association of a functional class of genes within the geneset analysed.

The top functional groups identified within the set of genes regulated in the total RNA samples were genes encoding phosphoproteins, genes of the Sprouty family, genes involved in response to oxidative stress, and genes encoding sequence specific DNA binding domains (table 6:2). The group of phosphoproteins was the largest at 71 genes, representing over 50% of the genes identified as significantly altered in expression, and was not therefore helpful in identifying patterns of gene expression.

The sprouty (Spry) and sprouty related proteins (Spred) are negative regulators of MAPK signaling. Spry2 is a target of MNK1[66], which is able to phosphorylate and hence stabilise Spry2, potentially creating a negative feedback loop in the MAPK signaling pathway. Although there is no known link between Spry or Spred transcription and MNK activity, the link with a known target of MNK1 would support the activity of CGP57380 through the MNK kinases.

Several genes were identified with a function involved in the response to oxidative stress. Signaling through the MAPK signaling cascade is involved in the cellular response to oxidative stress, in particular the balance between ERK and JNK signaling pathways[174]. The MNKs are activated by ERK and p38 MAPK but not JNK, and it may be that by inhibiting MNK activity a change in the balance of signaling through these different aspects of the MAPK signaling pathway is achieved, manifesting in altered regulation of genes involved in oxidative stress. It must also be born in mind that DMSO vehicle control was used to treat the cells in these experiments, which itself has anti-oxidant properties. Both treated and control cells were exposed to the same concentration of DMSO for the same time course, so differential expression of genes related to DMSO exposure should not be seen.

The third functional group identified was sequence specific DNA binding, representing several transcription factors (table 6:2). The gene within this group with the highest level of fold change was fos-like antigen 1 (FOSL1) which was also represented in the oxidative stress group. FOSL1 binds members of the JUN family to form the AP-1 transcription factor. AP-1 has been identified as a regulator of both c-MYC and cyclin D1 transcription, and can be itself be regulated through inhibition of mTOR in cells with activated AKT[175]. It is therefore possible that cyclin D1 transcription could also be regulated at a transcriptional level by the MNK proteins through this mechanism.

Functional Group/ Feature ID	Gene symbol/name	EASE Fold Change
Sprouty		**p<0.01**
212558_at	SPRY1/sprouty homolog 1	-2.1
235074_at	SPRED1/sprouty-related, EVH1 domain containing 1	-2.4
214026_s_at	SPRED2/sprouty-related, EVH1 domain containing 2	-2.2
Response to oxidative stress		**p<0.01**
204420_at	FOSL1/FOS-like antigen 1	-6.6
230711_at	EPAS1/endothelial PAS domain protein 1	+2.2
218120_s_at	HMOX2/heme oxygenase (decycling) 2	-2.9
242956_at	IDH1/isocitrate dehydrogenase 1 (NADP+), soluble	+2.4
238408_at	OXR1/oxidation resistance 1	+2.0
232375_at	STAT1/signal transducer and activator of transcription 1	+2.2
201008_s_at	TXNIP/thioredoxin interacting protein	+3.9
Sequence Specific DNA Binding		**p<0.01**
212501_at	CEBPB/ CCAAT/enhancer binding protein (C/EBP), beta	+3.4
203973_s_at	CEBPD/ CCAAT/enhancer binding protein (C/EBP), delta	+2.3
204420_at	FOSL1/FOS-like antigen 1	-6.6
205313_at	HNF1B/HNF1 homeobox B	-2.1
202672_s_at	ATF3/activating transcription factor 3	+2.9
230711_at	EPAS1/endothelial PAS domain protein 1	+2.2
1553613_s_at	FOXC1/forkhead box C1	-2.4
208025_s_at	HMGA2/high mobility group AT-hook 2	-4.6
214639_s_at	HOXA1/homeobox A1	-2.0
232375_at	STAT1/signal transducer and activator of transcription 1	+2.2
244521_at	TSHZ2/teashirt zinc finger homeobox 2	+2.9
217367_s_at	ZHX3/zinc fingers and homeoboxes 3	-2.1

Table 6:2 Functional groups statistically over-represented within genes with altered expression following treatment with CG57380. Total RNA samples

Analysis of those genes differentially expressed in the polysome fraction revealed 1155 features with a significant difference in expression ($p \leq 0.05$). Limiting this to those with at least a 2 fold change revealed 264 features, 142 of which were down regulated and 122 up regulated (Fig 6:9). This gene set included MCL-1 with a 3.8 fold reduction in the polysome fraction between treated and untreated cells. This is consistent with a reduction of translation of this transcript, and with the findings of protein analysis in response to treatment of cells with CGP57380.

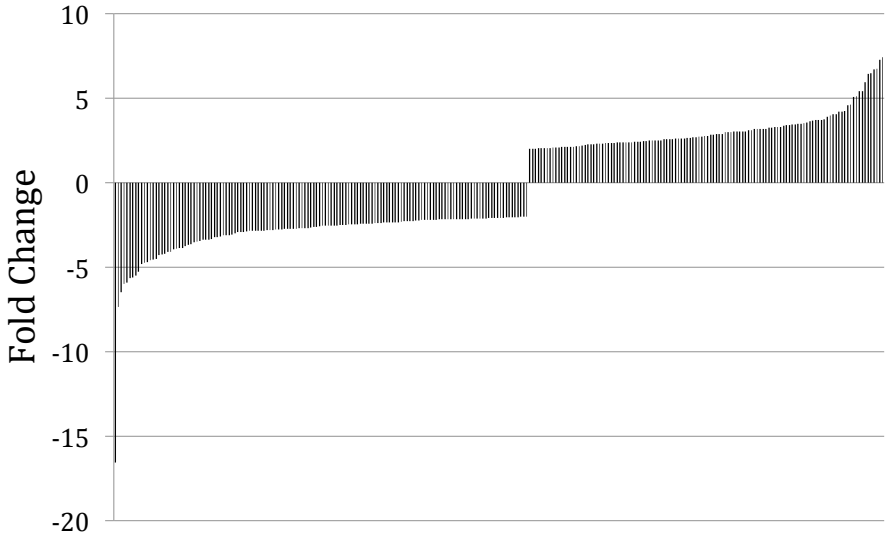

Figure 6:9 Genes differentially expressed in polysome associated RNA samples
Fold change for 264 features showing a significant difference ($p \leq 0.05$) in expression between CGP57380 treated and untreated cells with a fold change of at least 2.

The highest changing gene in the polysome fraction was MAFF with a decrease of 16 fold. The Maf proteins are transcriptional regulators which are able to form homo-dimers, or heterodimers with other transcription factors including the collar and cuff (CNC) family[176]. This includes the Nrf proteins which act as transcription factors, binding antioxidant response elements (AREs) in the nucleus to induce antioxidant genes when cells are exposed to oxidative and electrophile stresses. Nrf2 has been implicated both in carcinogenesis, such that induction of Nrf2 is protective against the development of the malignant phenotype, but also in the

resistance to cancer therapy, with induction of Nrf2 in response to chemotherapeutics[177].

In order to explore the changes in regulation of translation due to treatment of cells with CGP57380, an analysis of the shift in mRNA from the total to the polysome fraction was made, based on previous analyses by Bushell et al[178]. The ratio of polysome associated to total mRNA was calculated for each gene to define the level of translation. In this calculation, genes with a higher level of expression in the polysome fraction i.e. being actively translated, compared to the total sample i.e. being transcribed, would be regarded as being more efficiently translated. A percent rank function was used to define the position of each gene within the genome with respect to its translational efficiency. In order to exclude genes in which changes in transcription rather than translation were the cause of changes in the ratio, only those genes with a significant absolute change in polysome associated mRNA were selected. The change in position within the percent rank was then calculated for each gene. In order to exclude genes in which small changes in low levels of expression (therefore appearing to have a large relative change) were seen, only those genes with a change in percent rank (delta percent rank) of greater than 20 were included. Two populations of genes were established, those with a negative value for delta percent rank, i.e. those in which inhibition of MNK proteins resulted in a reduction in translational efficiency, and those with a positive delta percent rank in which inhibition of the MNKs resulted in an enhanced level of transcriptional efficiency. 203 genes were identified in which translation appeared to have decreased, with a further 284 genes with a positive delta percent rank of greater than 20, where translational efficiency appeared to have increased giving a total of 487 genes in which translation seemed to have been significantly altered by treatment of the cells with CGP57380.
Using functional annotation clustering as described above, 55 functional groups were identified with a significant EASE score. Due to the redundancy within functional groups, these can be combined into higher order groups containing similar functions. In this way a broader group containing multiple similar functional subgroups is obtained. Using this method, the top three clusters contained genes associated with; intracellular non-membrane bound organelles, post-transcriptional

gene silencing, and transition metal ion binding. These three groups contained 77, 4 and 83 genes respectively (table 6:3).

Functional Group Cluster / Gene Name	Delta percent rank
Intracellular non-membrane bound organelles	
AT rich interactive domain 4B (RBP1-like)	-20.5
CDC14 cell division cycle 14 homolog A (S. cerevisiae)	+28.9
CDC5 cell division cycle 5-like (S. pombe)	-55.6
DEAD (Asp-Glu-Ala-Asp) box polypeptide 20	-40.8
Post-transcriptional gene silencing	
Mov10, Moloney leukemia virus 10, homolog (mouse)	+45.6
lin-28 homolog B (C. elegans)	-24.1
protein kinase, interferon-inducible double stranded RNA dependent activator	-38.0
zinc finger, CCHC domain containing 11	+46.5
Transition metal ion binding	
ADAM metallopeptidase domain 5 pseudogene	+35.4
ADAM metallopeptidase with thrombospondin type 1 motif, 2	-32.9
ATP/GTP binding protein-like 5	+26.7
ArfGAP with RhoGAP domain, ankyrin repeat and PH domain 2	+22.7

Table 6:3 Functional annotation clustering of genes with delta percent rank greater than 20
Genes in which the ratio of polysome to total expression is altered. Three gene clusters were identified. The top 4 ranked genes for each cluster are shown.

A relatively large number of genes are clearly influenced by CGP57380 at the translational level with both increases and decreases in delta percent rank seen suggesting the ability of this compound to both promote and inhibit translation. Of note several genes involved in cell cycle regulation have been identified in the intracellular non-membrane bound organelle cluster. AT rich interactive domain 4B is often over-expressed in breast cancer, and has a dual role in the regulation of cell proliferation, through an ability to bind retinoblastoma protein, and also to from part of a histone deacetylase-dependent transcriptional co-repressor complex[179]. CDC14 is a homolog of a gene well described in S. cerevisiae with an important function in the exit from mitosis. CDC14 is a phosphatase and is responsible for inactivation of cyclin dependent kinases at the end of mitosis[180]. Equally in the post-transcriptional gene silencing group, Mov10 is a putative RNA helicase, with activity against INK4a, itself an inhibitor of cell cycle progression[181].

6.5. Discussion

Having established in earlier chapters that inhibition of the MNK proteins with CGP57380 can inhibit cell cycle progression in association with a reduction in cyclin D1 protein, the work in this chapter has investigated in more detail the mechanisms underlying the regulation of cyclin D1 at a transcriptional and translational level. In addition novel targets for regulation by the MNK proteins have been investigated.

Previous work has identified nuclear export of cyclin D1 RNA as the method of regulation of cyclin D1 protein in response to inhibition of the MNKs with CGP57380[12]. The work in this chapter has however clearly shown that on treating cells with CGP57380 not only is a reduction in cyclin D1 protein seen, but also in total cellular cyclin D1 RNA as measured using quantitative RT-PCR. This effect has been reproduced using siRNA targeted at the MNK proteins suggesting that it is indeed specific to an effect of CGP57380 on eIF4E phosphorylation, rather than an off target effect on other kinases identified in in vitro kinase screening assays[124].

Potential mechanisms for a reduction in total cyclin D1 cellular RNA would have to result from either a reduction in newly synthesised cyclin D1 RNA, i.e. regulation of transcription, or through enhanced degradation. In order for transcriptional regulation of cyclin D1 RNA to solely account for the reduction seen, the stability of the existing pool of RNA would have to be such that on complete inhibition of transcription, existing RNA would rapidly degrade. Treating cells with Actinomycin D in order to inhibit transcription however, showed stability of cyclin D1 RNA at 6 h, the time point in which a reduction in cyclin D1 RNA was seen on treatment with CGP57380. A reporter assay was performed to directly investigate the effect of CGP57380 on transcription. Surprisingly this assay demonstrated enhanced cyclin D1 promoter activity in response to CGP57380, compatible with increased rather than decreased transcription, but contrary to the effects of CGP57380 seen on cyclin D1 protein and RNA as investigated by western blotting and qRT-PCR respectively.

Further evidence for enhanced degradation of RNA rather than reduced transcription was seen when cells were treated with 4-thiouracil in order to label newly synthesised RNA. Although treatment with CGP57380 showed a reduction in both labelled (newly synthesised) and unlabelled RNA, the larger reduction in

unlabelled RNA would suggest this to be the driver of the reduction in total RNA seen. A model could therefore be suggested where degradation of RNA predominantly effects the existing pool, with some degradation of newly synthesised RNA also occurring, at a rate greater than transcription.

In order to investigate the localisation of cyclin D1 RNA within the cell following treatment of cells with CGP57380, cellular fractionation was performed. This showed a reduction in cyclin D1 RNA in all cellular compartments, however when the absolute levels of RNA were normalised to the levels of total cellular RNA, a relative accumulation of cyclin D1 RNA was seen within the nuclear compartment. Existing data shows an effect of inhibition of cyclin D1 RNA on nuclear export. The results described above suggest that to account for a reduction in total RNA in the absence of an effect on transcription, enhanced RNA degradation must occur. Thus on inhibition of eIF4E phosphorylation, RNA messages regulated by CGP57380 may first be retained within the nucleus, and then undergo degradation. This hypothesis would be supported by the data shown.

A limited analysis of genes regulated in the polysome cell fraction was carried out by Bianchini et al[74] using a gene microarray limited to a geneset associated with prostate cancer. This identified several genes associated with cell cycle control to be reduced in the polysome fraction. Within the polysome fractions examined by geneome wide analysis in the experiments described above *cdc5* was identified as having a 2 fold reduction in the polysome fraction, a gene involved in G2/M transition[182], however other cell cycle regulatory proteins were not identified in the polysome fraction. Within the total RNA samples, however cyclin D1 was identified as down regulated, with two probes for this gene showing 3.5 and 3.8 fold down regulation respectively, a similar change to that seen in previous qRT-PCR experiments. Additional genes with cell cycle regulatory roles were also identified which were regulated at the level of translation, as identified by changes in relative polysome loading (delta percent rank). These included genes directly involved in cell cycle regulation such as CDC14, and those with indirect action such as Mov10. Large numbers of genes have been identified within this genome wide array analysis which are influenced by CGP57380, both in respect to the total amount of RNA which can be measured in the cell, but also in polysome recruitment. This would support the hypothesis that eIF4E controls a regulon of mRNA molecules, with activity both at the level of nuclear export, but also initiation of translation[14].

Analysis of these results raises a number of issues. Although many genes were identified with statistically significant results using a two sided t test, when analysing such a large number of data points, statistical correction for multiple testing should be made. A variety of methods exist for such corrected analysis including the false discovery rate[183], which accounts for the large numbers of statistical tests involved in analysis of an array experiment. When the results obtained from the array experiments described in this chapter were subjected to a false discovery rate analysis, the level of statistical significance was >0.05 in all cases. There may be a variety of explanations for this. It is possible that all of the results obtained could be false positives due to multiple testing. However the fact that genes previously identified as regulated both at the protein level through immunoblotting, and RNA level through qRT-PCR, were identified in the array experiment would suggest that this is not universally the case. The experiments performed were duplicate rather than triplicate repeats due to the cost of performing such analyses. When using an inherently unstable molecule such as RNA, the inter-experimental variation is likely to be high, and it may be that larger numbers of repeat samples are required to obtain sufficient statistical power to show significance in a false discovery rate calculation. Although some of the array results can be retrospectively validated, as the changes in cyclin D1 RNA seen in qRT-PCR experiments are replicated in the array dataset, clearly further validation of these results is required with qRT-PCR analysis of additional targets identified from this experiment. Several interesting targets are however identified which would be worthy of further analysis.

7. Final discussion and future work

The work described in this thesis has confirmed the ability of CGP57380, through inhibition of the MNK proteins, to inhibit the proliferation of both breast and kidney cancer cell lines. This would suggest that the MNK proteins are a therapeutic target worthy of further investigation in these cancer types.

Although previous work has identified the ability of CGP57380 to inhibit the proliferation of HER2 overexpressing breast cancer cells[73], this work has extended this growth inhibitory effect to breast cancer cells of all clinical phenotypes, including HER2 overexpressing, oestrogen receptor positive, and triple negative cell lines. Within the cell lines investigated there was a correlation between the basal levels of phosphorylated eIF4E and the ability of CGP57380 to inhibit proliferation, such that the line with low levels of eIF4E phosphorylation (MCF7) showed no growth inhibitory effect. Within the breast tumour tissue samples examined there was significant variation in the levels of phosphorylated eIF4E. These two features together would suggest that levels of phosphorylated eIF4E could be investigated further as a biomarker of response to inhibition of the MNK proteins should this be taken forward as a therapeutic strategy in breast cancer.

The role of eIF4E phosphorylation in the proliferation of renal cancer cell lines has not previously been investigated. Previous work in prostate cancer cell lines has however identified HIFα as a target for regulation by phosphorylated eIF4E[74]. Thus as HIFα has been identified as critical in the pathogensis of VHL mutant clear cell renal cell cancer[184], this would appear an attractive disease to target with inhibition of the MNK proteins. Not only has this work identified the ability of inhibition of the MNK proteins to inhibit the proliferation of renal cancer cell lines, it has shown this effect in both VHL wild-type and mutant cell lines. This would suggest therefore that HIFα is not the relevant target of the MNK kinases in renal cancer cell lines, for the regulation of proliferation.

The mechanisms underlying inhibition of proliferation in both breast and renal cancer cell lines have been investigated. Both cyclin D1 and Mcl-1 have previously

been identified as targets for regulation by phosphorylated eIF4E[12,69,170], and have been shown in this work to be inhibited on treatment of cells with an inhibitor of the MNK proteins. Thus both inhibition of cell cycle progression and induction of apoptosis are potential mechanisms underlying the anti-proliferative effects seen in breast and kidney cancer cells. Using a combination of techniques, cell cycle arrest has been identified as the dominant mechanism of inhibition of proliferation, with little or no effect on induction of apoptosis in either of the cancer types investigated. This correlates with other work where the effects of treatment of solid tumour cells with CGP57380 have been investigated [74]. The effects of CGP57380 on the proliferation of B cell lymphoma cells has previously been investigated[75]. This is the only published work in which CGP57380 has been used as an anti-cancer agent in an animal model, and confirmed the ability of this compound to inhibit the growth of a lymphoma xenograft. The effects of inhibition of eIF4E phosphorylation on cyclin D1 protein were confirmed in these cells, however an increase in apoptosis in lymphoma cells treated with CGP57380 was also identified. Mcl-1 is however highly expressed in high grade lymphomas and is implicated in the survival of lymphoma cells[185]. Thus although a reduction in cyclin D1 was identified in this study, it is likely that Mcl-1 is the dominant regulator of cell survival in this cell type, and as such the use of an agent known to inhibit Mcl-1 translation would be likely to induce apoptosis in these circumstances.

The specificity of CGP57380 for the MNK proteins has been questioned using in vitro protein kinase assays[124]. Criteria have also been suggested for the demonstration of the specificity of kinase inhibitors for in vivo experiments[186]. These include the ability of the kinase inhibitor to induce cellular effects at a concentration shown to induce inhibition of phosphorylation of known targets of the kinase of interest. The proliferation experiments described in breast and kidney cancer cells have indeed been at doses in which inhibition of eIF4E phosphorylation has been demonstrated. Additional criteria include that no effect of the compound should be seen in cells in which a drug resistant mutant of the protein kinase has been induced. In this work a phospho-mimetic mutant of eIF4E was induced to generate resistance to CGP57380 and showed partial resistance in proliferation and cell cycle assays, again supporting the specificity of the action of CGP57380 through the MNK proteins.

The effect of inhibition of eIF4E phosphorylation on cyclin D1 protein has been highly reproducible both in this work and in other groups investigating the effects of CGP57380[12,20,75]. eIF4E is able to regulate translation of mRNA both through translation initiation, and mRNA nuclear export[14], and it is the latter which has been identified as regulating cyclin D1[13]. Inhibition of eIF4E phosphorylation has not however previously been shown to impact on total cyclin D1 RNA. Having established a reduction in cyclin D1 RNA in renal cancer cell lines, no effect has been shown on inhibition of transcription using a reporter assay. By demonstrating the stability of cyclin D1 RNA to be longer than the time period over which a reduction in cyclin D1 RNA is seen after treatment with CGP57380, a hypothesis is generated in which enhanced degradation of RNA is induced. When taken together with experimental data showing a relative accumulation of cyclin D1 RNA within the nuclear compartment, this hypothesis can be extended to suggest that inhibition of eIF4E phosphorylation leads to a nuclear accumulation of cyclin D1 RNA, and subsequent degradation within the nuclear compartment. Further work is clearly required to prove this hypothesis, which could be achieved by combining some of the assays used in the work described in this thesis. By labeling newly synthesised RNA with 4-thiouracil, treating cells with CGP57380, and then fractionating cells at sequential time points, a clearer picture of the fate of both existing and newly synthesised RNA could be achieved.

The final part of this project has investigated novel targets under the control of phosphorylated eIF4E using genome wide microarray. Multiple targets have been identified. Identifying changes in total cellular RNA would suggest regulation prior to translation, with the hypothesis suggested above that this is through RNA degradation within the nucleus. As has been previously alluded to, the results of this assay reached a level of statistical significance with a conventional t-test, but this did not hold up using false discovery rate. The results of this assay are therefore purely hypothesis generating, although did correlate with earlier qRT-PCR analysis of cyclin D1 RNA. Several genes with key functions in cell metabolism were identified in this group suggesting the induction of a metabolic switch from aerobic glycolysis to oxidative phosphorylation, a reversal of the Warburg effect[179], and a therapeutic strategy increasingly being investigated in

cancer[175]. By investigating changes in RNA within the polysome fraction, and in particular shifts in the ratio of total to polysome associated RNA a picture of those genes regulated at the translational level can be obtained. Clearly a change in the expression of multiple genes is seen at this level, and of particular note both up-regulation and down-regulation of gene expression at the level of translation is seen. Given the proposed established mechanisms of eIF4E function, either through induction of cap binding, or control of nuclear export, it would seen unlikely that a direct effect in up-regulating gene expression would be achieved by blocking the phosphorylation of eIF4E. It is more likely however that following the down-regulation of transcription and other factors involved in the regulation of gene expression by inhibiting eIF4E phosphorylation, subsequent events may result in an up-regulation of gene expression.

Although CGP57380 is active in inhibition of eIF4E phosphorylation and induction of cell cycle arrest at relatively high concentrations, it is certainly not sufficiently potent to be used as a therapeutic agent. Work is underway by other groups to develop more active inhibitors of the MNK proteins. A compound has recently been identified via high throughput screening with inhibition of the MNK kinases in the nanomolar range, and a preferential inhibitory effect on MNK2. This agent, cercosporamide, is orally active in animal models, and has shown the ability to prevent the growth of colon cancer and melanoma human xenografts in a mouse model[187]. The MNK kinases should thus be pursued for further development as therapeutic targets and their inhibitors should ultimately enter the arsenal of molecularly targeted agents as cancer therapy enters the age of personalised medicine.

8. References

1. Hanahan D, Weinberg RA. The hallmarks of cancer. Cell 2000;100:57-70.

2. Rousseau D, Kaspar R, Rosenwald I, Gehrke L, Sonenberg N. Translation initiation of ornithine decarboxylase and nucleocytoplasmic transport of cyclin D1 mRNA are increased in cells overexpressing eukaryotic initiation factor 4E. Proc Natl Acad Sci U S A 1996;93:1065-70.

3. De Benedetti A, Harris AL. eIF4E expression in tumors: its possible role in progression of malignancies. Int J Biochem Cell Biol 1999;31:59-72.

4. Altmann M, Handschin C, Trachsel H. mRNA cap-binding protein: cloning of the gene encoding protein synthesis initiation factor eIF-4E from Saccharomyces cerevisiae. Mol Cell Biol 1987;7:998-1003.

5. Lazaris-Karatzas A, Montine KS, Sonenberg N. Malignant transformation by a eukaryotic initiation factor subunit that binds to mRNA 5' cap. Nature 1990;345:544-7.

6. McClusky DR, Chu Q, Yu H, et al. A prospective trial on initiation factor 4E (eIF4E) overexpression and cancer recurrence in node-positive breast cancer. Ann Surg 2005;242:584-90; discussion 90-2.

7. Nathan CO, Franklin S, Abreo FW, Nassar R, De Benedetti A, Glass J. Analysis of surgical margins with the molecular marker eIF4E: a prognostic factor in patients with head and neck cancer. J Clin Oncol 1999;17:2909-14.

8. Wang R, Geng J, Wang JH, Chu XY, Geng HC, Chen LB. Overexpression of eukaryotic initiation factor 4E (eIF4E) and its clinical significance in lung adenocarcinoma. Lung Cancer 2009.

9. Berkel HJ, Turbat-Herrera EA, Shi R, de Benedetti A. Expression of the translation initiation factor eIF4E in the polyp-cancer sequence in the colon. Cancer Epidemiol Biomarkers Prev 2001;10:663-6.

10. Schmelzle T, Hall MN. TOR, a central controller of cell growth. Cell 2000;103:253-62.

11. Cullen BR. Nuclear RNA export. J Cell Sci 2003;116:587-97.

12. Topisirovic I, Ruiz-Gutierrez M, Borden KL. Phosphorylation of the eukaryotic translation initiation factor eIF4E contributes to its transformation and mRNA transport activities. Cancer Res 2004;64:8639-42.

13. Culjkovic B, Topisirovic I, Skrabanek L, Ruiz-Gutierrez M, Borden KL. eIF4E promotes nuclear export of cyclin D1 mRNAs via an element in the 3'UTR. J Cell Biol 2005;169:245-56.

14. Culjkovic B, Topisirovic I, Skrabanek L, Ruiz-Gutierrez M, Borden KL. eIF4E is a central node of an RNA regulon that governs cellular proliferation. J Cell Biol 2006;175:415-26.

15. Cohen N, Sharma M, Kentsis A, Perez JM, Strudwick S, Borden KL. PML RING suppresses oncogenic transformation by reducing the affinity of eIF4E for mRNA. Embo J 2001;20:4547-59.

16. Lai HK, Borden KL. The promyelocytic leukemia (PML) protein suppresses cyclin D1 protein production by altering the nuclear cytoplasmic distribution of cyclin D1 mRNA. Oncogene 2000;19:1623-34.

17. Hudes G, Carducci M, Tomczak P, et al. Temsirolimus, interferon alfa, or both for advanced renal-cell carcinoma. N Engl J Med 2007;356:2271-81.

18. Motzer RJ, Escudier B, Oudard S, et al. Efficacy of everolimus in advanced renal cell carcinoma: a double-blind, randomised, placebo-controlled phase III trial. Lancet 2008;372:449-56.

19. Graff JR, Konicek BW, Carter JH, Marcusson EG. Targeting the eukaryotic translation initiation factor 4E for cancer therapy. Cancer Res 2008;68:631-4.

20. Wang X, Yue P, Chan CB, et al. Inhibition of mammalian target of rapamycin induces phosphatidylinositol 3-kinase-dependent and Mnk-mediated eukaryotic translation initiation factor 4E phosphorylation. Mol Cell Biol 2007;27:7405-13.

21. Gingras AC, Kennedy SG, O'Leary MA, Sonenberg N, Hay N. 4E-BP1, a repressor of mRNA translation, is phosphorylated and inactivated by the Akt(PKB) signaling pathway. Genes Dev 1998;12:502-13.

22. Gingras AC, Gygi SP, Raught B, et al. Regulation of 4E-BP1 phosphorylation: a novel two-step mechanism. Genes Dev 1999;13:1422-37.

23. Loewith R, Jacinto E, Wullschleger S, et al. Two TOR complexes, only one of which is rapamycin sensitive, have distinct roles in cell growth control. Mol Cell 2002;10:457-68.

24. Chung J, Grammer TC, Lemon KP, Kazlauskas A, Blenis J. PDGF- and insulin-dependent pp70S6k activation mediated by phosphatidylinositol-3-OH kinase. Nature 1994;370:71-5.

25. Kim DH, Sarbassov DD, Ali SM, et al. GbetaL, a positive regulator of the rapamycin-sensitive pathway required for the nutrient-sensitive interaction between raptor and mTOR. Mol Cell 2003;11:895-904.

26. Inoki K, Zhu T, Guan KL. TSC2 mediates cellular energy response to control cell growth and survival. Cell 2003;115:577-90.

27. Saucedo LJ, Gao X, Chiarelli DA, Li L, Pan D, Edgar BA. Rheb promotes cell growth as a component of the insulin/TOR signalling network. Nat Cell Biol 2003;5:566-71.

28. Zhang Y, Gao X, Saucedo LJ, Ru B, Edgar BA, Pan D. Rheb is a direct target of the tuberous sclerosis tumour suppressor proteins. Nat Cell Biol 2003;5:578-81.

29. Inoki K, Li Y, Zhu T, Wu J, Guan KL. TSC2 is phosphorylated and inhibited by Akt and suppresses mTOR signalling. Nat Cell Biol 2002;4:648-57.

30. Roux PP, Ballif BA, Anjum R, Gygi SP, Blenis J. Tumor-promoting phorbol esters and activated Ras inactivate the tuberous sclerosis tumor suppressor complex via p90 ribosomal S6 kinase. Proc Natl Acad Sci U S A 2004;101:13489-94.

31. Kandel ES, Hay N. The regulation and activities of the multifunctional serine/threonine kinase Akt/PKB. Exp Cell Res 1999;253:210-29.

32. McManus EJ, Collins BJ, Ashby PR, et al. The in vivo role of PtdIns(3,4,5)P3 binding to PDK1 PH domain defined by knockin mutation. Embo J 2004;23:2071-82.

33. Sarbassov DD, Guertin DA, Ali SM, Sabatini DM. Phosphorylation and regulation of Akt/PKB by the rictor-mTOR complex. Science 2005;307:1098-101.

34. Engelman JA, Luo J, Cantley LC. The evolution of phosphatidylinositol 3-kinases as regulators of growth and metabolism. Nat Rev Genet 2006;7:606-19.

35. Maehama T, Dixon JE. The tumor suppressor, PTEN/MMAC1, dephosphorylates the lipid second messenger, phosphatidylinositol 3,4,5-trisphosphate. J Biol Chem 1998;273:13375-8.

36. Sansal I, Sellers WR. The biology and clinical relevance of the PTEN tumor suppressor pathway. J Clin Oncol 2004;22:2954-63.

37. Spitaler M, Cantrell DA. Protein kinase C and beyond. Nat Immunol 2004;5:785-90.

38. Bos JL. ras oncogenes in human cancer: a review. Cancer Res 1989;49:4682-9.

39. Davies H, Bignell GR, Cox C, et al. Mutations of the BRAF gene in human cancer. Nature 2002;417:949-54.

40. Waskiewicz AJ, Flynn A, Proud CG, Cooper JA. Mitogen-activated protein kinases activate the serine/threonine kinases Mnk1 and Mnk2. Embo J 1997;16:1909-20.

41. Egan SE, Giddings BW, Brooks MW, Buday L, Sizeland AM, Weinberg RA. Association of Sos Ras exchange protein with Grb2 is implicated in tyrosine kinase signal transduction and transformation. Nature 1993;363:45-51.

42. Barbacid M. ras genes. Annu Rev Biochem 1987;56:779-827.

43. Morrison DK, Cutler RE. The complexity of Raf-1 regulation. Curr Opin Cell Biol 1997;9:174-9.

44. Nakielny S, Cohen P, Wu J, Sturgill T. MAP kinase activator from insulin-stimulated skeletal muscle is a protein threonine/tyrosine kinase. Embo J 1992;11:2123-9.

45. Therrien M, Chang HC, Solomon NM, Karim FD, Wassarman DA, Rubin GM. KSR, a novel protein kinase required for RAS signal transduction. Cell 1995;83:879-88.

46. Stokoe D, Campbell DG, Nakielny S, et al. MAPKAP kinase-2; a novel protein kinase activated by mitogen-activated protein kinase. Embo J 1992;11:3985-94.

47. Hodge C, Liao J, Stofega M, Guan K, Carter-Su C, Schwartz J. Growth hormone stimulates phosphorylation and activation of elk-1 and expression of c-fos, egr-1, and junB through activation of extracellular signal-regulated kinases 1 and 2. J Biol Chem 1998;273:31327-36.

48. Fukunaga R, Hunter T. MNK1, a new MAP kinase-activated protein kinase, isolated by a novel expression screening method for identifying protein kinase substrates. Embo J 1997;16:1921-33.

49. Slentz-Kesler K, Moore JT, Lombard M, Zhang J, Hollingsworth R, Weiner MP. Identification of the human Mnk2 gene (MKNK2) through protein interaction with estrogen receptor beta. Genomics 2000;69:63-71.

50. O'Loghlen A, Gonzalez VM, Pineiro D, Perez-Morgado MI, Salinas M, Martin ME. Identification and molecular characterization of Mnk1b, a splice variant of human MAP kinase-interacting kinase Mnk1. Exp Cell Res 2004;299:343-55.

51. Parra JL, Buxade M, Proud CG. Features of the catalytic domains and C termini of the MAPK signal-integrating kinases Mnk1 and Mnk2 determine their differing activities and regulatory properties. J Biol Chem 2005;280:37623-33.

52. Scheper GC, Morrice NA, Kleijn M, Proud CG. The mitogen-activated protein kinase signal-integrating kinase Mnk2 is a eukaryotic initiation factor 4E kinase with high levels of basal activity in mammalian cells. Mol Cell Biol 2001;21:743-54.

53. Waskiewicz AJ, Johnson JC, Penn B, Mahalingam M, Kimball SR, Cooper JA. Phosphorylation of the cap-binding protein eukaryotic translation initiation factor 4E by protein kinase Mnk1 in vivo. Mol Cell Biol 1999;19:1871-80.

54. Scheper GC, Parra JL, Wilson M, et al. The N and C termini of the splice variants of the human mitogen-activated protein kinase-interacting kinase Mnk2 determine activity and localization. Mol Cell Biol 2003;23:5692-705.

55. Shveygert M, Kaiser C, Bradrick SS, Gromeier M. Regulation of eukaryotic initiation factor 4E (eIF4E) phosphorylation by mitogen-activated protein kinase occurs through modulation of Mnk1-eIF4G interaction. Mol Cell Biol 2010;30:5160-7.

56. Pyronnet S, Imataka H, Gingras AC, Fukunaga R, Hunter T, Sonenberg N. Human eukaryotic translation initiation factor 4G (eIF4G) recruits mnk1 to phosphorylate eIF4E. Embo J 1999;18:270-9.

57. Parra-Palau JL, Scheper GC, Wilson ML, Proud CG. Features in the N and C termini of the MAPK-interacting kinase Mnk1 mediate its nucleocytoplasmic shuttling. J Biol Chem 2003;278:44197-204.

58. Minich WB, Balasta ML, Goss DJ, Rhoads RE. Chromatographic resolution of in vivo phosphorylated and nonphosphorylated eukaryotic translation initiation factor eIF-4E: increased cap affinity of the phosphorylated form. Proc Natl Acad Sci U S A 1994;91:7668-72.

59. Scheper GC, van Kollenburg B, Hu J, Luo Y, Goss DJ, Proud CG. Phosphorylation of eukaryotic initiation factor 4E markedly reduces its affinity for capped mRNA. J Biol Chem 2002;277:3303-9.

60. Knauf U, Tschopp C, Gram H. Negative regulation of protein translation by mitogen-activated protein kinase-interacting kinases 1 and 2. Mol Cell Biol 2001;21:5500-11.

61. Morley SJ, Naegele S. Phosphorylation of Eukaryotic Initiation Factor (eIF) 4E Is Not Required for de Novo Protein Synthesis following Recovery from Hypertonic Stress in Human Kidney Cells. J Biol Chem 2002;277:32855-9.

62. Phillips A, Blaydes JP. MNK1 and EIF4E are downstream effectors of MEKs in the regulation of the nuclear export of HDM2 mRNA. Oncogene 2008;27:1645-9.

63. Lachance PED, Miron M, Raught B, Sonenberg N, Lasko P. Phosphorylation of Eukaryotic Translation Initiation Factor 4E Is Critical for Growth. Mol Cell Biol 2002;22:1656-63.

64. Ueda T, Watanabe-Fukunaga R, Fukuyama H, Nagata S, Fukunaga R. Mnk2 and Mnk1 are essential for constitutive and inducible phosphorylation of eukaryotic initiation factor 4E but not for cell growth or development. Mol Cell Biol 2004;24:6539-49.

65. Chrestensen CA, Eschenroeder A, Ross WG, et al. Loss of MNK function sensitizes fibroblasts to serum-withdrawal induced apoptosis. Genes Cells 2007;12:1133-40.

66. DaSilva J, Xu L, Kim HJ, Miller WT, Bar-Sagi D. Regulation of sprouty stability by Mnk1-dependent phosphorylation. Mol Cell Biol 2006;26:1898-907.

67. Hefner Y, Borsch-Haubold AG, Murakami M, et al. Serine 727 phosphorylation and activation of cytosolic phospholipase A2 by MNK1-related protein kinases. J Biol Chem 2000;275:37542-51.

68. Buxade M, Parra JL, Rousseau S, et al. The Mnks are novel components in the control of TNF alpha biosynthesis and phosphorylate and regulate hnRNP A1. Immunity 2005;23:177-89.

69. Wendel HG, Silva RL, Malina A, et al. Dissecting eIF4E action in tumorigenesis. Genes Dev 2007;21:3232-7.

70. Ueda T, Sasaki M, Elia AJ, et al. Combined deficiency for MAP kinase-interacting kinase 1 and 2 (Mnk1 and Mnk2) delays tumor development. Proc Natl Acad Sci U S A 2010;107:13984-90.

71. Furic L, Rong L, Larsson O, et al. eIF4E phosphorylation promotes tumorigenesis and is associated with prostate cancer progression. Proc Natl Acad Sci U S A 2010;107:14134-9.

72. Yoshizawa A, Fukuoka J, Shimizu S, et al. Overexpression of phospho-eIF4E is associated with survival through AKT pathway in non-small cell lung cancer. Clin Cancer Res 2010;16:240-8.

73. Chrestensen CA, Shuman JK, Eschenroeder A, Worthington M, Gram H, Sturgill TW. MNK1 and MNK2 regulation in HER2-overexpressing breast cancer lines. J Biol Chem 2007;282:4243-52.

74. Bianchini A, Loiarro M, Bielli P, et al. Phosphorylation of eIF4E by MNKs supports protein synthesis, cell cycle progression and proliferation in prostate cancer cells. Carcinogenesis 2008.

75. Muta D, Makino K, Nakamura H, Yano S, Kudo M, Kuratsu J. Inhibition of eIF4E phosphorylation reduces cell growth and proliferation in primary central nervous system lymphoma cells. J Neurooncol 2011;101:33-9.

76. Li Y, Yue P, Deng X, et al. Protein phosphatase 2A negatively regulates eukaryotic initiation factor 4E phosphorylation and eIF4F assembly through direct dephosphorylation of Mnk and eIF4E. Neoplasia 2010;12:848-55.

77. Westermarck J, Hahn WC. Multiple pathways regulated by the tumor suppressor PP2A in transformation. Trends Mol Med 2008;14:152-60.

78. Janssens V, Goris J. Protein phosphatase 2A: a highly regulated family of serine/threonine phosphatases implicated in cell growth and signalling. Biochem J 2001;353:417-39.

79. Chen J, Martin BL, Brautigan DL. Regulation of protein serine-threonine phosphatase type-2A by tyrosine phosphorylation. Science 1992;257:1261-4.

80. Usui H, Inoue R, Tanabe O, et al. Activation of protein phosphatase 2A by cAMP-dependent protein kinase-catalyzed phosphorylation of the 74-kDa B'' (delta) regulatory subunit in vitro and identification of the phosphorylation sites. FEBS Lett 1998;430:312-6.

81. Lee J, Stock J. Protein phosphatase 2A catalytic subunit is methyl-esterified at its carboxyl terminus by a novel methyltransferase. J Biol Chem 1993;268:19192-5.

82. Kranias G, Watt LF, Carpenter H, et al. Protein phosphatase 2A carboxymethylation and regulatory B subunits differentially regulate mast cell degranulation. Cell Signal 2010;22:1882-90.

83. Chalfant CE, Kishikawa K, Mumby MC, Kamibayashi C, Bielawska A, Hannun YA. Long chain ceramides activate protein phosphatase-1 and protein phosphatase-2A. Activation is stereospecific and regulated by phosphatidic acid. J Biol Chem 1999;274:20313-7.

84. Al-Murrani SW, Woodgett JR, Damuni Z. Expression of I2PP2A, an inhibitor of protein phosphatase 2A, induces c-Jun and AP-1 activity. Biochem J 1999;341 (Pt 2):293-8.

85. Baldin V, Lukas J, Marcote MJ, Pagano M, Draetta G. Cyclin D1 is a nuclear protein required for cell cycle progression in G1. Genes & Development 1993;7:812-21.

86. Gillett C, Fantl V, Smith R, et al. Amplification and Overexpression of Cyclin D1 in Breast Cancer Detected by Immunohistochemical Staining. Cancer Res 1994;54:1812-7.

87. Jiang W, Kahn SM, Tomita N, Zhang Y-J, Lu S-H, Weinstein IB. Amplification and Expression of the Human Cyclin D Gene in Esophageal Cancer. Cancer Res 1992;52:2980-3.

88. Bosch F, Jares P, Campo E, et al. PRAD-1/cyclin D1 gene overexpression in chronic lymphoproliferative disorders: a highly specific marker of mantle cell lymphoma. Blood 1994;84:2726-32.

89. Sherr CJ. The Pezcoller lecture: cancer cell cycles revisited. Cancer Res 2000;60:3689-95.

90. Zwijsen RML, Buckle RS, Hijmans EM, Loomans CJM, Bernards R. Ligand-independent recruitment of steroid receptor coactivators to estrogen receptor by cyclin D1. Genes & Development 1998;12:3488-98.

91. Knudsen KE, Cavenee WK, Arden KC. D-Type Cyclins Complex with the Androgen Receptor and Inhibit Its Transcriptional Transactivation Ability. Cancer Res 1999;59:2297-301.

92. Hu J, Colburn NH. Histone Deacetylase Inhibition Down-Regulates Cyclin D1 Transcription by Inhibiting Nuclear Factor-Œ ∫ B/p65 DNA Binding. Molecular Cancer Research 2005;3:100-9.

93. Shan J, Zhao W, Gu W. Suppression of cancer cell growth by promoting cyclin D1 degradation. Mol Cell 2009;36:469-76.

94. Karp JE, Smith BD, Levis MJ, et al. Sequential Flavopiridol, Cytosine Arabinoside, and Mitoxantrone: A Phase II Trial in Adults with Poor-Risk Acute Myelogenous Leukemia. Clinical Cancer Research 2007;13:4467-73.

95. Lamb J, Ramaswamy S, Ford HL, et al. A Mechanism of Cyclin D1 Action Encoded in the Patterns of Gene Expression in Human Cancer. Cell 2003;114:323-34.

96. Xu X, Vatsyayan J, Gao C, Bakkenist CJ, Hu J. HDAC2 promotes eIF4E sumoylation and activates mRNA translation gene specifically. J Biol Chem 2010;285:18139-43.

97. Olsen EA, Kim YH, Kuzel TM, et al. Phase IIB Multicenter Trial of Vorinostat in Patients With Persistent, Progressive, or Treatment Refractory Cutaneous T-Cell Lymphoma. Journal of Clinical Oncology 2007;25:3109-15.

98. Brunner TB, Hahn SM, Gupta AK, Muschel RJ, McKenna WG, Bernhard EJ. Farnesyltransferase Inhibitors. Cancer Research 2003;63:5656-68.

99. Manning G, Whyte DB, Martinez R, Hunter T, Sudarsanam S. The protein kinase complement of the human genome. Science 2002;298:1912-34.

100. Hanks S, Hunter T. Protein kinases 6. The eukaryotic protein kinase superfamily: kinase (catalytic) domain structure and classification. FASEB J 1995;9:576-96.

101. Chow JPH, Siu WY, Ho HTB, Ma KHT, Ho CC, Poon RYC. Differential Contribution of Inhibitory Phosphorylation of CDC2 and CDK2 for Unperturbed Cell Cycle Control and DNA Integrity Checkpoints. Journal of Biological Chemistry 2003;278:40815-28.

102. Moran MF, Polakis P, McCormick F, Pawson T, Ellis C. Protein-tyrosine kinases regulate the phosphorylation, protein interactions, subcellular distribution, and activity of p21ras GTPase-activating protein. Mol Cell Biol 1991;11:1804-12.

103. Harper JW. A phosphorylation-driven ubiquitination switch for cell-cycle control. Trends in Cell Biology 2002;12:104-7.

104. Knighton D, Zheng J, Ten Eyck L, et al. Crystal structure of the catalytic subunit of cyclic adenosine monophosphate-dependent protein kinase. Science 1991;253:407-14.

105. Jauch R, Cho MK, Jakel S, et al. Mitogen-activated protein kinases interacting kinases are autoinhibited by a reprogrammed activation segment. Embo J 2006;25:4020-32.

106. Johnson LN, Noble MEM, Owen DJ. Active and Inactive Protein Kinases: Structural Basis for Regulation. Cell 1996;85:149-58.

107. Kampa D, Burnside J. Computational and Functional Analysis of the Putative SH2 Domain in Janus Kinases. Biochemical and Biophysical Research Communications 2000;278:175-82.

108. Pendergast AM, Muller AJ, Havlik MH, Clark R, McCormick F, Witte ON. Evidence for regulation of the human ABL tyrosine kinase by a cellular inhibitor. Proceedings of the National Academy of Sciences of the United States of America 1991;88:5927-31.

109. Jauch R, Jakel S, Netter C, et al. Crystal structures of the Mnk2 kinase domain reveal an inhibitory conformation and a zinc binding site. Structure 2005;13:1559-68.

110. Omura S, Iwai Y, Hirano A, et al. A new alkaloid AM-2282 OF Streptomyces origin. Taxonomy, fermentation, isolation and preliminary characterization. J Antibiot (Tokyo) 1977;30:275-82.

111. Link JT, Raghavan S, Gallant M, Danishefsky SJ, Chou TC, Ballas LM. Staurosporine and ent-Staurosporine: The First Total Syntheses, Prospects for a Regioselective Approach, and Activity Profiles1. Journal of the American Chemical Society 1996;118:2825-42.

112. Tamaoki T, Nomoto H, Takahashi I, Kato Y, Morimoto M, Tomita F. Staurosporine, a potent inhibitor of phospholipid/Ca++dependent protein kinase. Biochem Biophys Res Commun 1986;135:397-402.

113. Nakano H, Kobayashi E, Takahashi I, Tamaoki T, Kuzuu Y, Iba H. Staurosporine inhibits tyrosine-specific protein kinase activity of Rous sarcoma virus transforming protein p60. J Antibiot (Tokyo) 1987;40:706-8.

114. Akinaga S, Gomi K, Morimoto M, Tamaoki T, Okabe M. Antitumor activity of UCN-01, a selective inhibitor of protein kinase C, in murine and human tumor models. Cancer Res 1991;51:4888-92.

115. Meggio F, Donella Deana A, Ruzzene M, et al. Different susceptibility of protein kinases to staurosporine inhibition. Kinetic studies and molecular bases for the resistance of protein kinase CK2. Eur J Biochem 1995;234:317-22.

116. Prade L, Engh RA, Girod A, Kinzel V, Huber R, Bossemeyer D. Staurosporine-induced conformational changes of cAMP-dependent protein kinase catalytic subunit explain inhibitory potential. 1997;5:1627-37.

117. Furet P, Caravatti G, Lydon N, et al. Modelling study of protein kinase inhibitors: binding mode of staurosporine and origin of the selectivity of CGP 52411. J Comput Aided Mol Des 1995;9:465-72.

118. Buchdunger E, Zimmermann J, Mett H, et al. Inhibition of the Abl protein-tyrosine kinase in vitro and in vivo by a 2-phenylaminopyrimidine derivative. Cancer Res 1996;56:100-4.

119. Druker BJ, Tamura S, Buchdunger E, et al. Effects of a selective inhibitor of the Abl tyrosine kinase on the growth of Bcr-Abl positive cells. Nat Med 1996;2:561-6.

120. O'Brien SG, Guilhot F, Larson RA, et al. Imatinib Compared with Interferon and Low-Dose Cytarabine for Newly Diagnosed Chronic-Phase Chronic Myeloid Leukemia. N Engl J Med 2003;348:994-1004.

121. Huse M, Kuriyan J. The conformational plasticity of protein kinases. Cell 2002;109:275-82.

122. Azam M, Latek RR, Daley GQ. Mechanisms of autoinhibition and STI-571/imatinib resistance revealed by mutagenesis of BCR-ABL. Cell 2003;112:831-43.

123. Shah NP, Kantarjian HM, Kim D-W, et al. Intermittent Target Inhibition With Dasatinib 100 mg Once Daily Preserves Efficacy and Improves Tolerability in Imatinib-Resistant and -Intolerant Chronic-Phase Chronic Myeloid Leukemia. J Clin Oncol 2008;26:3204-12.

124. Bain J, Plater L, Elliott M, et al. The selectivity of protein kinase inhibitors: a further update. Biochem J 2007;408:297-315.

125. Beatson C. On treatment of inoperable cases of carcinoma of the mamma: suggestions for a new method of treatment with illustrative cases. Lancet 1896;2:104–7.

126. Tamoxifen for early breast cancer: an overview of the randomised trials. Early Breast Cancer Trialists' Collaborative Group. Lancet 1998;351:1451-67.

127. Coussens L, Yang-Feng TL, Liao YC, et al. Tyrosine kinase receptor with extensive homology to EGF receptor shares chromosomal location with neu oncogene. Science 1985;230:1132-9.

128. Slamon DJ, Clark GM, Wong SG, Levin WJ, Ullrich A, McGuire WL. Human breast cancer: correlation of relapse and survival with amplification of the HER-2/neu oncogene. Science 1987;235:177-82.

129. Eiermann W. Trastuzumab combined with chemotherapy for the treatment of HER2-positive metastatic breast cancer: pivotal trial data. Ann Oncol 2001;12 Suppl 1:S57-62.

130. Perou CM, Sorlie T, Eisen MB, et al. Molecular portraits of human breast tumours. Nature 2000;406:747-52.

131. Sorlie T, Perou CM, Tibshirani R, et al. Gene expression patterns of breast carcinomas distinguish tumor subclasses with clinical implications. Proc Natl Acad Sci U S A 2001;98:10869-74.

132. Rouzier R, Perou CM, Symmans WF, et al. Breast cancer molecular subtypes respond differently to preoperative chemotherapy. Clin Cancer Res 2005;11:5678-85.

133. Neve RM, Chin K, Fridlyand J, et al. A collection of breast cancer cell lines for the study of functionally distinct cancer subtypes. Cancer Cell 2006;10:515-27.

134. Storkel S, Eble JN, Adlakha K, et al. Classification of renal cell carcinoma: Workgroup No. 1. Union Internationale Contre le Cancer (UICC) and the American Joint Committee on Cancer (AJCC). Cancer 1997;80:987-9.

135. Latif F, Tory K, Gnarra J, et al. Identification of the von Hippel-Lindau disease tumor suppressor gene. Science 1993;260:1317-20.

136. Kovacs G, Erlandsson R, Boldog F, et al. Consistent chromosome 3p deletion and loss of heterozygosity in renal cell carcinoma. Proc Natl Acad Sci U S A 1988;85:1571-5.

137. Gnarra JR, Tory K, Weng Y, et al. Mutations of the VHL tumour suppressor gene in renal carcinoma. Nat Genet 1994;7:85-90.

138. Herman JG, Latif F, Weng Y, et al. Silencing of the VHL tumor-suppressor gene by DNA methylation in renal carcinoma. Proc Natl Acad Sci U S A 1994;91:9700-4.

139. Maxwell PH, Wiesener MS, Chang GW, et al. The tumour suppressor protein VHL targets hypoxia-inducible factors for oxygen-dependent proteolysis. Nature 1999;399:271-5.

140. Huang LE, Gu J, Schau M, Bunn HF. Regulation of hypoxia-inducible factor 1alpha is mediated by an O2-dependent degradation domain via the ubiquitin-proteasome pathway. Proc Natl Acad Sci U S A 1998;95:7987-92.

141. Jaakkola P, Mole DR, Tian YM, et al. Targeting of HIF-alpha to the von Hippel-Lindau ubiquitylation complex by O2-regulated prolyl hydroxylation. Science 2001;292:468-72.

142. Hon WC, Wilson MI, Harlos K, et al. Structural basis for the recognition of hydroxyproline in HIF-1 alpha by pVHL. Nature 2002;417:975-8.

143. Lonergan KM, Iliopoulos O, Ohh M, et al. Regulation of hypoxia-inducible mRNAs by the von Hippel-Lindau tumor suppressor protein requires binding to complexes containing elongins B/C and Cul2. Mol Cell Biol 1998;18:732-41.

144. Kamura T, Koepp DM, Conrad MN, et al. Rbx1, a component of the VHL tumor suppressor complex and SCF ubiquitin ligase. Science 1999;284:657-61.

145. Semenza GL. Targeting HIF-1 for cancer therapy. Nat Rev Cancer 2003;3:721-32.

146. Schmidt L, Duh FM, Chen F, et al. Germline and somatic mutations in the tyrosine kinase domain of the MET proto-oncogene in papillary renal carcinomas. Nat Genet 1997;16:68-73.

147. Fischer J, Palmedo G, von Knobloch R, et al. Duplication and overexpression of the mutant allele of the MET proto-oncogene in multiple hereditary papillary renal cell tumours. Oncogene 1998;17:733-9.

148. Moghul A, Lin L, Beedle A, et al. Modulation of c-MET proto-oncogene (HGF receptor) mRNA abundance by cytokines and hormones: evidence for rapid decay of the 8 kb c-MET transcript. Oncogene 1994;9:2045-52.

149. Besser D, Bardelli A, Didichenko S, et al. Regulation of the urokinase-type plasminogen activator gene by the oncogene Tpr-Met involves GRB2. Oncogene 1997;14:705-11.

150. Weidner KM, Sachs M, Birchmeier W. The Met receptor tyrosine kinase transduces motility, proliferation, and morphogenic signals of scatter factor/hepatocyte growth factor in epithelial cells. J Cell Biol 1993;121:145-54.

151. Leibovich BC, Blute ML, Cheville JC, et al. Prediction of progression after radical nephrectomy for patients with clear cell renal cell carcinoma: a stratification tool for prospective clinical trials. Cancer 2003;97:1663-71.

152. Interferon-alpha and survival in metastatic renal carcinoma: early results of a randomised controlled trial. Medical Research Council Renal Cancer Collaborators. Lancet 1999;353:14-7.

153. Motzer RJ, Hutson TE, Tomczak P, et al. Overall survival and updated results for sunitinib compared with interferon alfa in patients with metastatic renal cell carcinoma. J Clin Oncol 2009;27:3584-90.

154. Escudier B, Pluzanska A, Koralewski P, et al. Bevacizumab plus interferon alfa-2a for treatment of metastatic renal cell carcinoma: a randomised, double-blind phase III trial. Lancet 2007;370:2103-11.

155. Albanese C, Johnson J, Watanabe G, et al. Transforming p21ras mutants and c-Ets-2 activate the cyclin D1 promoter through distinguishable regions. J Biol Chem 1995;270:23589-97.

156. Kozma SC, Bogaard ME, Buser K, et al. The human c-Kirsten ras gene is activated by a novel mutation in codon 13 in the breast carcinoma cell line MDA-MB231. Nucleic Acids Res 1987;15:5963-71.

157. rDhanjaland P, R.Fry J. Determinants of MTT reduction in rat hepatocytes. Biomarkers 1997;2:111 - 6.

158. Frisch SM, Francis H. Disruption of epithelial cell-matrix interactions induces apoptosis. J Cell Biol 1994;124:619-26.

159. Moro L, Venturino M, Bozzo C, et al. Integrins induce activation of EGF receptor: role in MAP kinase induction and adhesion-dependent cell survival. Embo J 1998;17:6622-32.

160. Khwaja A, Rodriguez-Viciana P, Wennstrom S, Warne PH, Downward J. Matrix adhesion and Ras transformation both activate a phosphoinositide 3-OH kinase and protein kinase B/Akt cellular survival pathway. Embo J 1997;16:2783-93.

161. Chow KC, Ross WE. Topoisomerase-specific drug sensitivity in relation to cell cycle progression. Mol Cell Biol 1987;7:3119-23.

162. Jin X, Jin HR, Lee D, Lee JH, Kim SK, Lee JJ. A quassinoid 6alpha-tigloyloxychaparrinone inhibits hypoxia-inducible factor-1 pathway by inhibition of eukaryotic translation initiation factor 4E phosphorylation. Eur J Pharmacol 2008;592:41-7.

163. Nicol D, Hii SI, Walsh M, et al. Vascular endothelial growth factor expression is increased in renal cell carcinoma. J Urol 1997;157:1482-6.

164. Motzer RJ, Hutson TE, Tomczak P, et al. Sunitinib versus interferon alfa in metastatic renal-cell carcinoma. N Engl J Med 2007;356:115-24.

165. Escudier B, Eisen T, Stadler WM, et al. Sorafenib for Treatment of Renal Cell Carcinoma: Final Efficacy and Safety Results of the Phase III Treatment Approaches in Renal Cancer Global Evaluation Trial. J Clin Oncol 2009.

166. Sternberg CN, Davis ID, Mardiak J, et al. Pazopanib in locally advanced or metastatic renal cell carcinoma: results of a randomized phase III trial. J Clin Oncol 2010;28:1061-8.

167. Rixe O, Bukowski RM, Michaelson MD, et al. Axitinib treatment in patients with cytokine-refractory metastatic renal-cell cancer: a phase II study. Lancet Oncol 2007;8:975-84.

168. Shinojima T, Oya M, Takayanagi A, Mizuno R, Shimizu N, Murai M. Renal cancer cells lacking hypoxia inducible factor (HIF)-1Œ± expression maintain vascular endothelial growth factor expression through HIF-2Œ±. Carcinogenesis 2006;28:529-36.

169. Yu C, Bruzek LM, Meng XW, et al. The role of Mcl-1 downregulation in the proapoptotic activity of the multikinase inhibitor BAY 43-9006. Oncogene 2005;24:6861-9.

170. Culjkovic B, Topisirovic I, Borden KL. Controlling gene expression through RNA regulons: the role of the eukaryotic translation initiation factor eIF4E. Cell Cycle 2007;6:65-9.

171. Reich M, Liefeld T, Gould J, Lerner J, Tamayo P, Mesirov JP. GenePattern 2.0. Nat Genet 2006;38:500-1.

172. Marin-Hernandez A, Rodriguez-Enriquez S, Vital-Gonzalez PA, et al. Determining and understanding the control of glycolysis in fast-growth tumor cells. Flux control by an over-expressed but strongly product-inhibited hexokinase. FEBS J 2006;273:1975-88.

173. Yalcin A, Telang S, Clem B, Chesney J. Regulation of glucose metabolism by 6-phosphofructo-2-kinase/fructose-2,6-bisphosphatases in cancer. Exp Mol Pathol 2009;86:174-9.

174. Kim J-w, Dang CV. Cancer's Molecular Sweet Tooth and the Warburg Effect. Cancer Research 2006;66:8927-30.

175. Le A, Cooper CR, Gouw AM, et al. Inhibition of lactate dehydrogenase A induces oxidative stress and inhibits tumor progression. Proceedings of the National Academy of Sciences 2010;107:2037-42.

176. Katsuoka F, Motohashi H, Ishii T, Aburatani H, Engel JD, Yamamoto M. Genetic Evidence that Small Maf Proteins Are Essential for the Activation of Antioxidant Response Element-Dependent Genes. Mol Cell Biol 2005;25:8044-51.

177. Hayes JD, McMahon M. NRF2 and KEAP1 mutations: permanent activation of an adaptive response in cancer. Trends in Biochemical Sciences 2009;34:176-88.

178. Bushell M, Stoneley M, Kong YW, et al. Polypyrimidine tract binding protein regulates IRES-mediated gene expression during apoptosis. Mol Cell 2006;23:401-12.

179. Warburg O. On the origin of cancer cells. Science 1956;123:309-14.

180. Mohl DA, Huddleston MJ, Collingwood TS, Annan RS, Deshaies RJ. Dbf2,ÄìMob1 drives relocalization of protein phosphatase Cdc14 to the cytoplasm during exit from mitosis. The Journal of Cell Biology 2009;184:527-39.

181. El Messaoudi-Aubert S, Nicholls J, Maertens GN, Brookes S, Bernstein E, Peters G. Role for the MOV10 RNA helicase in polycomb-mediated repression of the INK4a tumor suppressor. Nat Struct Mol Biol 2010;17:862-8.

182. Lei X, Shen X, Xu X, Bernstein H. Human Cdc5, a regulator of mitotic entry, can act as a site-specific DNA binding protein. J Cell Sci 2000;113:4523-31.

183. Reiner A, Yekutieli D, Benjamini Y. Identifying differentially expressed genes using false discovery rate controlling procedures. Bioinformatics 2003;19:368-75.

184. Gordan JD, Lal P, Dondeti VR, et al. HIF-alpha effects on c-Myc distinguish two subtypes of sporadic VHL-deficient clear cell renal carcinoma. Cancer Cell 2008;14:435-46.

185. Cho-Vega JH, Rassidakis GZ, Admirand JH, et al. MCL-1 expression in B-cell non-Hodgkin's lymphomas. Hum Pathol 2004;35:1095-100.

186. Cohen P. Guidelines for the effective use of chemical inhibitors of protein function to understand their roles in cell regulation. The Biochemical journal 2010;425:53-4.

187. Konicek BW, Stephens JR, McNulty AM, et al. Therapeutic Inhibition of MAP Kinase Interacting Kinase Blocks Eukaryotic Initiation Factor 4E Phosphorylation and Suppresses Outgrowth of Experimental Lung Metastases. Cancer Research 2011;71:1849-57.